

POLITECNICO DI TORINO

Master's degree in Structural Engineering

Master's degree Thesis

Structural Health Monitoring (SHM), Heritage building information modelling (HBIM) and remote sensing for existing bridge.



Tutor Candidate

Prof. Francesco Tondolo

Co-tutor

Prof. Anna Osello

Prof. Marco Piras

Candidate:

Gianluca Colia

Abstract:

Much of the world's historical, artistic, and cultural built heritage has internal or exposed damage and require ordinary or extraordinary maintenance. From an engineering point of view, several techniques have been developed over time to solve this problem, such as structural health monitoring (SHM) which involves the management of structural damage using internal or external sensors or through visual damage inspection.

As for the existing structures, after the data is generated, it must be collected, managed and stored in an appropriate manner and consequently one needs to work in an HBIM context, also known as Historical Building information Modelling. Following this methodology, it is essential to work with a unified and parametric 3D model, able to manage new model integrations by updating its database with different types of data.

In most cases, existing structures are characterized by complex geometries that would have to be modelled directly in a BIM environment, with a great deal of time. With this in mind, new techniques have been developed such as Scan-to-BIM or Mesh-to-BIM which are based on remote sensing through the use of laser scanners, photogrammetric techniques and, recently, also drones with cameras that have characteristic of rotating 180°. These techniques make the reconstruction of the model more expeditious, even if currently there are still problems of interoperability between software to use them in an optimal way.

The main objective of this research is to generate a workflow to perform the detection and characterization of damage in a bridge, through the SHM and remote sensing techniques, working in an HBIM environment.

At the beginning, we looked for a methodology to import the mesh and texture of a 3D object, a Rubik's cube, into the Revit software, following a mesh-to-BIM procedure which, however, turned out to be a non-automatic and very time-consuming procedure. Another methodology was then followed, namely scan-to-BIM, by importing the dense point cloud of a damaged pier cap beam of a dismantled bridge into the Revit software and identifying the damage through a user interface, with the help of CloudCompare software and Dynamo.

After finding a quick methodology, the same work-flow was followed for the Stura Bridge located between Turin and Turin-Caselle Airport. In the first phase, an in situ survey of the bridge was carried out with laser scanner and drone. The point clouds were generated and processed using the software Faro-Scene, Agisoft Metashape and CloudCompare. Subsequently, through the use of Recap, the point cloud was imported into Revit. Finally, damage was identified through CloudCompare, software capable of managing more detailed dense point clouds, and with Dynamo a user interface was created to import the damage identified, directly into Revit.

To conclude, it is possible to guess that in future it will be possible to automate different processes in order to directly implement SHM and remote sensing techniques directly in an HBIM environment, but currently there are still problems due to interoperability between software that make some phases the process still manual, time-consuming and at best cases semi-automatic.

Index:

1. SHM

- 1.1 General aspects
- 1.2 Definition
- 1.3 Operating principles and levels of identification
- 1.4 SHM and visual inspection

2. BIM

- 2.1 Introduction
- 2.2 Definition
- 2.3 Level of development Lod: Log, Lol
- 2.4 HBIM: heritage building information model
- 2.5 Scan to BIM – Mesh to BIM

3. Remote sensing

- 3.1 Introduction
- 3.2 Photogrammetry
 - 3.2.1 Definition
- 3.3 Historical concept
 - 3.3.1 Photogrammetry of the plane table
 - 3.3.2 Analog photogrammetry
 - 3.3.3 Analytical photogrammetry
 - 3.3.4 Digital photogrammetry
- 3.4 Basic concept of photogrammetry
 - 3.4.1 Detection and photogrammetric rendering
 - 3.4.2 From photographs to digital frames
- 3.5 Lidar and Laser scanner
 - 3.5.1 Principle of operation
 - 3.5.2 Land and aerial survey
- 3.6 Drones
 - 3.6.1 Anafi Work Parrot

4. RUBIK'S CUBE: mesh-to-BIM

- 4.1 Dense point cloud and mesh with Metashape
- 4.2 Eliminate distortions and separate faces with Meshmixer and Meshlab

- 4.3 Import into Revit
- 5. PIER CAP: mesh and scan to BIM
 - 5.1 Mesh to BIM
 - 5.2 Solid Family
 - 5.3 Scan to Bim
 - 5.3.1 Mesh generation in CloudCompare
 - 5.3.2 Dynamo Code
- 6. STURA BRIDGE
 - 6.1 Linee guida per la classificazione e gestione del rischio, la valutazione della sicurezza ed il monitoraggio dei ponti esistenti
 - 6.2 Laser scanner data processing with FARO SCENE
 - 6.2.1 Creating a project and importing scans
 - 6.2.2 Registration of scans
 - 6.2.3 Registration of scans
 - 6.2.4 Colouring of scans and export of point clouds
 - 6.3 UAV data processing with AGISOFT METASHAPE
 - 6.3.1 Upload and align photos to generate sparse point cloud
 - 6.3.2 Upload and align photos to generate sparse point cloud
 - 6.3.3 Build dense cloud
 - 6.4 Generating the full dense cloud with CloudCompare
 - 6.4.1 Importing, cleaning, and merging point clouds
 - 6.4.2 Span 4 mesh generation and damage detection
 - 6.4.3 Damage recognition and machine learning algorithm
 - 6.5 Scan to BIM: Recap, dynamo, Revit.
- 7. Conclusions
 - 7.1 Future developments

List of figures:

Figure 1. Similarity between the SHM and the nervous system of humans. Source: Mohamed Abdel-Basset Abdo, 2014, pp. 17	11
Figure 2. Principle and organization of a SHM system. Source: Daniel Balageas et al., 2006, pp. 14.....	14
Figure 3. Drone used for the survey	17
Figure 4. Loss of information caused by disruptions in the digital information flow. Source: Andre Borrmann et al.,2018, pp. 3.....	18
Figure 5. The concept of Building Information Modeling. Source: Andre Borrmann et al, 2018, pp. 5.	20
Figure 6. the increasing of the LOD of a precast Structural Column. Source: Jim Bedrick et al. 2020, pp. 44.23	
Figure 7. Example table of the UNI LODs - A.Pavan et al., 2017.	23
Figure 8. Mesh to BIM process. Source: Cettina Santagati et al., 2021, pp. 8.	26
Figure 9. Drone used and auxiliary devices	27
Figure 10. Stura bridge	28
Figure 11. Woodcut by Duerer The Draughtsman And The Lute. Source: History of Photogrammetry.....	30
Figure 12. Photogrammetric perspective by Hauck. Source: History of Photogrammetry.....	31
Figure 13. Nadar obtaining photography from a ballon. Source: History of Photogrammetry	32
Figure 14. Meydenbauer's principles of photogrammetry. Source: History of Photogrammetry.....	33
Figure 15. Meydenbauer's camera developed in 1872. Source: History of Photogrammetry.....	33
Figure 16. Deville's Stereo Planigraph. Source: History of Photogrammetry.....	34
Figure 17. von Orel's patent for Stereoisohypsograph. Source: History of Photogrammetry.	34
Figure 18. Hugershoff Autocartograph. Source: History of Photogrammetry.	35
Figure 19. Stereocomparator developed by Hugershoff. Source: History of Photogrammetry.	35
Figure 20. Duane Brown with the CRC-1 camera. Source: History of Photogrammetry.....	36
Figure 21. BC4 Satellite Triangulation Camera station operated by the U.S. Coast and Geodetic Survey. Source: History of Photogrammetry.	37
Figure 22. Raytheon-Wild B8 Stereomat. Source: History of Photogrammetry.	38
Figure 23. Gestalt Photo Mapper. Source: History of Photogrammetry.....	39
Figure 24. The central projection as an idealization of the grip. Source: Manzano, A., n.d Geomatica.	40
Figure 25. Two frames are needed to measure a 3D object. Source: Manzano, A., n.d Geomatica.	41
Figure 26. Intersection pattern of homologous rays. Source: Manzano, A., n.d Geomatica.....	42
Figure 27. The "restitution" in the case of nadiral holds. Source: Manzano, A., n.d Geomatica.....	42
Figure 28. Flight plan design. Source: Manzano, A., n.d Geomatica.	43
Figure 29. The internal reference system. Source: Manzano, A., n.d Geomatica.....	44
Figure 30. The model reference system. Source: Manzano, A., n.d Geomatica.	44
Figure 31. Spatial rotations. Source: Manzano, A., n.d Geomatica.....	45
Figure 32. Primary rotation. Source: Manzano, A., n.d Geomatica.....	46
Figure 33. Secondary rotation. Source: Manzano, A., n.d Geomatica.	46
Figure 34. Tertiary rotation. Source: Manzano, A., n.d Geomatica.....	47
Figure 35. From object to image. Source: Manzano, A., n.d Geomatica.....	48
Figure 36. from image to object. Source: Manzano, A., n.d Geomatica.	49
Figure 37. Digital image. Source: Lingua Andrea, Chiabrando Filiberto, Aicardi Irene, n.d. Droni P1-10	51
Figure 38. Black and white discretization. Source: Source: Manzano, A., n.d Geomatica.	51
Figure 39. Gray tones discretization. Source: Lingua Andrea, Chiabrando Filiberto, Aicardi Irene, n.d. Droni P1-10.....	52

Figure 40. True color discretization. Source: Lingua Andrea, Chiabrandò Filiberto, Aicardi Irene, n.d. Droni P1-10.....	52
Figure 41. Laser scanner principle operation. Source: Manzino, A., n.d Geomatica.	54
Figure 42. Non-intelligent procedure. Source: Manzino, A., n.d Geomatica.	54
Figure 43. Measurement system. Source: Manzino, A., n.d Geomatica.	55
Figure 44. Aerial survey. Source: Manzino, A., n.d Geomatica.	58
Figure 45. Drones Market. Source: Lingua Andrea, Chiabrandò Filiberto, Aicardi Irene, n.d. Droni P1-10....	59
Figure 46. Structure from motion. Source: Lingua Andrea, Chiabrandò Filiberto, Aicardi Irene, n.d. Droni P1-10.....	60
Figure 47. Complete kit Anafi parrot drone. Source: https://www.dronext.eu/certificazione-parrot-anafi-work	61
Figure 48. Anafi work drone. Source: https://www.dronext.eu/certificazione-parrot-anafi-work	61
Figure 49. App pix4Dcapture. Source: https://www.pix4d.com/product/pix4dcapture	62
Figure 50. App Parrot FreeFlight6. Source: https://www.parrot.com/us/apps-and-services	62
Figure 51. Rubik's cube photographs	63
Figure 52. Point alignment	64
Figure 53. Dense cloud.	65
Figure 54. Dense cloud cleaned.....	65
Figure 55. Mesh.....	66
Figure 56. Imported cube with distortions.....	67
Figure 57. Reshaped cube in Meshmixer.	67
Figure 58. Cube's face in Meshlab.....	68
Figure 59. orthophotos of the model.....	68
Figure 60. Creation of new materials with orthophotos in Revit.....	69
Figure 61. Rubik's cube imported into Revit.	69
Figure 62. Largo grosseto overpass during its useful life.	70
Figure 63. Grosseto overpass during demolition.	70
Figure 64. Dense point cloud of the pier cup in CloudCompare.....	71
Figure 65. Mesh of the pier cap in CloudCompare.....	71
Figure 66. Back view in CloudCompare	72
Figure 67. Bottom view in CloudCompare.	72
Figure 68. Left side view in CloudCompare.....	73
Figure 69. Right side view in CloudCompare.....	73
Figure 70. Top View in CloudCompare.....	73
Figure 71. "Magic selection" tool in Paint3D.....	74
Figure 72. Cleaning the background in Paint3D.....	74
Figure 73. Exporting the left side view without background.....	75
Figure 74. back view without background.....	75
Figure 75. Bottom view without background.....	76
Figure 76. Front view without background.....	76
Figure 77. Left view without background.....	76
Figure 78. Right view without background.....	77
Figure 79. Top view without background.....	77
Figure 80. Pier cup's face selected in Meshlab.	78
Figure 81. Pier cup's wireframe in Revit.....	78
Figure 82. Creation of new materials with orthophotos.....	79
Figure 83. Pier cup imported in Revit.....	79
Figure 84. Solid geometry modelled in Revit.	80
Figure 85. Solid Family with orthophotos.	81

Figure 86. Pier cap with dense point cloud in Revit.	82
Figure 87. High zoom level.	83
Figure 88. Mesh generated in CloudCompare.....	84
Figure 89. Mesh with selected points.	85
Figure 90. Import points code.	87
Figure 91. First damage interface code.	88
Figure 92. First damage interface.....	88
Figure 93. Second damage interface code.	90
Figure 94. Second damage interface.	90
Figure 95. Full dynamo code.	91
Figure 96. Pier cup with imported points.....	92
Figure 97. Location of Ponte Stura on the RA10 motorway junction.....	93
Figure 98. Sensors installed in 2018. Source: ANAS S.p.A. and SYSDEV – Monitoraggio struttrale di ponti e viadotti.....	93
Figure 99. dense point cloud of the span 1 and 2.	94
Figure 100. surveys carried out in the years 2020/21.....	94
Figure 101. Pag 1/11 “bridges census cards” ATTACHMENT A. Source: (Linee guida per la classificazione e gestione della sicurezza e il monitoraggio dei ponti esistenti, 2020).	95
Figure 102. Page 2/24 "defect cards" ATTACHMENT B. Source: (Linee guida per la classificazione e gestione della sicurezza e il monitoraggio dei ponti esistenti, 2020).	96
Figure 103. Page 31/131 "defect cards" ATTACHMENT C. Source: (Linee guida per la classificazione e gestione della sicurezza e il monitoraggio dei ponti esistenti, 2020).	97
Figure 104. Multilevel approach and relationships between levels of analysis. Source: (Linee guida per la classificazione e gestione della sicurezza e il monitoraggio dei ponti esistenti, 2020).....	98
Figure 105. Example of bending stress relationship calculated with the Normale n.8 of 1933 and the D.M. 17.01.2018. Source: (Linee guida per la classificazione e gestione della sicurezza e il monitoraggio dei ponti esistenti, 2020).	99
Figure 106. laser scanner used for the survey of the Stura bridge	100
Figure 107. Drag & Drop.....	101
Figure 108. quick view Stura_scan003	101
Figure 109. References imported.	102
Figure 110. cloud-to-cloud point errors	103
Figure 111. natural point 5/327	104
Figure 112. Natural points collimated for each scan.....	104
Figure 113. Tension of the target.	105
Figure 114. first span scans	105
Figure 115. second span scans	106
Figure 116. Third span scans	106
Figure 117. laser scanner's positions.....	106
Figure 118. 3D view stura_scan003.....	107
Figure 119. Full 3D dense cloud view	107
Figure 120. Exported scans sorted in .e57 format	108
Figure 121. Extraction of 1/30 images with VLC	109
Figure 122. photos extracted for the third span	109
Figure 123. photos extracted for the fourth span.....	110
Figure 124. photos extracted for the fifth span	110
Figure 125. sparse cloud span 3	111
Figure 126. sparse cloud span 4	112
Figure 127. sparse cloud span 5	112

Figure 128. coordinates of natural points in .txt format.....	113
Figure 129. marker 69/327.....	114
Figure 130. third span residual error.....	115
Figure 131. residual error fourth span	115
Figure 132. fifth span residual error.....	115
Figure 133. dense cloud span 3	116
Figure 134. Dense cloud span 4.....	116
Figure 135. Dense cloud span 5.....	117
Figure 136. Global Shift & Scale proposed by CloudCompare	118
Figure 137. Scans span 4, 5, 6 joined (2021)	119
Figure 138. Dense cloude from laser scanner cleaned.....	120
Figure 139. dense cloud of span 3	120
Figure 140. dense cloud of span 4	120
Figure 141. dense cloude of span 5.....	121
Figure 142. Final dense cloud	121
Figure 143. Span mesh generation 4.....	122
Figure 144. span 4 Stura bridge.....	123
Figure 145. Drone image VS mesh.....	123
Figure 146. Output of machine learning	124
Figure 147. damage detection by polyline	125
Figure 148. identification by point	125
Figure 149. identification by polyline and machine learning	126
Figure 150. span damage detection 4	126
Figure 151. Final dense cloud in Recap	127
Figure 152. Final dense cloud imported in Revit.....	127
Figure 153. spheres created in revit.....	128
Figure 154. .txt point vs polyline	129
Figure 155. corruptions imported into Revit.....	129
Figure 156. damages hypothesized in CloudCompare	131
Figure 157. generating phases in Revit	131
Figure 158. damage evolution 2021-2030-2040	132
Figure 159. damage situation hypothesized in 2040.....	132

1 SHM

1.1 General aspects

Structures and infrastructures including bridges, buildings, dams and ducts are complex engineering systems that degrade and accumulate damage progressively over their useful life. This deterioration is due to various reasons including fatigue failure caused by repetitive traffic loads, environmental effects and extreme events such as an earthquake.

As these systems age and deteriorate, their proper inspection, monitoring and maintenance becomes increasingly important.

If the damage is not detected, the structure may have a low safety margin or have maintenance problems. As a result, the integrity of the structural system has great potential for collapse, resulting in loss of life and economic damage.

In this sense, it is necessary to promptly monitor this progressive damage process to detect the occurrence of a critical state, thus avoiding collapses and catastrophes in the worst case scenario.

In Italy, the growing concern for the state of existing structures, especially after the collapse of the Morandi bridge (Genoa, 14/08/18), has motivated numerous studies on the detection of damage using various non-destructive tools.

Structural health monitoring (SHM) therefore appears to be of fundamental importance, to ensure the correct functioning of the structures, avoiding catastrophes and significant economic damage.

The main goal is to identify anomalies and deteriorations that can affect the safety of a structure, performing the same task as the human nervous system. In fact, as reported in the book "Structural Health monitoring, History, applications and future" written by Mohamed Abdel-Basset Abdo:

"The human nervous system consists of a complex collection of specialized nerves and cells and the main processing unit (brain). Nerve cells transmit signals between different parts of the body and the brain. The brain is the primary control unit for receiving and processing information, as well as giving instructions. Likewise, SHM consists of a sensory network to collect information and a unit control for data processing and decision making "

The similarity between SHM and the human nervous system is illustrated in the following image.

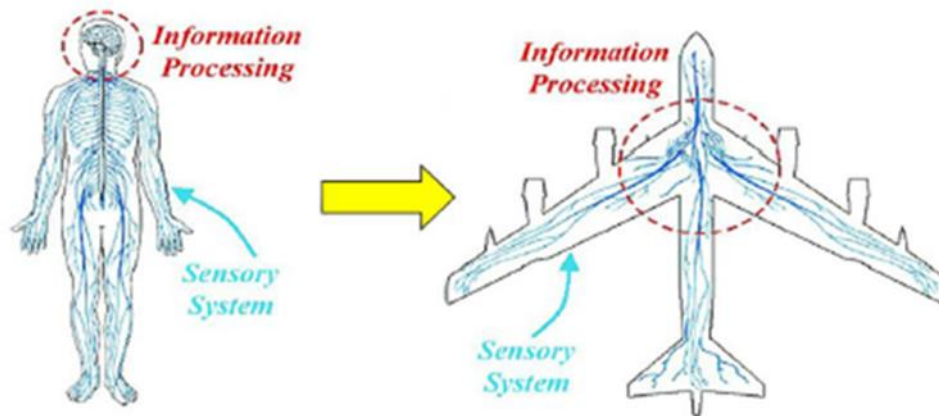


Figure 1. Similarity between the SHM and the nervous system of humans. Source: Mohamed Abdel-Basset Abdo, 2014, pp. 17

It is important to remember that in addition to damage detection, the objectives of structural monitoring systems must be extended to include above all the construction process where the structure experiences different stress states from those it will then have during its useful life.

For an existing structure, the various structural elements that constitute it are generally not known in detail, furthermore the stress state, which is radically conditioned by the construction phases, is not easy to evaluate numerically.

Conventional practice regarding structural monitoring is based on periodic human visual inspection, so inspections are generally carried out visually, collecting damage to the structure by filling in attached graphs.

Obviously, in order for this to be carried out, the damaged area must be easily accessible, and its position must be known.

However, the visual inspection is partially inadequate, in fact, in addition to being subjective it is completely ineffective for monitoring critical issues such as the progressive evolution of internal cracks not visible to the human eye.

Furthermore, the problem of current practice appears to be exacerbated by the shortage of experienced inspectors and the inevitable delay caused by a thorough structural analysis.

To solve these problems, in certain situations it is possible to use sensors in order to collect information, without carrying out destructive tests.

In recent decades, many non-destructive testing methodologies have been proposed for structural health monitoring. Some non-destructive methods are modal analysis, deformation analysis, photo elastic techniques, and ultrasonic and acoustic emissions.

With technological evolution, it has become possible to reliably and quickly transmit the structural response signal data digitally. Programs were then developed to acquire data in near real time from instrumented facilities.

Despite the use of sensors, it is complicated to manage all the information in a single model that groups together all the knowledge obtained also through visual inspections and tests.

Furthermore, after having classified the damaged structure or infrastructure, there is no universal database where to store all the damage detected in the various structures to make a comparison between the most common damages, in order to facilitate their identification and characterization.

The new guidelines for monitoring and risk of bridges, published in April 2020 by the Italian Transport Infrastructure Minister, aim to standardize damage classification methodologies.

They are composed of three parts, on the census and classification of risk, the verification of safety and the surveillance and monitoring of existing bridges and viaducts.

The classification of the risk or class of attention is based on a multilevel approach that from the simple census of the works of art to be analysed leads to the determination of a class of attention on the basis of which, in the cases provided for by the methodology itself, the verification of safety.

In this sense, the methodology for the classification of risk and the assessment of security provides for 5 levels which, proceeding from level 0 to level 5, increase in complexity, degree of detail and onerousness of the investigations.

1.2 Definition

As reported in the bridge monitoring guidelines, SHM can be described as follows:

"The instrumental monitoring methodologies (Structural Health Monitoring) are based on the installation for quite long periods of time (several months or years) or for the entire operational life of a structure, of sensor networks managed by hardware / software systems that acquire the data from the sensors and process it automatically or semi-automatically, identifying the presence of malfunctions through appropriate algorithms. "

From this definition it is clear that regardless of the installation time of the sensors, they must allow the identification of the malfunction or damage of a structure or part of it in a timely manner.

In this sense, the SHM appears to be a methodology capable of detecting structural criticalities in an early and more reliable way than conventional practices that are based primarily on visual observation.

Another definition is that reported in the book "Structural Health monitoring, written by Daniel Balageas, Claus-Peter Fritzen and Alfredo Guemes":

"Structural Health Monitoring (SHM) aims to provide, in every moment of the life of a structure, a diagnosis of the" state "of the constituent materials, of the different parts, and of the complete assembly of these constituent parts of the structure as a whole. The state of the structure must remain in the domain specified in the project, even if this can be altered by normal aging due to use, by the action of the environment and by accidental events. The complete historical database of the structure and, with the help of Usage Monitoring, it can also provide a prognosis (damage evolution, residual life, etc.). "

In other words, Structural Health Monitoring (SHM) must continuously provide a diagnosis of the condition of the elements that make up the structure and of the structure as a whole during the useful life of a structure before these produce evident manifestations. This procedure is effective if included in a process of analysing and managing data over time.

1.3 Operating principles and levels of identification

The operating principle underlying the SHM consists of two phases:

- Damage sensor detection
- Sending the signal to the acquisition system

A sensor converts stimuli or inputs such as pressure, temperature and strain into electrical signals that are passed through an interface that converts them into a binary code and transmits it to a computer for processing, as shown in the following image.

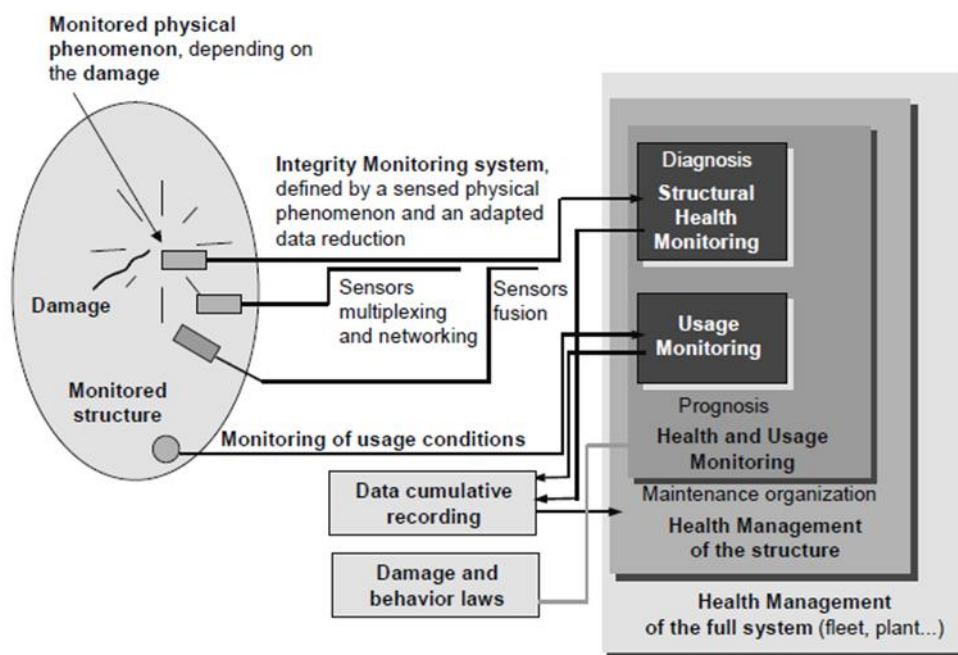


Figure 2. Principle and organization of a SHM system. Source: Daniel Balageas et al., 2006, pp. 14.

Generally, several sensors of the same type are installed in a structure that make up a network and their data can be combined with those coming from other types of sensors.

Known the information from the different families of sensors, through the knowledge of the mechanics of damage and the laws of behavior, it is possible to manage any maintenance and repair of the structure.

In other words, the ability to monitor a facility and detect damage quickly provides the ability to develop maintenance strategies by providing accurate forecasts of remaining life.

The detection of damage in structural systems involves the identification of the damage, followed by the knowledge of its location, type and severity.

In this sense, an SHM system is composed of the following levels of damage identification:

- LEVEL 1: identification of the damage, obtaining information regarding the possible existence of the damage
- LEVEL 2: knowledge of the geometric position of the damage
- LEVEL 3: type of damage, indicating its nature
- LEVEL 4: severity of the damage, estimating the extent and describing any effects
- LEVEL 5: forecast of the residual life of the structure

As the level of assessment increases, knowledge of the damage and health conditions of the structure increases, but also the economic costs and the difficulty in acquiring such information.

Consequently, the criteria for selecting the level to be achieved depend on the number, type, and cost of available and usable sensors and on the deterioration conditions of the structure.

1.4 SHM and visual inspection

One of the oldest techniques for carrying out monitoring is visual inspection used for assessing bridges in service. It consists of a collection of data concerning the structures that show damage, through the defect cards, by an expert inspector. The results of these inspections are used to make an assessment of the structure and the structural elements that compose it.

In particular, the visual inspections have the purpose of collecting information regarding the geometric and structural characteristics of the work for the description as objective as possible of the work and the surrounding environment, also detecting geometry, position and criticality of any damage present.

To document a visual inspection it is necessary to use a basic instrumentation consisting of measuring instruments to detect the geometry of the structure, photographic tools suitable for carrying out surveys especially of the areas characterized by criticality and other photogrammetric survey instruments, such as the total station and the laser scanner useful for correct documentation of the survey.

This technique has always been combined with the SHM of existing works, since in addition to being the oldest method to carry out a survey, it provides details on the geometry and degradation of the structure, albeit superficial.

An advantage of visual inspection is that the critical elements are surveyed quickly, as the operator identifies surface defects due to degradation phenomena on the basis of his knowledge. As a result, damage can be reported immediately for structures that are in critical condition and need immediate maintenance, without having to reprocess the data.

Visual inspection for monitoring existing works was found to be a technique adequate to the standards of the time for a long period of time. However, with the passage of time, the continuous growth of the design complexity and the development of know-how in the construction phases of the new structures, have allowed the construction of large-scale works such as bridges in areas that are difficult to access and remote.

In this regard, this technique if used alone has many defects. Consider a bridge that crosses a valley. Visual inspections require an examination of the extrados, the intrados and each element of the bridge in order to carry out a complete inspection of the work. In such a case, in addition to putting the operators' lives at risk to inspect the soffit of the bridge and increase the inspection time which leads to an increase in expenses.

In addition, visual inspections are able to monitor visible deterioration, such as surface cracks and wetlands. The problem is that these phenomena are easily recognizable in the most exposed elements of a bridge, but it is difficult to determine their position and severity in the difficult to access or hidden elements of a bridge.

Equally important is the aspect linked to the subjectivity of identifying damage. It appears to be completely based on the inspector's knowledge of the various types of deterioration, consequently there is always a degree of uncertainty in the survey.

With this in mind, new alternative or complementary techniques to visual inspection were sought, such as the use of drones in order to reduce costs and increase the efficiency of the process.

The use of drones to monitor bridges appears to be an economical methodology, capable of reducing the problems related to the safety of inspectors and increasing the quality of the survey, especially in areas that are inaccessible or difficult to navigate.

Currently there are numerous latest generation professional drones on the market suitable for capturing high-resolution images and videos, with cameras attached to the system with a rotational capacity of 180 °.

Consequently, it is possible to photograph the intrados of a viaduct from bottom to top with the use of a drone without reducing the image quality. In general, it is possible to photograph many critical parts of a bridge with the use of a drone.



Figure 3. Drone used for the survey

2 BIM

2.1 Introduction

In recent years, most industrial sectors are going through a transition period due to digitization. In particular, the construction industry is increasingly adopting digital tools for the design, construction and management of structures and infrastructures. However, compared to other sectors in the architecture, engineering, construction (AEC) sector, the information is not completely exchanged in digital form. A lot of information is lost for various reasons causing interruptions in the workflow, which cause delays in both design and delivery. For example, drawings made by hand or printed on paper are one of the main causes of delays in the life cycle of a project because they cannot be automatically implemented in a digital format.

Even if it were possible to automatically implement the drawings in paper format in the computer, there would be shortcomings regarding the parametric information that a digital model can contain compared to a paper drawing.

Furthermore, most of the information is lost even when you are in possession of information in digital format but on software or calculation programs that are incompatible with each other. As a result, when you need to connect and merge different digital models together, usually a lot of data is lost and must be re-created.

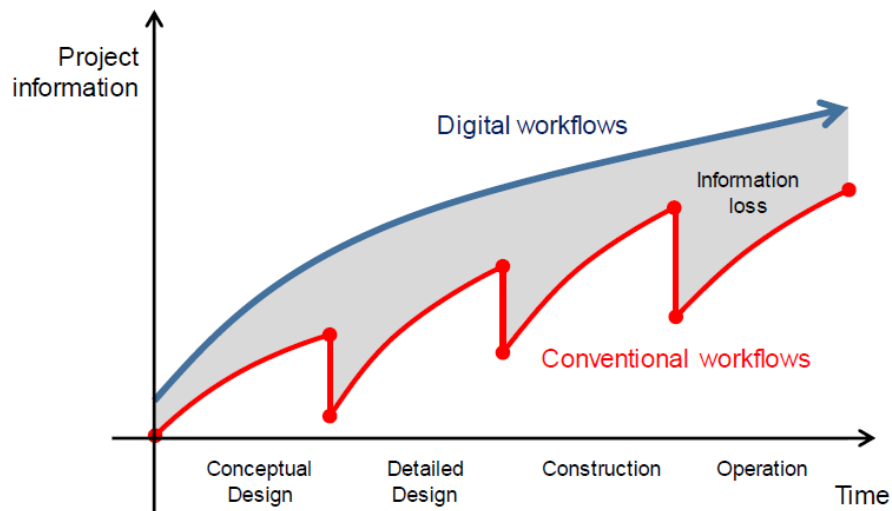


Figure 4. Loss of information caused by disruptions in the digital information flow. Source: Andre Borrmann et al., 2018, pp. 3.

With this in mind, Building Information Modeling (BIM) comes into play. A BIM model is a digital representation of a structure or infrastructure, characterized by a database of information greater than the only geometric information offered by paper drawings. In particular, the real revolution of this new way of designing lies in having in a single model both the geometric part and the parametric part linked to all the information that can be contained in a single digital model.

One of the main features of a Building information Model is its ability to transmit semantics, so all the objects that make up a model in addition to geometric information also have a meaning, that is, they are instances of types of objects such as a wall, beam or column. This makes it possible to facilitate all the design phases, in which all the subjects involved collaborate using a single reference model in a shared environment, which can be easily implemented and updated.

In this sense, using the BIM methodology, a reduction in repetitive work is achieved, through the automation of documentation and modelling processes, using a database of parametric architectural elements that can be adapted as needed.

In Bim the concept of three-dimensionality takes on a wider meaning, in fact it is possible to manage information that goes beyond 3D geometric information.

In this regard, the UNI 11337 standards have adopted this classification:

- 3D: three-dimensional modelling. Using the "traditional" 3D graphic model, the building object is displayed during all its life stages. In this way it is possible to manage the modelling effectively, reducing errors both in the execution and maintenance phases.
- 4D: time management. In this dimension, time management is planned. We could think of it as a sort of time schedule of the works associated with the model in order to reduce, or rather cancel, the possibility of interference between the processes during the life phases of the project. Times and coordination between the workers involved during the life of the building are optimized.
- 5D: economic management. the fifth "BIM-dimension" allows, through the 3D model and the 4D BIM, to have full control of costs over time. This possibility allows to obtain efficient and convenient constructions.
- 6D: life cycle and maintenance. 6D BIM allows you to optimize the management and maintenance of the building object throughout its life cycle. It provides information on the individual components: from technical systems to finishes
- 7D: sustainability. With this dimension we have the analysis of the energy consumption of the building. Analyzing the energy performance right from the project phases allows the adoption of the most suitable technical solutions to ensure lower energy consumption, guaranteeing the sustainability of the project.

2.2 Definition

Over the years, different definitions have been attributed to BIM. In particular, some define BIM as a building information model and therefore as a 3D digital model, while others interpret BIM as a building information modeling, therefore as a new methodology for designing. defines BIM as follows (NIBS, 2012): "A Building Information Model (is a digital representation of physical and functional characteristics of a facility As such it serves as a shared knowledge resource for information about a facility forming a reliable basis for decisions during its lifecycle from inception onward A basic premise of BIM is collaboration by different stakeholders at different phases of the life cycle of a facility to insert, extract, update or modify information in the BIM to support and reflect the roles of that stakeholder The BIM is a shared digital representation founded on open standards for interoperability ".

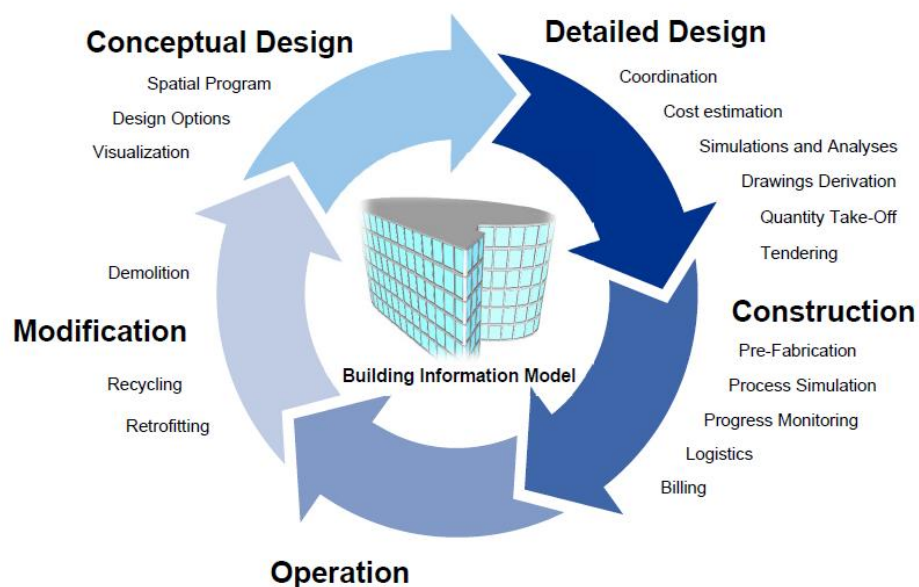


Figure 5. The concept of Building Information Modeling. Source: Andre Borrmann et al, 2018, pp. 5.

Another definition given by Autodesk is this one:

“Building Information Modelling (BIM) is the holistic process of creating and managing information for a built asset. Based on an intelligent model and enabled by a cloud platform, BIM integrates structured, multi-disciplinary data to produce a digital representation of an asset across its lifecycle, from planning and design to construction and operations.”

2.3 Level of development Lod: Log, Lol

The design of a structure or infrastructure involves the processing of paper technical drawings. In particular, these drawings can provide various information that depend on the geometric scale with which they are plotted. As the geometric scale decreases, the level of detail increases.

In the world of digital models, is not present a geometric scale on which the level of detail depends as for the drawings. However, an analogy was found to reflect the concept of geometric resolution and degree of processing.

Initially, in the digital models, the LOD was introduced, intended as a "level of detail", but in order not to emphasize the exclusively geometric aspect, the LOD was subsequently understood as a "level of development". In fact, there are important differences in that the level of detail is essentially the amount of detail included in the element, while the level of development indicates the degree to which the geometry and related alphanumeric information of a model have been designed.

Basically, the level of detail can be considered as an input for the element, while the level of development is an output.

The LOD, intended as a development level, therefore provides indications both on the LOG "geometry level" and on the LOI "information level", for example on alphanumeric information.

To manage and share these geometric and alphanumeric data, the regulations of different states have tried to create reference scales to define the degree of detail, in order to create a common approach system between professionals working in BIM.

The US BIMForum has defined six standard LODs expressed in hundreds, ranging from 100 to 500, as can be seen below:

- LOD 100

The Model Element may be graphically represented in the Model with a symbol or other generic representation, but does not satisfy the requirements for LOD 200. Information related to the Model Element (i.e. cost per square foot, tonnage of HVAC, etc.) can be derived from other Model Elements.

BIMForum Interpretation: LOD 100 elements are not geometric representations. Examples are information attached to other model elements or symbols showing the existence of a component but not its shape, size, or precise location. Any information derived from LOD 100 elements must be considered approximate.

- LOD 200

The Model Element is graphically represented within the Model as a generic system, object, or assembly with approximate quantities, size, shape, location, and orientation. Non-graphic information may also be attached to the Model Element.

BIMForum interpretation: At this LOD elements are generic placeholders. They may be recognizable as the components they represent, or they may be volumes for space reservation. Any information derived from LOD 200 elements must be considered approximate.

- LOD 300

The Model Element is graphically represented within the Model as a specific system, object or assembly in terms of quantity, size, shape, location, and orientation. Non-graphic information may also be attached to the Model Element.

BIMForum interpretation: The quantity, size, shape, location, and orientation of the element as designed can be measured directly from the model without referring to non-modeled information such as notes or dimension call-outs. The project origin is defined and the element is located accurately with respect to the project origin.

- LOD 350

The Model Element is graphically represented within the Model as a specific system, object, or assembly in terms of quantity, size, shape, location, orientation, and interfaces with other building systems. Non-graphic information may also be attached to the Model Element.

BIMForum interpretation. Parts necessary for coordination of the element with nearby or attached elements are modeled. These parts will include such items as supports and connections. The quantity, size, shape, location, and orientation of the element as designed can be measured directly from the model without referring to non-modeled information such as notes or dimension call-outs.

- LOD 400

The Model Element is graphically represented within the Model as a specific system, object or assembly in terms of size, shape, location, quantity, and orientation with detailing, fabrication, assembly, and installation information. Non-graphic information may also be attached to the Model Element.

BIMForum interpretation. An LOD 400 element is modeled at sufficient detail and accuracy for fabrication of the represented component. The quantity, size, shape, location, and orientation of the element as designed can be measured directly from the model without referring to non-modeled information such as notes or dimension call-outs.

- LOD 500 [NOT USED]

The Model Element is a field verified representation in terms of size, shape, location, quantity, and orientation. Non-graphic information may also be attached to the Model Elements.

BIMForum interpretation. Since LOD 500 relates to field verification and is not an indication of progression to a higher level of model element geometry or non-graphic information, this Specification does not define or illustrate it.

For example, It can be seen the increasing of the LOD of a precast Structural Column (concrete) from 200 to 350:

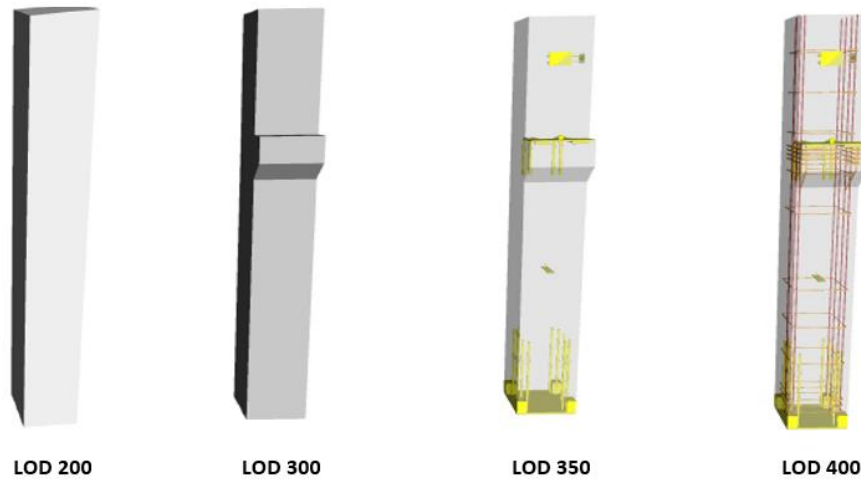


Figure 6. the increasing of the LOD of a precast Structural Column. Source: Jim Bedrick et al. 2020, pp. 44.

The Italian classification system - 11337: 2017-4 - derives from the Stanutense classification of LODs, which divides the lodges into an alphabetical scale:

- LOD A symbolic object
- LOD B generic object
- LOD C defined object
- LOD D detailed object
- LOD E specific object
- LOD F object performed
- LOD G object updated

It can be seen an example from this extract from the UNI 11337: 2017 standard

LOD A	LOD B	LOD C	LOD D	LOD E
<p>Geometria Elemento architettonico verticale o pseudoverticale rappresentato mediante un simbolo 2D.</p> <p>Oggetto Grafica 2D (linee e campiture 2D)</p> <p>Caratteristiche Posizionamento di massima</p> <p>Usi consentiti</p> <ul style="list-style-type: none"> • Semplici ingombri • Studio schemi compositivi 	<p>Geometria Solido generico per rappresentazione elemento architettonico verticale o pseudoverticale con forma, spessore e posizione approssimata</p> <p>Oggetto Solido 3D</p> <p>Caratteristiche Semplici geometrie d'ingombro</p> <p>Usi consentiti</p> <ul style="list-style-type: none"> • Studio preliminare • Computo metrico • Stima economica preliminare 	<p>Geometria Elemento architettonico (sistema e sottosistema) verticale o pseudoverticale rappresentato con ingombri calcolati secondo la normativa tecnica</p> <p>Oggetto Solido 3D strutturato</p> <p>Caratteristiche Definizione del sistema architettonico</p> <ul style="list-style-type: none"> • Spessore • Lunghezza • Larghezza • Volume • Definizione materiali • Definizione stratigrafie principali <p>Usi consentiti</p> <ul style="list-style-type: none"> • Dimensioni esecutive • Utilizzo per computo metrico estimativo • Verifica interferenze con altre discipline 	<p>Geometria Elemento architettonico verticale o pseudoverticale rappresentato mediante un solido avente dimensioni pari alle dimensioni reali. Sono modellate tutte le stratigrafie.</p> <p>Oggetto Solido 3D complesso</p> <p>Caratteristiche Dettaglio dei componenti per gruppi e senza riferimenti a singoli prodotti</p> <ul style="list-style-type: none"> • Definizione stratigrafie dettagliate • Spessori componenti • Struttura • Isolamento • Camera d'aria • Sottotondo supporto • Finitura • Dettagli costruttivi <p>Usi consentiti</p> <ul style="list-style-type: none"> • Previsioni di scheduling di cantiere 	<p>Geometria Elemento architettonico verticale o pseudoverticale rappresentato mediante un solido avente dimensioni pari alle dimensioni reali. Sono incluse tutte le stratigrafie, i dati specifici del fornitore dei materiali e le finiture.</p> <p>Oggetto Solido 3D complesso</p> <p>Caratteristiche Dettaglio dei componenti con singolo prodotto. Informazioni di montaggio</p> <p>Materiale di supporto</p> <p>Schede tecniche singoli prodotti</p> <ul style="list-style-type: none"> • Tipo finitura interna • Superficie finitura interna • Tipo finitura esterna • Superficie finitura esterna • Composizione Materiale/Componente • Presenza certificazioni • Capacità strutturale • Trasmissione vapore • Valore R • Valore U • Valore assorbimento • Trasmissione acustica <p>Usi consentiti</p> <ul style="list-style-type: none"> • Caratterizzazione • Produzione • Manutenzione

Figure 7. Example table of the UNI LODs - A.Pavan et al., 2017.

In conclusion, it is possible to state that in general the structure of the US LOD is the most used reference in the world today.

2.4 HBIM: Heritage building information model

The great majority of the historical, artistic, and cultural heritage consists of existing works. In particular, several assets are currently in an advanced state of decay and therefore require maintenance.

The main problem is that there is no detailed information on these structures since they were built by the builders of the time and have undergone several changes over the course of history that may have also changed the static operating scheme, of which there is no trace in any drawings.

In 2009, Professor Maurice Murphy, defined and introduced the concept of HBIM which stands for Historic Building Information Modelling. This term denotes a methodology aimed at historic buildings that amplifies the possibilities of the BIM method born, instead, for the design of new building organisms.

In Europe, 80% of buildings were built before 1990 and consequently there are no BIM models available.

With this in mind, the main objective of HBIM is to manage existing buildings through parametric information, to carry out a three-dimensional architectural reconstruction by incorporating the existing building into a BIM methodology.

The main advantages of having a building built within a BIM methodology are, for example, having an estimate of maintenance costs, quantification of materials, data management, asset documentation, constructive analysis of the state and execution plans.

A first difference between BIM and HBIM lies in the type of information, as in addition to the parametric 3D model, in this case we have a series of multidisciplinary and implementable information such as, for example, archive documents, documents relating to the various campaigns. detection, identification of the state of conservation and the different forms of alteration and degradation, identification of the different construction phases and stratifications that have affected the work overtime.

A further difference lies in the workflow, in fact, while to create a 3D model in a BIM software we start from a design idea that is subsequently modelled and implemented, in the HBIM the parametric information to be treated relate to an existing building. Consequently, in the HBIM it is necessary to have a graphic documentation available, which represents the real starting point for the modelling of the artifact, such as a cloud of points or drawings and historical documents.

Through the use of digital photogrammetry, laser scanners and drones it is possible to generate with post-processing, which includes the elimination of noise, point clouds and textured meshes which are then inserted into the BIM software.

These technologies are also fundamental because the buildings of the built heritage have complex geometries that are often converted into digital models following techniques that are not only inaccurate but also time-consuming. As a result, remote sensing technologies have played a key role in recent years, as in addition to saving time, they have proven extremely accurate in recording irregular building geometries.

Once the graphic documentation of the heritage is available, the HBIM methodology foresees their knowledge, management, and archiving.

This method of proceeding obviously concerns a first approach to built heritage, but in the future the as-built BIM model can be performed as an update of an existing BIM model, without having to generate a new one.

2.5 Scan to BIM – Mesh to BIM

The starting point of HBIM modelling is based on photogrammetry, laser scanner and drone techniques, as, thanks to these techniques, it is possible to document the initial condition of the built heritage, detect possible construction errors, evaluate changes over time by updating from time to time. in turn the digital model.

The use of photogrammetry allows you to measure geometries that are difficult to detect manually, such as complex geometries or structural elements that are difficult to reach by operators. Furthermore, these survey techniques are useful when the use of traditional equipment would involve a considerable expenditure in terms of time or, even, would be impossible to carry out due to the size of the site or inaccessible places, such as roofs or soffits of high decks.

Compared to traditional survey techniques, for photogrammetric survey it is necessary to make sure that all the built heritage is detected through images that are sufficiently overlapping, avoiding large jumps between the photos. Furthermore, it is necessary that the climatic conditions are adequate since the quality of the photogrammetric survey and laser scanner output depends above all on the weather and lighting conditions in situ.

After carrying out the survey and post-processing, the current literature tells us that it is possible to potentially follow two working methods, namely scan to BIM and mesh to BIM.

Scan to BIM consists of two types of modelling: direct modelling and indirect modelling.

Direct modelling can be carried out if geometric primitives referring to the historical documentation of the heritage are available. It combines the original concept of HBIM based on historical documentation, with the concept of "as-built" based instead on real data obtained from photogrammetric techniques. The work is developed by first creating a 3D model of the building based on the knowledge of the geometric primitives, generally predicting the shape and some details of the building. Subsequently, the 3D point cloud is imported into the BIM environment where the parameters are checked and refined, and an evaluation of the assets is carried out in their current state. Then the shape of the building obtained through the knowledge of geometric primitives is remodelled through the superimposition of the 3D point cloud, based instead on the real relief.

Inverse modelling is used when dealing with a built heritage whose geometric primitives are not known. In this case, the structural and architectural elements they constitute are modelled starting directly from the point cloud or from other drawings that always derive from the point cloud, such as meshes and solids. There are software or plugins, for example "as-built for Revit", which automatically and quickly recognize the elements that make up the heritage, but this software adapt to planar elements such as walls, floors and some regular structural elements such as beams, and pillars with a rectangular section, while they are unable to detect structural elements characterized by a variable section along the curvilinear abscissa.

It can be said that scan to BIM remains mainly a manual process, even if there are currently software on the market that allow direct modelling.

Mesh to BIM modelling allows to obtain from a purely graphic point of view the same results obtained with the scan to BIM procedure, but in an even more automatic and quick way. In particular, the geometric primitives obtained through direct or inverse scan to BIM modelling consist of an editable geometric shape that can be refined at a later time, while the geometric primitives obtained through mesh to BIM modelling can also have parametric information , but their geometry cannot be modified. These primitive geometries generally derive from the existing solid geometry, that is from the point cloud that can be transformed into a mesh through triangular meshes. BIM platforms, such as Revit, allow the import of mesh objects in .obj or .dxf format, however the texture associated with the mesh can be implemented but through manual processes that require a great deal of time.

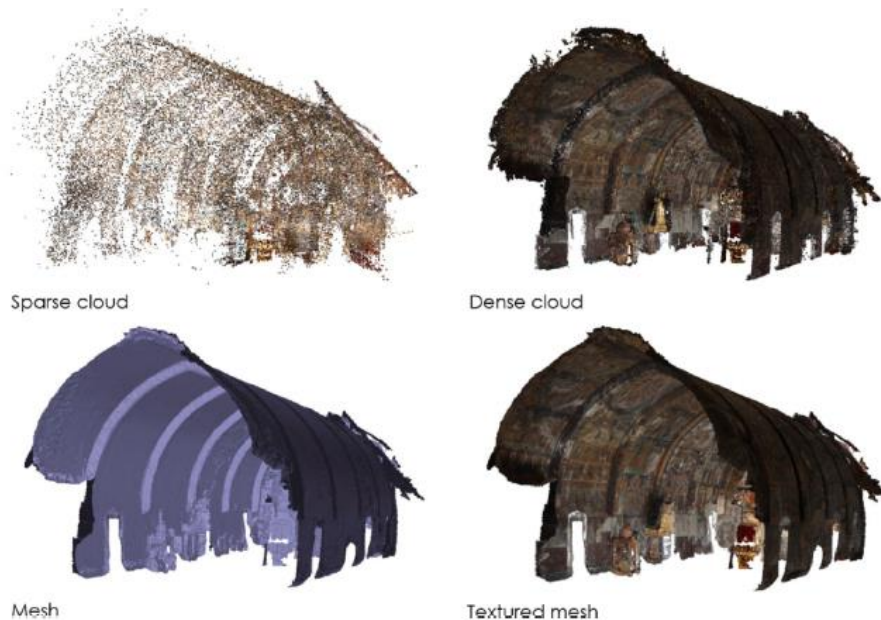


Figure 8. Mesh to BIM process. Source: Cettina Santagati et al., 2021, pp. 8.

The use of the mesh to BIM process turns out to be much more convenient in terms of timing, but it is not yet fully used also because if you wanted to export the 3D model obtained with the mesh to BIM in a calculation software, the mesh elements obtained from the point cloud of the built heritage they would not be importable.

3 Remote sensing

3.1 Introduction

Over time, there has been a need to obtain as-built models of a large part of the existing built heritage. In civil engineering, the documentation of built heritage is an aspect that has become increasingly important with the passage of time, due to various disasters that have occurred.

According to Gkoumas et al., there are more than 1234 km of road bridges with a length of over 100 m in Europe. The United States Bureau of Transportation Statistics reports 614,386 bridges in the United States at the end of 2016. Overall, there is a large number of bridges in use today. As such, bridges build and an integral part of the world's road infrastructure and are seen as the most vulnerable element of the road network. Most bridges in Western Europe were built in the aftermath of World War II in the 1950s, 1960s and 1970s, with a peak in construction activity in the 1970s. As a result, many bridges are between the ages of 40 and 50, so they are at the end of their useful life.

Consequently, many methodologies have been developed that aim to detect any type of structure and infrastructure, in order to classify the damage, verify its safety, carry out ordinary or extraordinary maintenance or possibly demolish the heritage to rebuild it. In particular, monitoring techniques that are increasingly efficient in terms of cost and time have been developed, including photogrammetry. The use of this methodology is essential to carry out a rapid monitoring not only of the structures and infrastructures, but also of the cultural heritage in order to preserve art and architecture.

The methods currently most used to survey the built heritage are LIDAR technology, photogrammetric techniques and drones equipped with an adequate camera. After collecting the data coming from the survey and carrying out the post-processing, the outputs that must be generated are usually orthophotos, point cloud and as-built 3D model.



Figure 9. Drone used and auxiliary devices



Figure 10. Stura bridge

LIDAR technology is based on the laser scanner which detects millions of points per second with high precision and rapid acquisition, generating a cloud of points, where each point is characterized by coordinates (x, y, z) and by a colour intensity (red, green and blue, RGB). The photogram techniques, on the other hand, allow to determine metrically the shape and position of objects, starting from at least two distinct frames that show the same object, based on mathematical principles such as collinearity equations. The use of drones, on the other hand, is a technique that has recently been implemented, using the same photogrammetric techniques, however, through images captured by a high-definition camera made integral with the drone.

Another useful tool to carry out a survey with a greater degree of precision and accuracy is georeferencing: it is used to connect the images and point clouds obtained with a reference coordinate system. In particular, through the use of a GPS / GNSS and marker, the detected object can be post-processed based not only on the information deriving from photogrammetric techniques, such as overlapping of pixels or overlapping point clouds by shape, but through superposition of fixed points, such as markers or natural points, and through scaling factors.

3.2 Photogrammetry

The word photogrammetry is the union of two words or "photogram", by which we do not mean a photo, and "metry", therefore the metric survey of an object at a distance. It is possible to state that photogrammetry is the technique through which it is possible to metrically determine the position and shape of objects from two or more distinct photographic sockets.

In general, through photogrammetry it is possible to obtain spatial measurements and other products derived in a geometric way from photographs.

Photography is a process that converts the real three-dimensional world into flat two-dimensional images, then through the camera you go from three to two dimensions with the consequent loss of depth. Instead, photogrammetry converts flat two-dimensional images into the real three-dimensional world. However, as information is lost in the photographic process, it is difficult to obtain all the information of the 3D world using photographs. At a minimum, we need two different photographs to reconstruct the three-dimensional world. If the photographs were taken from a perfect technical and environmental point of view, then the two photographs would be more than enough to reconstruct the three-dimensional model they represent. In reality, photographs and measurements are never carried out and are never carried out in an ideal way, consequently even the reconstruction of the three-dimensional model will prove to be imperfect. To solve this problem, it is possible to take several photographs, thus using more input data.

The fundamental principle of photogrammetry is triangulation. By taking photographs from at least two different positions, it is possible to develop the so-called "lines of sight" or "rays" that start from the gripping point and arrive at the points on the object. Through mathematical equations it is possible to produce three-dimensional coordinates of the points of interest. However, to triangulate a set of points you also need to know the position of the camera and the pointing or orientation angles for all images taken.

The outputs obtained thanks to photogrammetry are closely linked to the technical characteristics of the camera. Furthermore, in recent years, close-up photogrammetry methodologies have also been developed using cameras that can be rotated 360°, made integral with the drones.

3.2.1 Definition

As the book "Manual of Photogrammetry, ASPRS, 1980" says:

Photogrammetry is the science that allows you to obtain reliable information on physical objects and the surrounding environment through processes of recording, measuring and interpreting photographic and digital images formed by radiant electromagnetic energy and other physical phenomena.

A further definition [PE&RS, 1999] is the following:

Photogrammetry is the science that allows you to extract information from images and present them to the user effectively.

3.3 Historical concept

Currently photogrammetry is based on photographs which are digital images. In reality, photogrammetry has much more remote origins. Leonardo da Vinci in 1480 stated that:

“Perspective is nothing other than seeing an object behind a sheet of glass, smooth and fairly transparent, on the surface of which all things can be marked that are behind this glass. All things transmit their images to the eye by pyramid lines, and these pyramids are cut from this glass. The closer to the eye these intersect, the smaller the image of their cause will appear ”.

Already in 1492 Leonardo began experimenting with inventions such as the "magic lantern" (a term coined to indicate what today would be a device that acts in a very similar way to the daytime slide projector) thus working with perspective and central projections. These principles form the basis on which photogrammetry is based.

In 1525, Albrecht Dürer created a tool thanks to which it is possible to create a real perspective drawing.

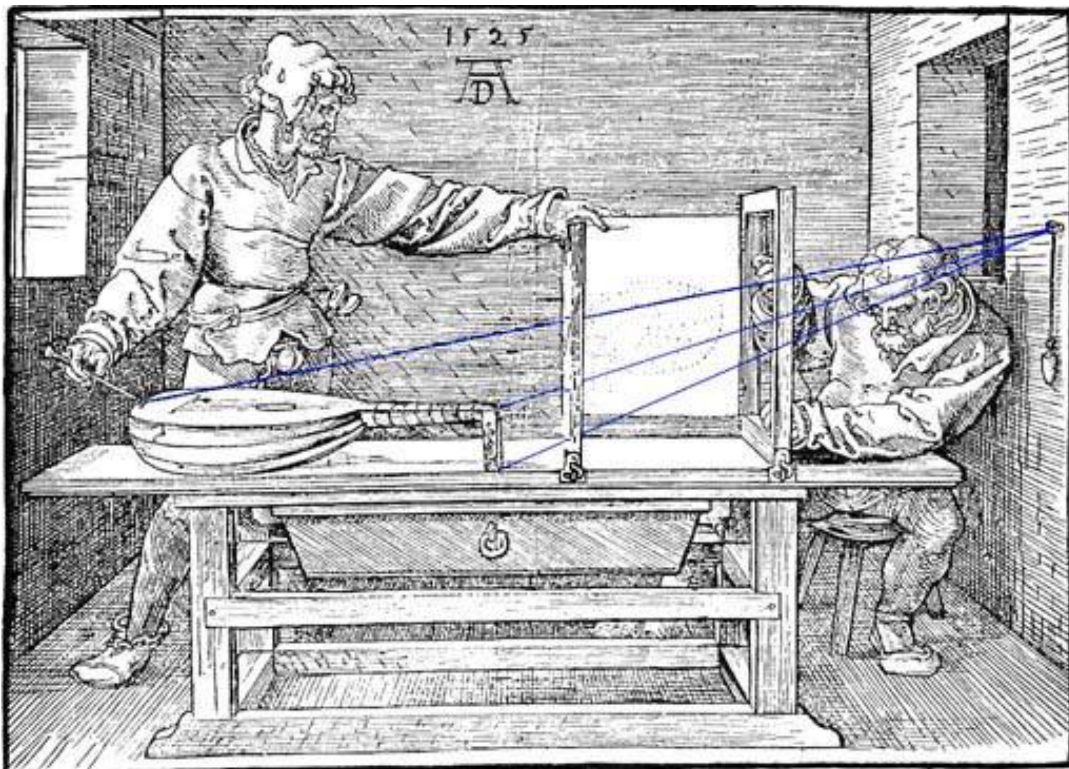


Figure 11. Woodcut by Duerer *The Draughtsman And The Lute*. Source: *History of Photogrammetry*.

Johan Heinrich Lambert, in 1759 in a treatise "perspectiva Liber" developed, using spatial resection, the mathematical principles of a perspective image using space resection to find a point in space from which a picture is made, while R. Sturm and Guido Hauck in 1883 they first found a relationship between projective geometry and photogrammetry.

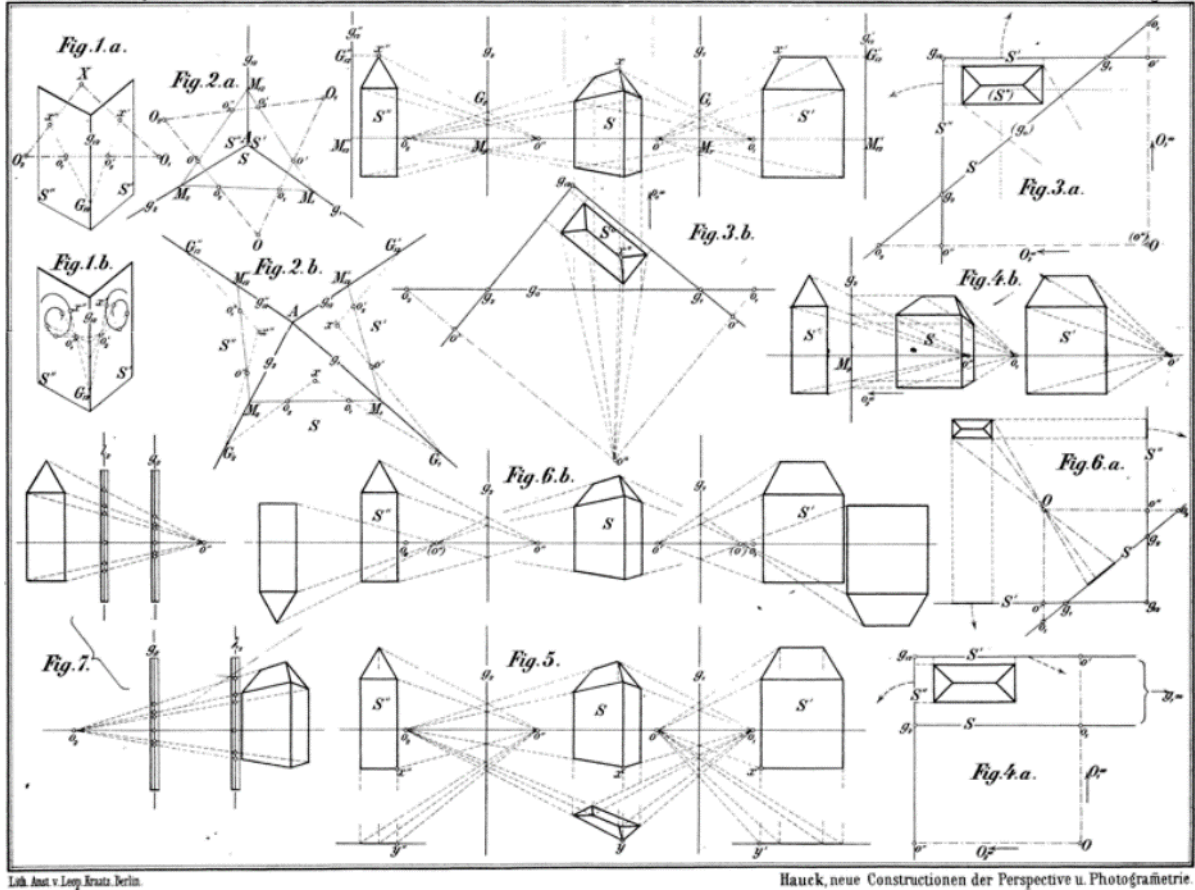


Figure 12. Photogrammetric perspective by Hauck. Source: History of Photogrammetry.

In general, the real developments of photogrammetry begin in 1850 and in particular it is possible to group all the evolution of photogrammetry into 4 periods of about 50 years:

- Photogrammetry of the flat panel, from 1850 to 1900,
- Analog photogrammetry, from 1900 to 1960,
- Analytical photogrammetry, from 1960 to today,
- Digital photogrammetry, which is a new methodology under development.

3.3.1 Photogrammetry of the plane table

Amie Laussedat, who is considered the father of photogrammetry, developed the first photogrammetry methods for terrestrial and aerial cartography, first taking pictures from kites, then he moved in a hot air balloon in order to make topographic maps. In 1855, Nadar (gaspar felix Tournachonn) used a hot air balloon flying 80 meters high to get the first aerial photograph.



Figure 13. Nadar obtaining photography from a ballon. Source: History of Photogrammetry

The photogrammetry of the plane table is an extension of the conventional relief plane of the table [Konecny, 1985]. Each exposure station was determined by resection and traced on the table top. The photos exhibited were oriented on the table top and the directions for the different objects were transferred to the map sheets.

The first person to use the term photogrammetry was Dr. Albrecht Meydenbauer, in fact he founded the Prussian institute of royal photogrammetry. Meydenbauer is known for making several architectural surveys using photogrammetry, designing his first wide-angle lens camera used for mapping.

His camera had the following characteristics:

- Robust body
- Permanently mounted lens
- Levels to level the camera
- Device for aligning the camera axis
- Definition of the image plane from a frame with signs of trust for the coordinated axes

3.3.2 Analog photogrammetry:

Two important developments were necessary to move to analog photogrammetry: stereoscopy and the airplane.

The first aerial photograph captured from an aircraft for mapping purposes was done by Captain Cesare Tardivo for a 1: 4,000 mosaic from Benghazi, Italy.

In 1896, Edouard Deville, a Canadian surveyor, invented the first stereoscopic chart called a stereo-planograph. Although this tool was a first attempt for the stereographic superimposition of photos, it was not used much due to its complexity.

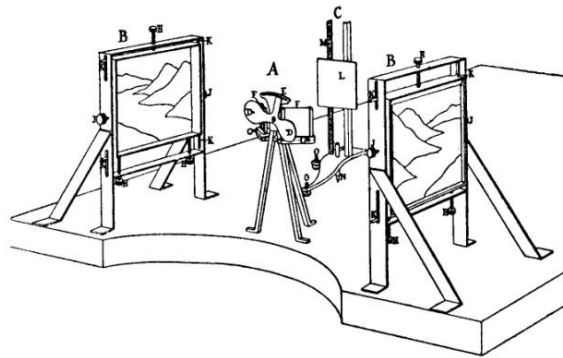


Figure 16. Deville's Stereo Planigraph. Source: History of Photogrammetry.

In 1908, in Germany, Eduard von Orel developed the first stereo autograph, which was very important because its construction principles made terrestrial photogrammetry practicable in mountainous areas, allowing the operator to directly trace contour lines. However, this plotter had the flaw that it could not be adapted to aerial photogrammetry.

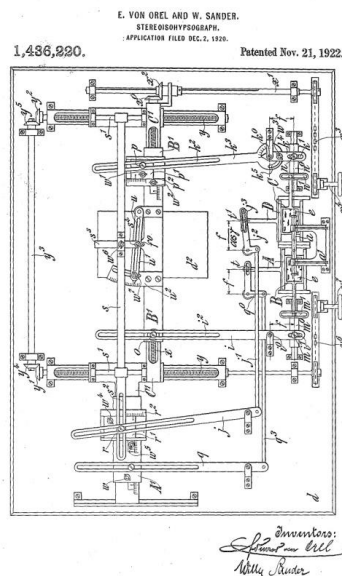


Figure 17. von Orel's patent for Stereoisohypsograph. Source: History of Photogrammetry.

In 1921, Professor Reinhard Hegershoff contributed a lot to the development of the survey and mapping instrumentation. He created the first analog plotter (Hegershoff Autocartograph) which was a very complex mechanical plotter incorporating two photogoniometers. In addition, he also developed an aerial camera using glass plates to attach the camera to the side of the plane.

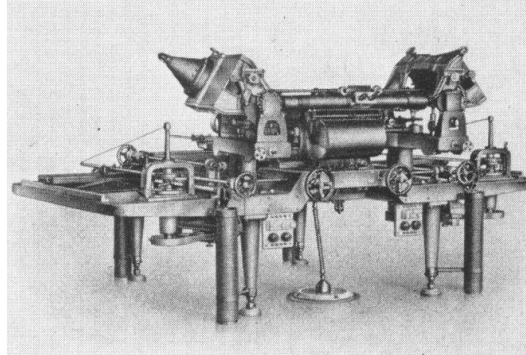


Figure 18. Hegershoff Autocartograph. Source: History of Photogrammetry.

One of the unique tools developed by Hegershoff was the stereo-comparator, it utilized a single light source and single measuring mark. The photographs were moved in X and Y tracks for the measurement process. This design was the predecessor to the Zeiss PSK stereo-comparator. These are just a few of the developments attributed to Reinhard Hegershoff. Later in life we worked with Zeiss Works in developing other photogrammetric equipment.

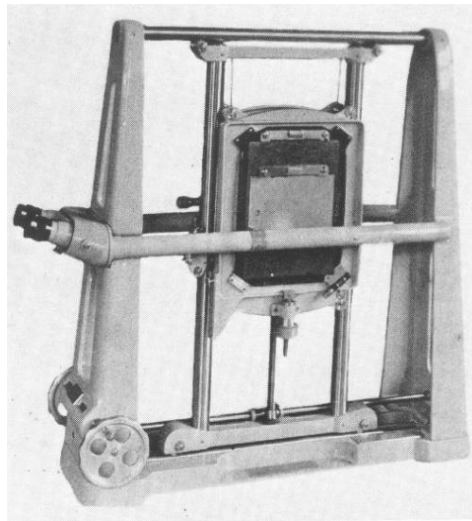


Figure 19. Stereocomparator developed by Hegershoff. Source: History of Photogrammetry.

As for the photogrammetry industry, one of the first leading companies was Zeiss. The reason why it dominated the market at the beginning of the twentieth century is due to the fact that many of the early pioneers of photogrammetry were employees of the company. Some of the innovative instruments at the time of the Zeiss are:

- 1901, Zeiss' first photogrammetric instrument, the Stereo-comparator, made using the design by Pulfrich
- 1921, Stereo-planigraph C1 produced
- 1930, C4 went into production

Later, in 1988, Kern and Wild merged to form a new company, Leica. In 2001, Leica was able to offer customers Lidar scanning systems and software for remote image detection and processing.

3.3.3 Analytical photogrammetry

The principles on which analytical photogrammetry is based are based on the inventions made to develop analog photogrammetry.

In this period numerous advances were made: a semi-analytical approach was found for analytical control where the orientation of the photos is done in a semi-graphic way, a series of solutions for camera calibration, space resection, external and internal orientation were developed, relative and absolute, extension of analytical control.

The real photogrammetric developments were carried out thanks to the invention of the computer (by Zure in Germany in 1941 and independently by Aitken in the United States in 1943).

In 1953, Dr. Hellmut Schmid developed the principles of modern multi-station analysis using matrix notation and his work included a correct least squares solution, a simultaneous solution of any number of photographs, and a comprehensive study of the propagation of mistakes.

G. H. Shut, from the National Research Council in Canada, used the concept of coplanarity for analytical triangulation. He recognized the limitations of the computer at the time and therefore developed a cantilever adjustment strip obtained by first calculating the relative orientation of each camera and after orienting each photograph along the strip, the strip's coordinates were adapted to ground control. .

In 1951, Duane Brown joined Schmid to work in the ballistics research laboratory to use ballistic cameras to determine the orbital path of the satellites. Subsequently, he developed new approaches for camera calibration and for the mathematical developments of beam adjustment, significant developments because it was a simultaneous solution of the camera's external orientation parameters, the coordinates of the survey points along the internal orientation and the systematic distortion of the radial lens.

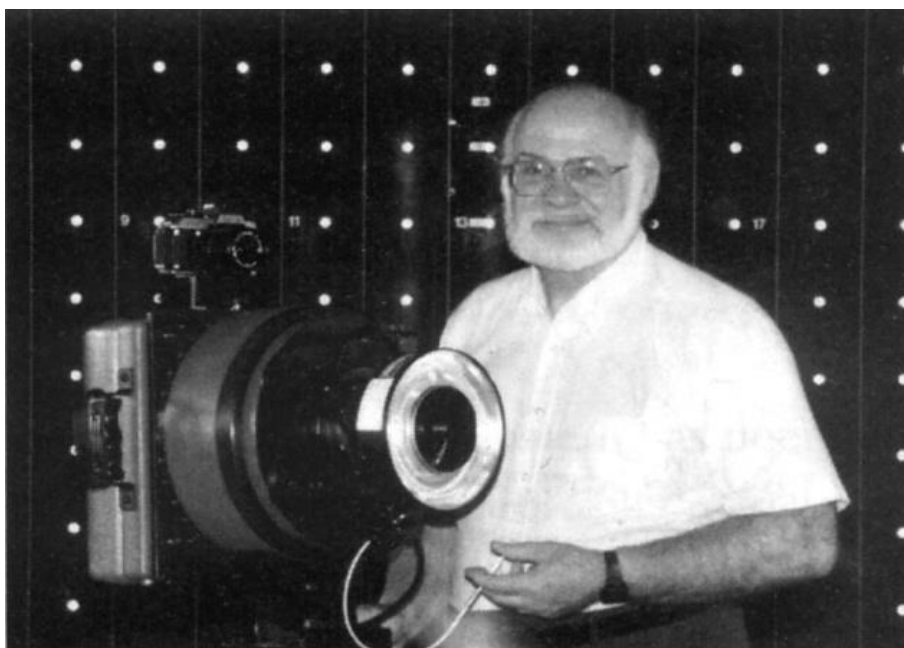


Figure 20. Duane Brown with the CRC-1 camera. Source: History of Photogrammetry

Brown, after joining the Instrument Corporation of Florida, continued to refine the package tuning for large photogrammetric blocks to include autotuning, which is important for improving the accuracy and reliability of photogrammetric tuning. Using the modified ballistic camera, he was able to apply his principles to the radio telescope survey in Greenbank, WN, reaching a degree of accuracy around the 1: 50000 level, so about 2mm.



Figure 21. BC4 Satellite Triangulation Camera station operated by the U.S. Coast and Geodetic Survey. Source: History of Photogrammetry.

Another big step Duane Brown took while at GIS was to take photogrammetry from an instrument that required highly skilled technicians to measure a system that could be directly used by customers. The new software was called STARS (Simultaneous Triangulation and Resection Software). Through this software, which later became a system, given that other software such as CRC-1 and Autaset-1 were added, it was possible to break the level of the micrometre in photogrammetric precision, achieving an accuracy better than 1: 1000000.

In 1957, Vilho Helava developed the analytical plotter used as a servo instead of the previous mechanical or optical construction, so the computer was now not only used to guide the instrument around the stereo model, but also to digitally transform the coordinates between the image and the map.

3.3.4 Digital photogrammetry

One of the pioneers of digital photogrammetry was Gilbert Louis Hobrough, who contributed to the development of photogrammetry by inventing the electronic printer and building an aerial profile recorder.

This instrument allowed the measurement of the distance from an aircraft to the ground with about one foot of precision, through the use of radar and a reference barometer with the same precision.

Hobrough demonstrated his concept of image correlation on a Kelsh plotter, but due to the technology of the time, the correlation process was analog, thus using hardware to compare the gray levels of the images. This development led to the creation of the Raytheon-Wild B8 stereomat, although the tool was unsuccessful as it was too innovative to use for the photogrammetric professionals of the time.

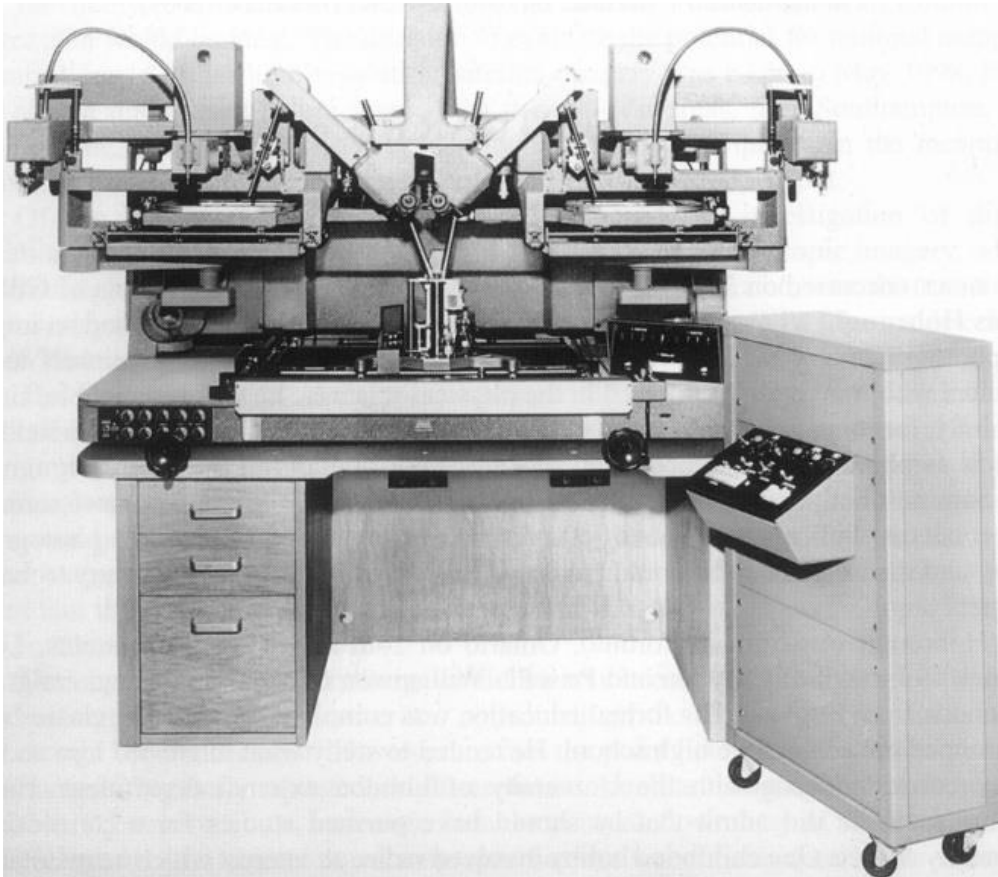


Figure 22. Raytheon-Wild B8 Stereomat. Source: History of Photogrammetry.

Hobrough later moved to California where he worked with George Wood on Automatic Stereoscopic Recording (ARES). The purpose of this tool was to correlate the resolution of the photographs taken for the survey with the high-precision photographs taken for the survey, in order to allow a more precise measurement of the changing conditions of the ground.

After moving to Canada in 1967, Hobrough developed the Gestalt Photo Mapper (GPM), which is an automated orthophotography that used stereo image correlation and consisted of a printer that was generally located in a darkroom, with a scanner system, correlator, and computer and an input and output device.



Figure 23. Gestalt Photo Mapper. Source: History of Photogrammetry.

In 1979, Uki Helava played an important role in the development of digital photogrammetry, first as a research scientist at Bendix and then at Helava associates, Inc, which later became a subsidiary of General Dynamics in 1986, making a huge contribution to the development of photogrammetric stations for the defense mapping agency (now called NIMA).

In 1997, Helava Associates formed a joint partnership with Leica Geosystem to form LH Systems, which has now joined the Leica Geosystems.

3.4 Basic concept of photogrammetry

Photogrammetry is a three-dimensional metric survey technique, that is, it is a technique that allows you to metrically determine the position and shape of an object starting from 2 and more photometric taken from distinct points in space, so you cannot start from multiple photos taken in the same point (except if the object is in motion).

In reality, we don't use photographs but frames, as we want the result to be metric. In fact, in them it is assumed that the grip geometry corresponds to the central projection, that is, the angles of entry to the camera are equal to the angles starting from the main camera and going to impress the image.

The system is metric from the angular point of view (there are no angular distortions) but not in the lengths.

Photogrammetry is based on the so-called Frames:

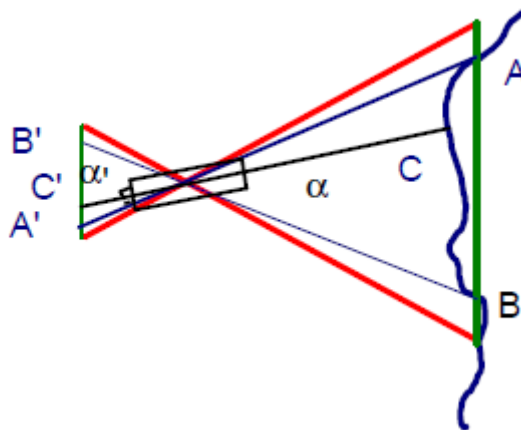


Figure 24. The central projection as an idealization of the grip. Source: Manzino, A., n.d Geomatica.

These are not simple photographs but are metric frames, i.e. the angle entering and the angle leaving the camera are the same. So, we talk about frame when $\alpha = \alpha'$, in a photograph this can happen since there can be angular distortions and therefore $\alpha \neq \alpha'$.

It is not possible to measure the image with the ruler, in fact, even if the angles are maintained, objects have points that are closer (they have a larger scale) and points that are more distant (smaller scale) from the gripping point.

If you are interested in having a cartography and therefore it is projected on the tangent plane (the approximation is good in the plan within 15 cm), in fact the points are projected in the frame, e.g. A in A'' and E in E''. But if you build the cartography in the field with a scale meter, instead of A'' if you would have A'. Therefore, except at the nadiral point, there are aberrations in the planimetric position. In this sense, we can speak of the average scale of the frame, in which we consider an average plane, and we have:

$$\frac{s}{B} = \frac{c}{H} = \frac{1}{n}$$

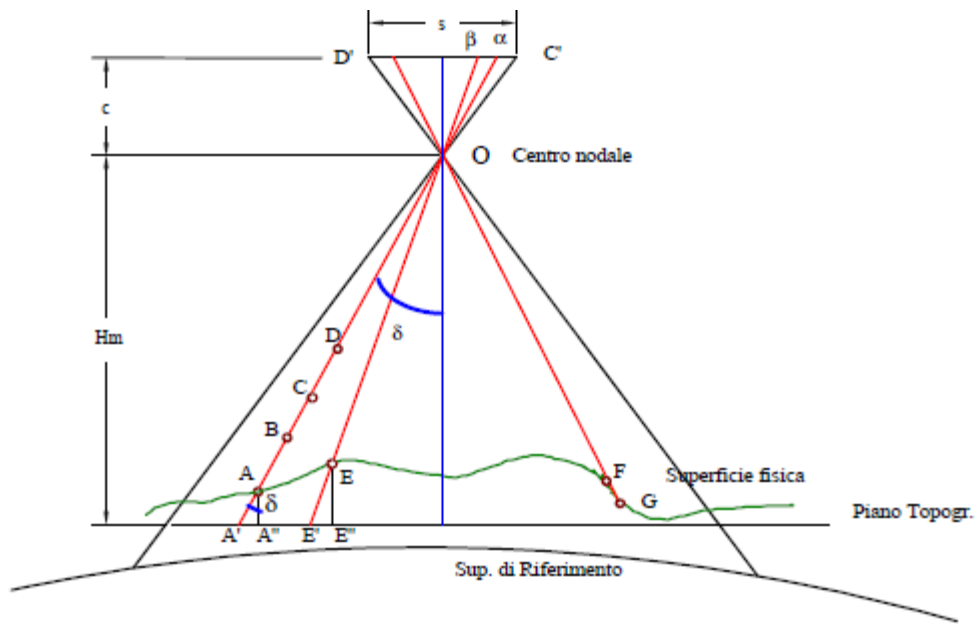


Figure 25. Two frames are needed to measure a 3D object. Source: Manzino, A., n.d Geomatica.

Where is it:

- s = frame size (size in the photo)
- B = hugging the ground (real size)
- c = focal distance
- H = average relative altitude of the flight
- n = Average scale factor
- s / B = average scale

The average frame scale is also the ratio between focal length and average altitude of the flight. However, we speak of "medium" scale because the closest points are on a larger scale and the farthest on a smaller scale.

To carry out a photogrammetric capture of an object, at least two frames are required that show the same portion of the object.

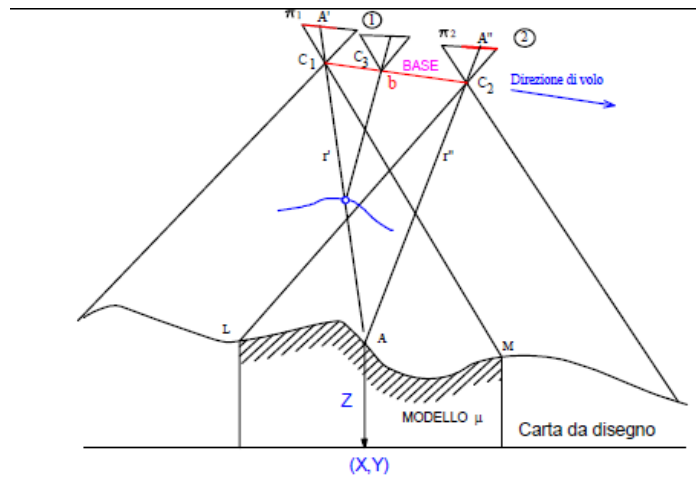


Figure 26. Intersection pattern of homologous rays. Source: Manzino, A., n.d Geomatica.

Imagine taking 2 frames from 2 distinct points that take up the same portion of land and therefore have a part in common. Note the position of the gripping points C1 and C2 and the angles of arrangement of the chambers 1 and 2 at the time of gripping, it is possible to derive the equation of the straight-line r' and r'' . From their intersection, the coordinates of the point under examination are obtained.

In particular, at the time of taking, in the frame you can see the points A' and a'' , said homologous points from the same point A.

The system consists of 2 bodies, each having 6 degrees of freedom, and therefore 12 information is needed. The position of the aircraft or tripod is obtained with the GPS, while the angular position is obtained with the help of inertial instruments. There are cases where it is not interesting to know the absolute position of the object but only the scale, such as an object that deforms.

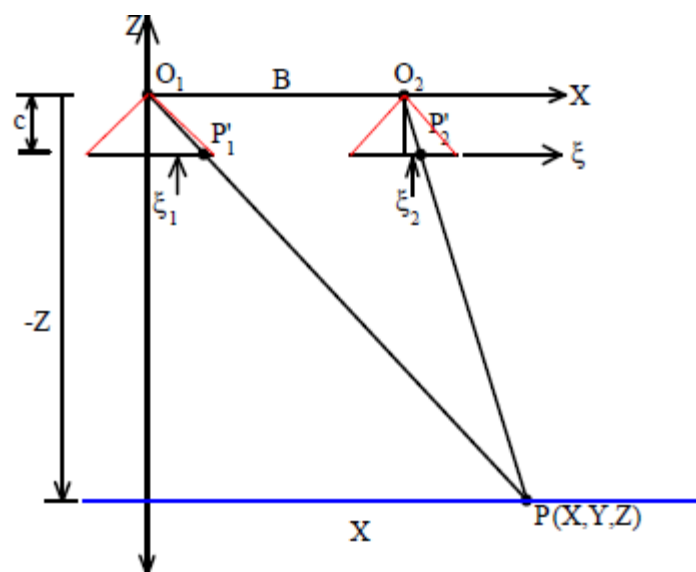


Figure 27. The "restitution" in the case of nadiral holds. Source: Manzino, A., n.d Geomatica.

It is noted that, by moving along the grip base C1 and C2 (the aircraft's route) while maintaining the same orientation as the camera, the homologous rays can be intersected and the object can be reconstructed, only with a smaller scale thus having only 6 degrees of freedom.

The conversion takes place through the restitutor which is a system that allows you to start from 2 frames. These, digitally, are two matrices having a certain number of rows and columns in which the elements are the pixels that can be in grayscale or in RGB colour tones.

From these matrices, the restitutor returns the three-dimensionality of the object. This happens as long as you enter some information called external orientation and internal orientation.

The external orientation implies the knowledge of the position of the two frames in space, while the internal orientation implies the knowledge of the characteristics of the camera and therefore the geometric reconstruction of the interior of the photogrammetric camera.

The frames are reminiscent of pyramids that have the tip pointing downwards. This means that the objects furthest to the right end up on the left in the image and vice versa, so there is an inversion with respect to the real arrangement in the ground

If you want to print a digital frame and have the position reset, an identical camera must be introduced under the image, having the same trim angles, with the gripping surface facing downwards and pointing upwards. Thus, the frame is reversed, and the positions are also restored in the image.

3.4.1 Detection and photogrammetric rendering

When it is necessary to reconstruct the 3D model of an object, to be sure that each point of the object is captured by at least 2 frames, it is necessary to be sure that the entire territory is covered with frames.

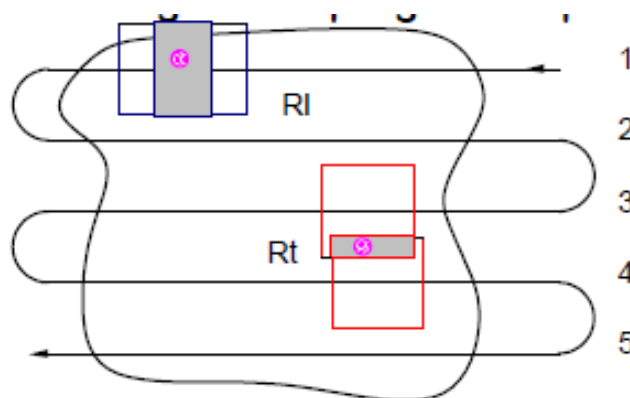


Figure 28. Flight plan design. Source: Manzano, A., n.d Geomatica.

Assuming for simplicity that the photogrammetric images are square, it is necessary that the overlap between the frames, along the direction of flight or catch, is at least 50%. In doing so, these overlap and cover everything.

Generally, an object or a ground, for example, is not flat and, depending on the scale, you can cover a certain area and find the missing part because it has a different height.

Therefore, a coverage of 50% is not adopted since it is a theoretical value valid for flat terrain and with the same trim angle (there are no skids). Therefore, the transversal coverage between frames must be between 60% and 80%, while for the longitudinal coverage the overlap must be between 10% and 20%.

To construct the straight lines, that is the homologous rays, which pass from the grip points to the homologous points, it is necessary to define a single reference system in which to compute them.

The internal orientation reference system of the machine cannot be used, i.e., the one defined in the pixel matrix and origin in the main point, since it is a plane reference system.

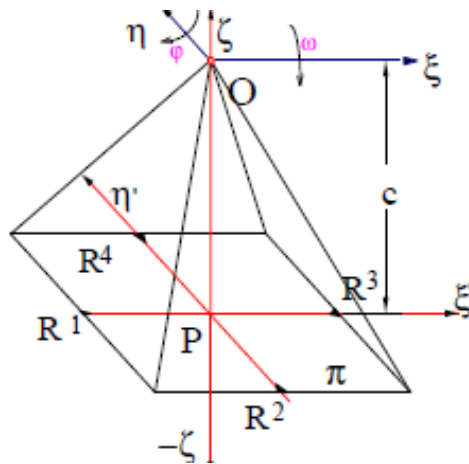


Figure 29. The internal reference system. Source: Manzino, A., n.d Geomatica.

In reality, to construct the straight lines and intersect them, it is necessary to use the East-North-Elevation ENQ reference system and in it know the coordinates of the grip points O_1 and O_2 , the attitude of Cameras 1 and 2 and the coordinates of the homologous points P_1 and P_2 .

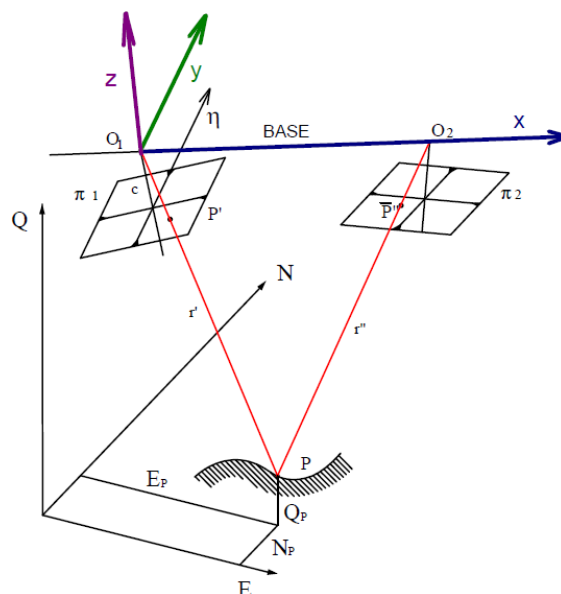


Figure 30. The model reference system. Source: Manzino, A., n.d Geomatica.

The problem is that the coordinates of the homologous points are given in pixels but affect the ENQ coordinates. In particular, it is necessary to rotate the reference system with respect to the known angles of the plane of the frame and a translation linked to the origin of the gripping points O1 and O2

The roto-translation in the plane is based on a rotation matrix consisting of the director cosines of the local reference system.

$$\begin{Bmatrix} X \\ Y \end{Bmatrix} = [R] \begin{Bmatrix} x \\ y \end{Bmatrix} = \begin{bmatrix} \cos xX & \cos yX \\ \cos xY & \cos yY \end{bmatrix} \begin{pmatrix} x \\ y \end{pmatrix} = \begin{bmatrix} \cos \alpha & -\sin \alpha \\ \sin \alpha & \cos \alpha \end{bmatrix} \begin{pmatrix} x \\ y \end{pmatrix} = \begin{bmatrix} i \\ j \end{bmatrix} \begin{pmatrix} x \\ y \end{pmatrix}$$

In space, the operation is more complex because there are more director cosines.

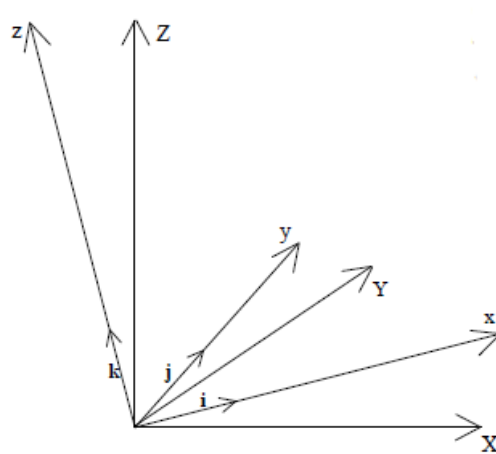


Figure 31. Spatial rotations. Source: Manzino, A., n.d Geomatica.

$$\begin{Bmatrix} X \\ Y \\ Z \end{Bmatrix} = \begin{bmatrix} \cos(xX) & \cos(yX) & \cos(zX) \\ \cos(xY) & \cos(yY) & \cos(zY) \\ \cos(xZ) & \cos(yZ) & \cos(zZ) \end{bmatrix} \begin{pmatrix} x \\ y \\ z \end{pmatrix}$$

To correctly derive the rotation matrix as a function of the attitude angles, it is necessary to give these rotations with a certain order.

Primary rotation:

A rotation ω around the x axis is initially applied. In this way, the $X = X_\omega$ axis remains unchanged while y and z vary. Therefore, the rotation matrix is a 3 x 3 matrix having in the first row and column the vector (1 0 0).

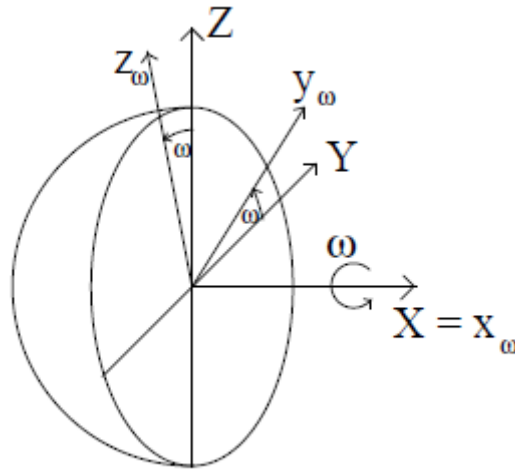


Figure 32. Primary rotation. Source: Manzano, A., n.d Geomatica.

$$\{x\} = \begin{bmatrix} 1 & 0 & 0 \\ 0 & \cos\omega & -\sin\omega \\ 0 & \sin\omega & \cos\omega \end{bmatrix} \begin{pmatrix} x_\omega \\ y_\omega \\ z_\omega \end{pmatrix} = [R_\omega]\{x_\omega\}$$

Secondary rotation:

subsequently, it rotates by an angle ϕ but not around the original Y axis, but on the new yw axis.

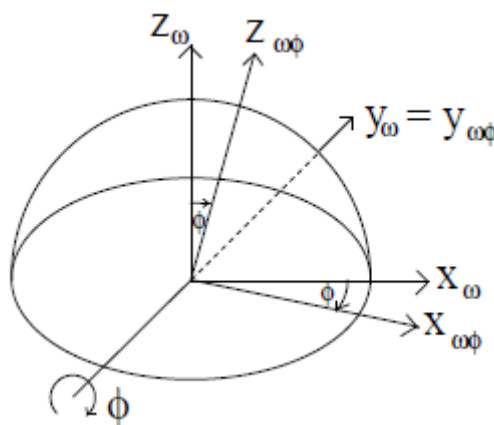


Figure 33. Secondary rotation. Source: Manzano, A., n.d Geomatica.

$$\{x_\omega\} = \begin{bmatrix} \cos\phi & 0 & \sin\phi \\ 0 & 1 & 0 \\ -\sin\phi & 0 & \cos\phi \end{bmatrix} \begin{pmatrix} x_{\omega\phi} \\ y_{\omega\phi} \\ z_{\omega\phi} \end{pmatrix} = [R_{\omega\phi}]\{x_{\omega\phi}\}$$

Tertiary rotation:

a rotation around the z axis is applied, which had been given a rotation of both ω and ϕ .

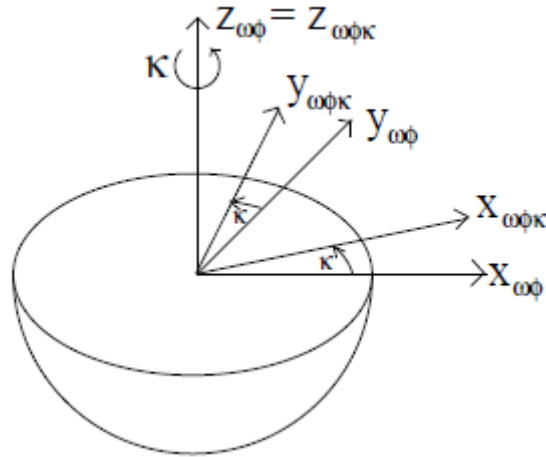


Figure 34. Tertiary rotation. Source: Manzino, A., n.d Geomatica.

$$\{x_{\omega\phi}\} = \begin{bmatrix} \cos\kappa & -\sin\kappa & 0 \\ \sin\kappa & \cos\kappa & 0 \\ 0 & 0 & 1 \end{bmatrix} \begin{pmatrix} x_{\omega\phi\kappa} \\ y_{\omega\phi\kappa} \\ z_{\omega\phi} \end{pmatrix} = [R_{\omega\phi\kappa}]\{x_{\omega\phi\kappa}\}$$

Thus, when the rotation matrix is obtained not as a function of the director cosines but of the angles ϕ , ω and κ , it is necessary to put the rotations in a certain order, otherwise the result changes.

$$\begin{aligned} [R] &= [R_{\omega}][R_{\phi}][R_{\kappa}] \\ &= \begin{bmatrix} \cos\phi\cos\kappa & -\cos\phi\sin\kappa & \sin\phi \\ \cos\omega\sin\kappa + \sin\omega\sin\phi\cos\kappa & \cos\omega\cos\kappa - \sin\omega\sin\phi\sin\kappa & -\sin\omega\cos\phi \\ \sin\omega\sin\kappa - \cos\omega\sin\phi\cos\kappa & \sin\omega\cos\kappa + \cos\omega\sin\phi\sin\kappa & \cos\omega\cos\phi \end{bmatrix} \end{aligned}$$

So, to simplify the matrix, it is possible to name its elements.

$$[R] = \begin{bmatrix} r_{11} & r_{12} & r_{13} \\ r_{21} & r_{22} & r_{23} \\ r_{31} & r_{32} & r_{33} \end{bmatrix}$$

In general, the internal axis system (ξ ; η) is known of the point P', while the main point does not lie on the origin of the matrix but has coordinates (ξ_0 ; η_0).

Furthermore, the plane of the frame is oriented according to the angles ω , ϕ and κ . It starts from the X'Y'Z' reference system having the same origin as the ground reference system, but parallel to the grip plane.

By projecting the point P' into P in the X'Y'Z' system, similitude equations can be established.

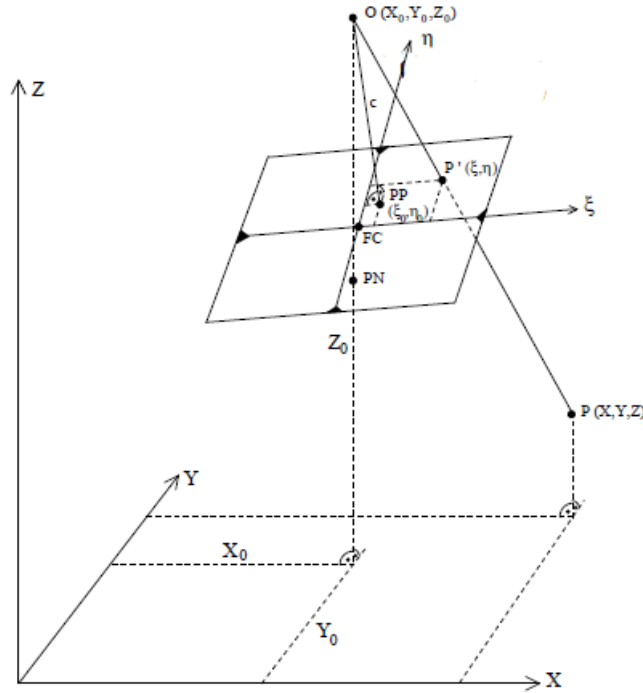


Figure 35. From object to image. Source: Manzano, A., n.d Geomatica.

Along ξ :

$$\frac{\xi - \xi_0}{c} = \frac{x' - x'_0}{z'_0 - z'} \rightarrow \xi = \xi_0 + c \frac{x' - x'_0}{z'_0 - z'}$$

Along η :

$$\frac{\eta - \eta_0}{c} = \frac{y' - y'_0}{z'_0 - z'} \rightarrow \eta = \eta_0 + c \frac{y' - y'_0}{z'_0 - z'}$$

Coordinate differences, i.e., vectors, appear in the terms on the right. These are evaluated in the X'Y'Z' reference system and, to indicate them in the XYZ reference system, a rotation is used.

$$\begin{pmatrix} x - x_0 \\ y - y_0 \\ z - z_0 \end{pmatrix} = [R] \begin{pmatrix} x' - x'_0 \\ y' - y'_0 \\ z' - z'_0 \end{pmatrix}$$

It is possible to obtain the vector on the right by multiplying the transpose of the rotation matrix.

$$\begin{pmatrix} x' - x'_0 \\ y' - y'_0 \\ z' - z'_0 \end{pmatrix} = [R]^T \begin{pmatrix} x - x_0 \\ y - y_0 \\ z - z_0 \end{pmatrix}$$

At this point I am going to make the various replacements within the similarity matrix.

$$\xi = \xi_0 - c \frac{r_{11}(x - x_0) + r_{21}(y - y_0) + r_{31}(z - z_0)}{r_{13}(x - x_0) + r_{23}(y - y_0) + r_{33}(z - z_0)} = \xi_0 - c \frac{Z_x}{N}$$

$$\eta = \eta_0 - c \frac{r_{12}(x - x_0) + r_{22}(y - y_0) + r_{32}(z - z_0)}{r_{13}(x - x_0) + r_{23}(y - y_0) + r_{33}(z - z_0)} = \eta_0 - c \frac{Z_y}{N}$$

3.4.2 From photographs to digital frames

The photographs with respect to the frames are images in which distortions are made, since they are obtained using simple cameras that are not metrics that from the angular point of view

There are three types of distortion:

- Radial distortion (positive or negative), described by three parameters, is a pincushion distortion and is the most frequent.
- Tangential distortion, described by three parameters
- Refinement bias, described by two parameters

These distortions must be determined.

In particular, the collinearity equations are no longer representative of the model. But we introduce corrective terms $\Delta\xi$ and $\Delta\eta$ which represent the contributions of the distortions and there are 8 more parameters to calculate.

$$\xi = \xi_0 - c \frac{N_x}{N_z} + \Delta\xi$$
$$\eta = \eta_0 - c \frac{N_y}{N_z} + \Delta\eta$$

In this case, it is necessary to determine both the internal orientation and the distortion parameters, starting from some support points on the ground of known coordinates. This process is called indirect calibration: after obtaining the distortions, if the image is digital, it is counter-deformed by removing the deformation and the frame is obtained.

The digital image consists of a two-dimensional matrix, the elements of which are called pixels. This matrix contains numbers, which provide radiometric information. Then a geometric discretization is performed (division into pixels) and a radiometric discretization.

In this sense, an object measurement is already made, since the geometry is discretized in two dimensions and the third dimension is radiometry. In the digital frames there are two discretizations, a geometric discretization since the frame is divided into pixels, it is a radiometric discretization since each pixel has an associated number that represents the gray tone of the pixel itself if the image is in black and white.

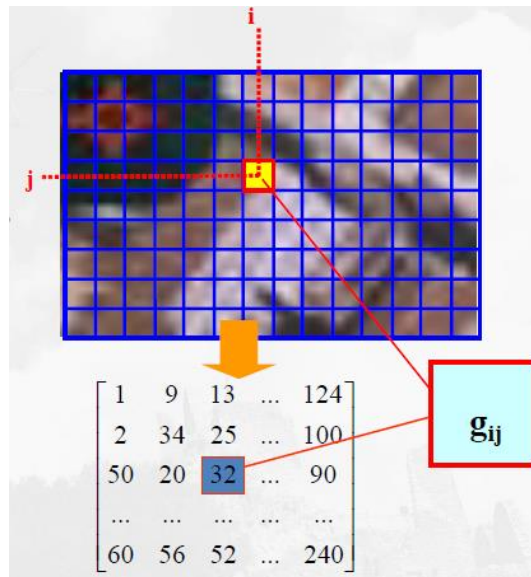


Figure 37. Digital image. Source: Lingua Andrea, Chiabrando Filiberto, Aicardi Irene, n.d. Droni P1-10

The number of pixels contained in predetermined length units expresses the geometric resolution of the image and for practicality all the pixels are usually square in size. By convention, it is expressed as the number of pixels contained in one inch (1 inch = 25.4 mm), with the unit of measure dpi.

Since a geometric discretization has been made, each pixel is identified by a row index i and a column index j that characterize it and, to each pixel, a numerical value is associated, which represents the average radiometric value, because a radiometric discretization that characterizes the portion of the image delimited by the edges of the pixel.

The choice of the relationship between radiometric value and number takes place according to the conventions with which the image is constructed, which can be black and white, in shades of gray, true colour and palette.

Black and white

The technique is used in the cadastre, where you are only interested in memorizing lines and associating the number 0 for white and the number 1 for black.

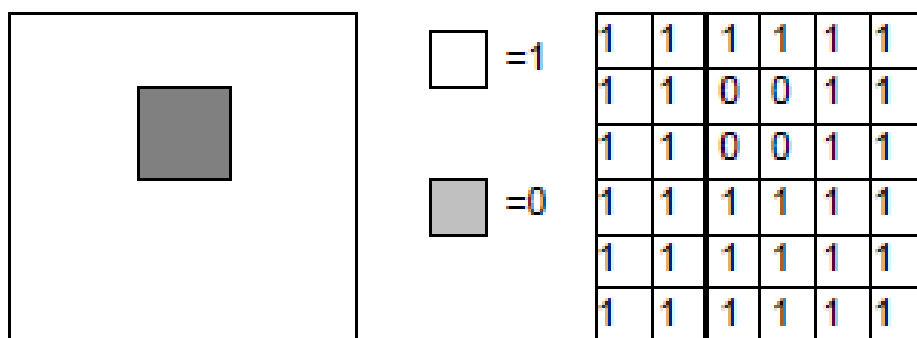


Figure 38. Black and white discretization. Source: Source: Manzino, A., n.d Geomatica.

In this way, images can be constructed with only 1 bit per pixel, but this discretization mode is not useful for photogrammetry.

Gray tones

The radiometric variation from white to black is divided into 256 intervals, with extreme values 0 corresponding to white and 255 corresponding to black.

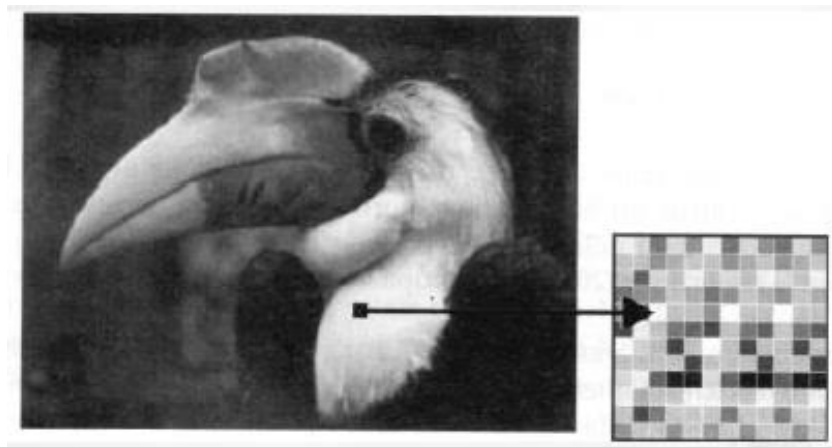


Figure 39. Gray tones discretization. Source: *Lingua Andrea, Chiabrando Filiberto, Aicardi Irene, n.d. Droni P1-10*

Now, storing a pixel requires one byte and therefore 8 bits.

True colour

Each colour can consist of three additive or subtractive colours which are red, green and blue (RGB). As a result, each colour can be defined with 3 bytes, where each byte contains the intensity of red, green or blue, so it takes up 3 times as much memory.

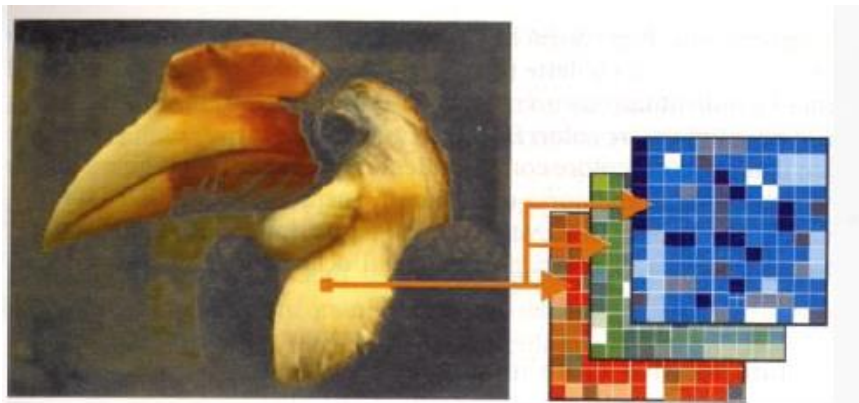


Figure 40. True color discretization. Source: *Lingua Andrea, Chiabrando Filiberto, Aicardi Irene, n.d. Droni P1-10*

Palette:

If you have a coloured image, you can only occupy one byte instead of 3 for each pixel if you use a certain way of filling the byte, that is, the colour palette.

In fact, there are many shades but less can be enough. So, we know that in each colour the intensities of R, G, B range from 0 to 255 and therefore, each colour is defined by a triad of numbers from 0 to 255. If there is a first colour, defined by a certain triad, then it is inserted in the palette as colour 0. The second colour is then inserted as colour one in the palette and so on, so the advantage is that there are usually 256³ possibilities in the true colour, while in the palette there are only 256 colours.

3.5 lidar and laser scanner

The term LIDAR means "Light Detection and Ranging", that is the emission of an electro-optical impulse towards an object and the reception of part of the reflected component, like wave spacers, which however need to use a prism to get the reflected signal.

This is possible thanks to a device that has inside both the transmitting apparatus and the receiving apparatus of the same signal which is composed of a sequence of impulses over time.

By being able to concentrate the large part of the energy in a limited time interval, a high-power signal is obtained. In particular, the signal is a coherent beam, i.e., a laser beam, in which all the waves are in phase (wavelength equal to 0.76 microns).

When an impulse hits an object, there are three possibilities

- If the surface of the object is a mirror and is tilted, nothing returns to the instrument because the ray is reflected in another direction
- If the surface of the object is rough and completely absorbent, then it does not come back again
- Usually, for a common surface, the light beam does not return all the way back, but the reflected light moves in different directions and only a small part of the signal returns to the source from which it was emitted.

The energy with which the signal returns is certainly less than the energy that the emitted signal possesses, so it is possible to detect objects that are within certain distances, usually within 300 meters.

3.5.1 Principle of operation

It has already been seen that, from a technological point of view, the instrument is simpler than a motorized total station because it does not have an azimuth and zenithal circle, but rather has high-precision motors that move the direction of a distance meter. Having known the position of the centre of the distance meter and known the directions from the distance vector (two directions in the earth survey are enough because the z axis is fixed), the coordinates of the observed point can be obtained. In particular, it passes from the spherical coordinates (d , δ , θ) measured to have the coordinates (x , y , z) of the observed point.

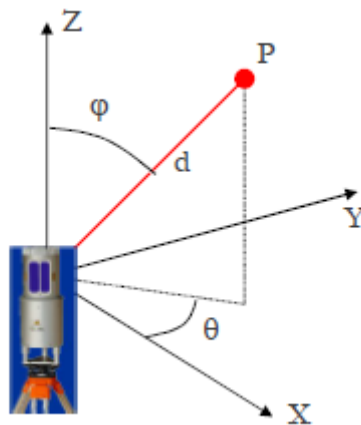


Figure 41. Laser scanner principle operation. Source: Manzino, A., n.d Geomatica.

During the survey, the measurements are made continuously, as we proceed in many angular steps. Hence a difference between the total station and LIDAR arises, in fact in the total station, the points necessary to define an object are detected, while in the Lidar a non-intelligent procedure is followed since the whole object is acquired, obtaining a cloud of coordinate points (x , y , z) in a reference system, without making choices.

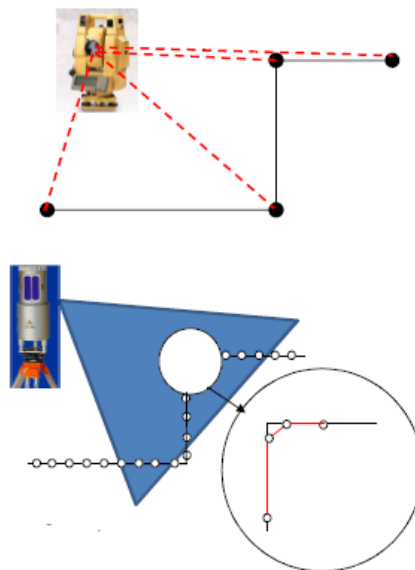


Figure 42. Non-intelligent procedure. Source: Manzino, A., n.d Geomatica.

The mechanism is similar in both terrestrial and aerial surveys, since there is a system of prisms that rotate at a very high-speed hitting the object with a beam of light. The difference is that in the aerial survey the aircraft moves during the survey itself, guaranteeing complete coverage of the terrain. For this reason, the Lidar is integrated with an inertial system and with a GNSS positioning system.

Since the instrument is in practice a distance meter, it typically uses laser beams, i.e., beams of coherent infrared light.

Like the pulse distance meters, there is a transmitter and a receiver that intercepts the signal emitted by the object. The process takes place at the speed of light, so thousands of values can be measured in seconds.

The distance is obtained by measuring the flight time:

a square wave is emitted, which is received after an interval of time. The same wave is not received, due to the noise caused by the atmosphere and the object hit by the beam. The flight time is made up of a whole part (i.e., complete cycles), which is measured by a wavelength counter, which gives the value of n . To this are added two fractional parts t_a and t_b , linked to the start and stop signals, which are measured by means of a micrometric circuit in which a capacitor charges and discharges (the measurement derives from the voltage variation).

$$\Delta t = nT + t_a + t_b$$

From here the distance is obtained through the relation:

$$d = \frac{v \Delta t}{2}$$

Where v is the speed of light corrected with atmospheric refraction.

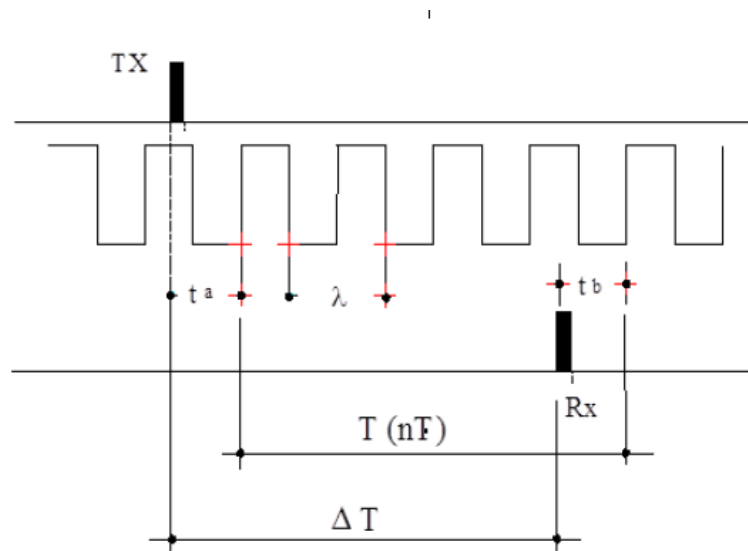


Figure 43. Measurement system. Source: Manzano, A., n.d Geomatica.

The accuracy of the pulse distance meters is high thanks to the accuracy of the time measurement system. In reality, accuracy also depends on the relationship between signal intensity and noise. The latter is related to the object hit and its distance, as they affect the amount of signal that is reflected by the object in the direction of transmission.

$$\sigma_d = \frac{1}{\sqrt{S/N}}$$

Where S is the signal and N the noise.

Vice versa, or distance meters with phase measurement measure the phase shift between emitted sine wave, re-entrant sine wave and add the whole number of wavelengths to this.

$$S_e(t) = A \sin(\omega t + \varphi_0)$$

$$S_r(t) = A \sin[\omega(t + \Delta t) + \varphi_0]$$

$$d = n \frac{\lambda}{2} + \frac{\lambda \Delta \varphi}{2\pi}$$

3.5.2 Land and aerial survey

In land surveying, the quality of the instrument is not only defined by precision and range, but also by other aspects:

- Detection speed: important for surveying in motion
- Resolution of the scan, which in theory is equal to the amplitude of the rotation angle of the laser beam between two adjacent points
- Divergence of the laser beam, which allows you to cross obstacles such as vegetation and hit the ground.
- Real range, linked to the medium, ie the refraction, roughness of the object, type of material and disturbing radiation.
- Measurement range, depending on the sending frequency of the square waves, there is a minimum and a maximum distance to be unambiguous, ie not to receive the same signal twice and interpret it as the first signal.
- RGB acquisition, there are tools that, in addition to the intensities, acquire the wavelength of the return signal and associate each point acquired with the radiometry detected on the laser impact area. Alternatively, they can have an external digital camera integral with the laser scanner (better system)

In the aerial laser scanner, the same principles as for terrestrial survey are followed, but now the laser beam is emitted at a point of known coordinates in the GNSS reference system and measures the distance, while the 3 components of the distance vector are known thanks to the presence of an inertial.

The laser beam falls into the infrared, also because this corresponds to one of the few wavelengths that penetrate long distances into the atmosphere and have a sufficiently powerful return signal. By appropriately modifying the wavelength, the signal also penetrates the water and a return signal can be returned up to a depth of 10-20 m, depending on the power used.

Typically, aerial instruments perform scans on the ground, creating a sort of serpentine, in order to detect profiles. In fact, the client always requires a certain number of points per m^2 and, since the Lidar has a constant rotation speed, to obtain a good density, the air-ground distance must be varied, and the ground must be surveyed with many swipes. This is very reminiscent of photogrammetry, but the difference is that now the angle of view is narrower and the number of steps to take is greater.

The accuracy of the aerial scan laser depends on several factors:

- Lidar errors, i.e. angular scan errors, assembly errors (i.e. alignment errors between instruments), inertial measurement and GNSS positioning errors
- Instrument synchronization error, because the reference systems of the 3 instruments must also be put together in a temporal sense, that is, they must be synchronous
- Systematic and accidental errors, generally lower than the sum of the others.
- In particular, if an object is measured in the zenith direction, the error can become very high depending on the distance from the object, in fact, depending on the distances, the distances can have errors of 10-40 cm, which result in large errors in the plan. and altimetry, even if the error in the planimetry is dominated.
- So the accuracy is not high but on the other hand it seems that there are thousands of measurements, you can filter the data and improve the accuracy.
- Among other things, altimetric error and planimetric error depend in a non-linear way on the scanning angle and, for this reason, its value is limited to openings of 30 ° - 50 ° instead of 90 °.
- Response echoes, caused by the divergence of the laser beam and the impact surface that is not punctual and its extension increases as the distance of the object increases. This extension becomes significant in the aerial survey, in which distances of 3000-4000 m are involved.

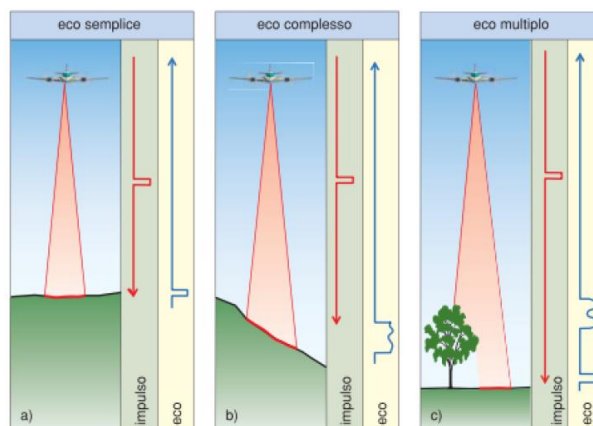


Figure 44. Aerial survey. Source: Manzino, A., n.d Geomatica.

If then the surface has roughness, a portion of the ray is reflected before the rest. The result is a series of return signals, known as response echoes.

This aspect is very important in the presence of vegetation because, thanks to its divergence, the laser beam penetrates through the spaces left by the vegetation and touches the ground. There are thus many response echoes, relative to both the canopy and the ground and from here a DTM or a DMS can be produced. On the other hand, not all echoes can be recorded by the instrument. Some instruments can record only one impulse, others also record the last impulse and still others also record two intermediate impulses.

3.6 Drones

The drones used for photogrammetry are born with military purposes and are part of a family of devices called UAVs (Unmanned Aerial Vehicles), which are unmanned reusable motorized aerial vehicles.

It is preferable to use UAVs for photogrammetric surveys due to an economic aspect linked to the high costs of digital photogrammetry carried out through piloted aircraft or helicopters.

For example, the possible applications of drones used for photogrammetry are surveys for cartographic purposes, bridge inspection, monitoring for forestry purposes, documentation and generation of 3D models for cultural heritage and

Their use is also convenient in case of emergency in order to carry out timely local monitoring.

In particular, the use of UAV devices is recommended for the detection of objects that are difficult to reach, detection of objects that are accessible but only for a certain period of time, detection of living organisms and for the detection of small objects

As for the drone market, it appears to be in strong growth both for the continuous technological progress that also characterizes drones from a mechanical point of view, but also for their versatility in carrying out certain operations quickly and economically.

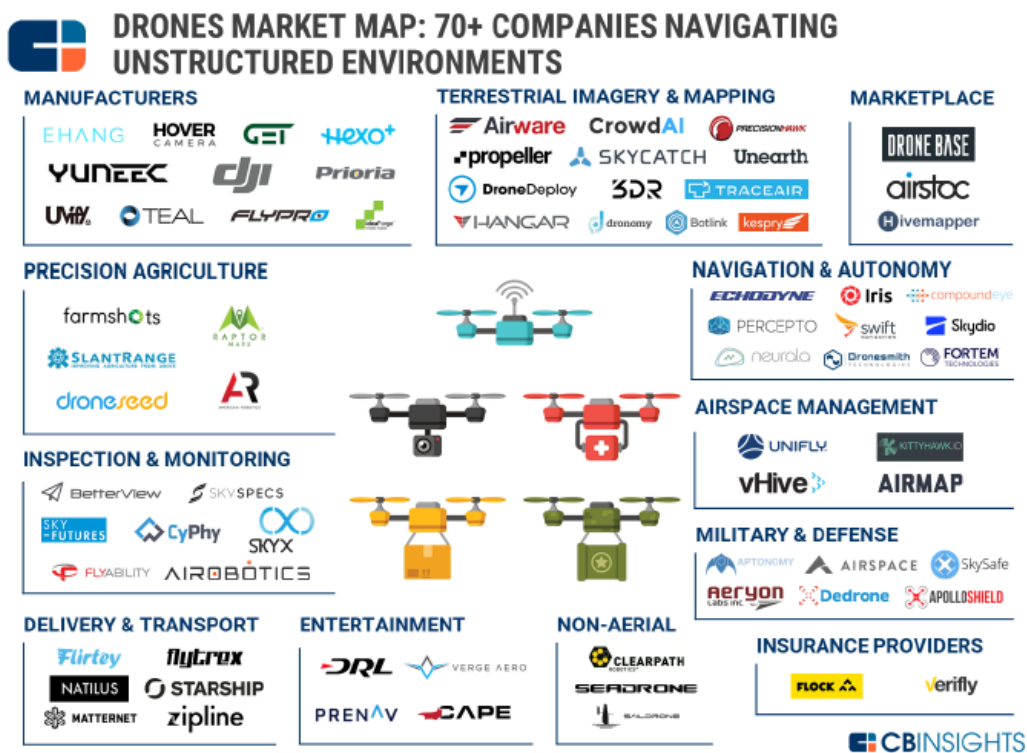


Figure 45. Drones Market. Source: Lingua Andrea, Chiabrando Filiberto, Aicardi Irene, n.d. Droni P1-10

The drone moves in space and can mainly perform two operations, namely record a video, or take photographs of the real object to be detected. These are saved in a memory inside the drone. These images are then used to return certain outputs.

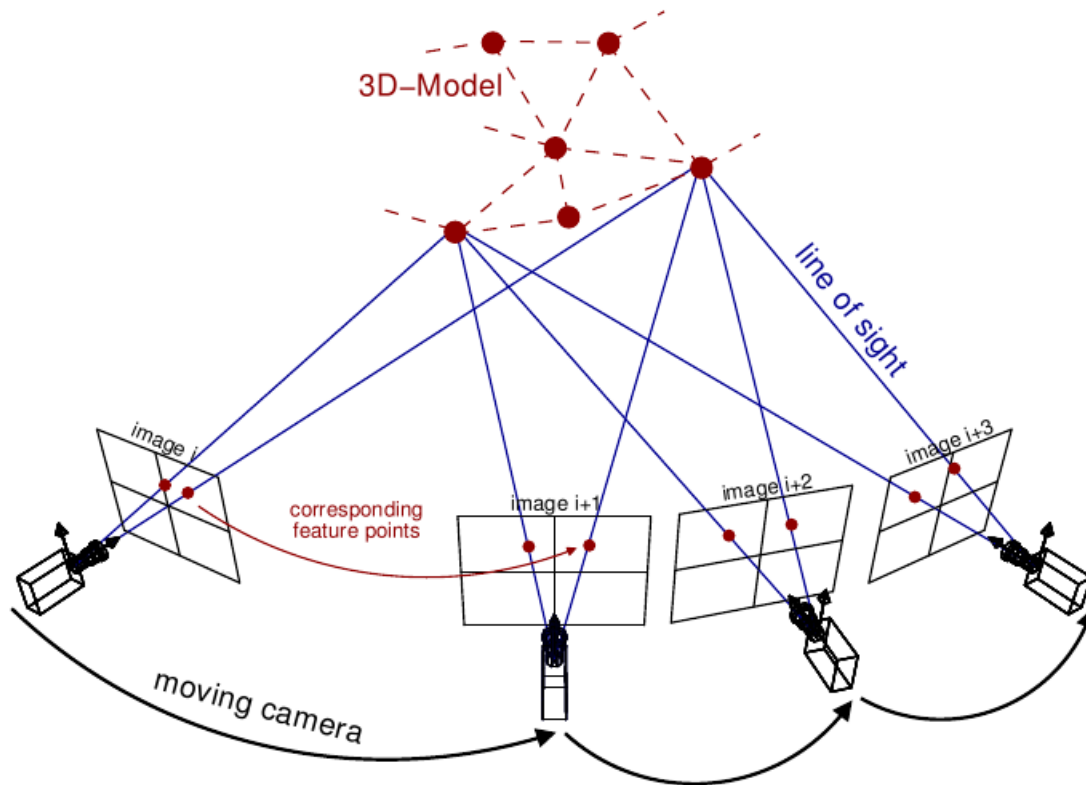


Figure 46. Structure from motion. Source: Lingua Andrea, Chiabrando Filiberto, Aicardi Irene, n.d. Droni P1-10

The procedure to follow is therefore the following:

1. Measure the image coordinates with great precision of significant points (preferably homologous) within the digital cameras.
2. Define the characteristics of the digital cameras (internal orientation parameters by means of calibration)
3. Position the digital images acquired by the cameras in space (external orientation parameters)
4. Calculate the X, Y, Z coordinates of the identified homologous points
5. Automatically recognize homologous significant points (feature extraction, description and matching)
6. Automatically recognize significant points (feature extraction, description and matching)
7. Automatically generate point clouds that describe the surface of the object (dense matching algorithms)
8. Generate the final products in the most automatic way possible (orthophoto, DTM, DSM, TIN, mesh...).

3.6.1 Anafi Work Parrot

In particular, for the thesis work the “Anafi work drone” of the manufacturer Parrot was purchased from the Turin Polytechnic.



Figure 47. Complete kit Anafi parrot drone. Source: <https://www.dronext.eu/certificazione-parrot-anafi-work>.

As can be seen from the data sheet, it is a professional multi-rotor drone that can capture high resolution images and videos. It is equipped with a 4K HDR camera and gimbal that can rotate 180 °, an optimal feature for inspecting a bridge soffit. It has a weight of 320 grams, characterized by a compact shape and folding frame in carbon fibers. The battery is a 4700mAh Li-PO with a duration of 25 minutes, so since 4 batteries are provided in the complete kit, the drone's flight autonomy is equal to 1h and 40 minutes.



Figure 48. Anafi work drone. Source: <https://www.dronext.eu/certificazione-parrot-anafi-work>.

To carry out a photogrammetric survey using the Parrot anafi work drone, you must have a mobile device in which some apps must be present such as the “parrot FreeFlight6” or the “pix4Dcapture”.

Pix4Dcapture is an app that allows you to design a photogrammetric survey mission.

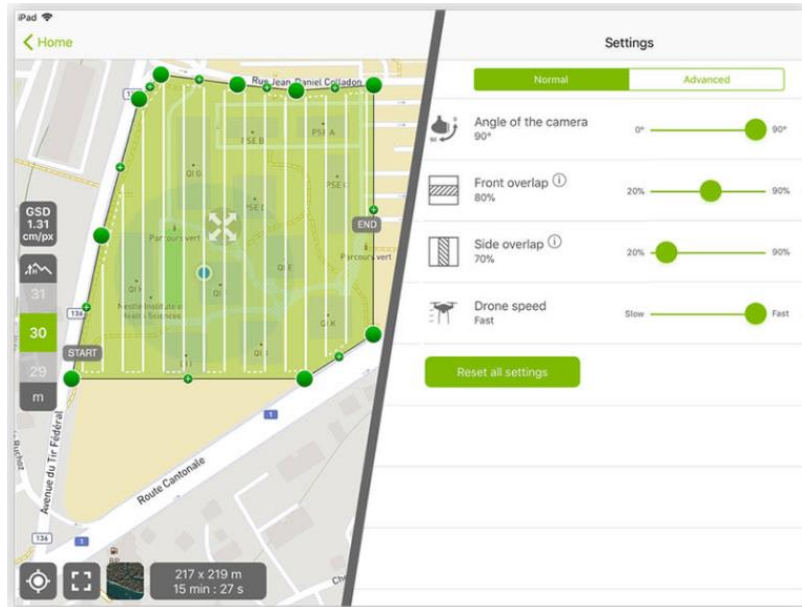


Figure 49. App pix4Dcapture. Source: <https://www.pix4d.com/product/pix4dcapture>

In particular, it is possible to program the flight plan through models available in grid, circular and polygonal configurations that allow you to carry out a survey by capturing videos or images from different perspectives, in order to obtain an adequate number of photos.

In addition, it is possible to set the altitude of the drone and the angle of the camera, depending on the object or area to be detected.

The Parrot FreeFlight6 is an app that allows you to program a flight plan and check the various data of the drone while it is in flight, such as the battery level. The various features are very similar to the pix4Dcapture app, and its use is more intuitive.



Figure 50. App Parrot FreeFlight6. Source: <https://www.parrot.com/us/apps-and-services>.

4 RUBIK'S CUBE: mesh-to-BIM

The final goal of the following thesis work is mainly to find a method through which to carry out the monitoring of the bridges in this case but of the heritage built in general not in situ but directly in the office having available all the outputs that photogrammetry and laser scanning can provide, such as mesh and point clouds.

To do this process, a research was carried out on the possible methods through which to import and export point clouds and meshes between the various software in order to determine the damages of a bridge. We therefore started from simplified models and such as importing a rubik's cube into the Revit software, to obtain a workflow through which both the mesh and the texture can be imported into the Revit software.

The main problem lies in the fact that the Revit software actually reads point clouds and meshes without problems that can be imported both in .dxf point format but also through the Revit Dynamo plugin, but currently Revit is not completely able to associate a 3D model created in Revit environment to associate the texture coming from photogrammetry and Lidar technique.

If you want to import the geometry but also the texture of any real object into Revit it is possible to do so but not automatically. If it were possible to do this automatically, it would be a great advantage because when we have the 3D model of a bridge and it would be possible to associate the texture of the real bridge with the actual state, then we could go directly to carry out the evaluation and recognition. of the various damages in order then to indicate the positions in which they are found to subsequently carry out the necessary precautions and then evaluate whether it is necessary to carry out extraordinary ordinary maintenance interventions or if it is necessary to completely demolish the work.

After carrying out research on the subject, the thesis work aims to find a methodology to carry out this operation which, however, has no longer been adopted because it is a completely manual and not automatic operation, so later we will see how it was then dealt with. the problem. We started by going to create the mesh of a Rubik's cube and then the first phase was to take pictures with a cube camera. The photographs were taken from different angles and from different distances for a total of about 30 photographs.

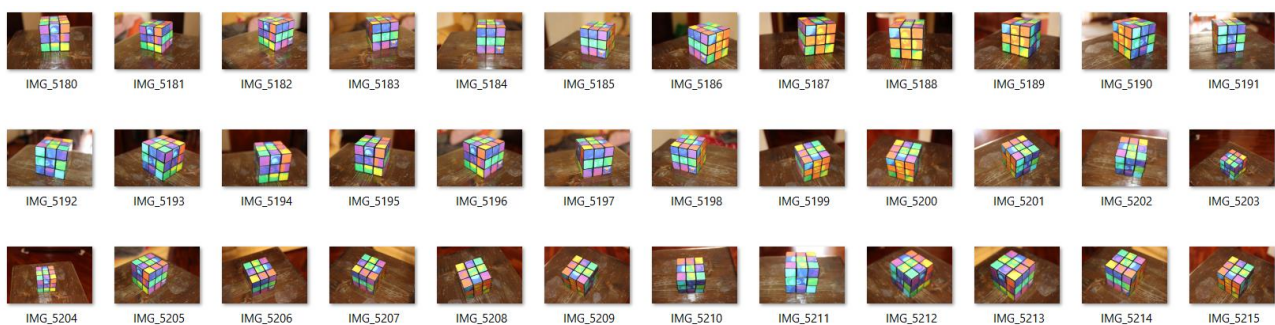


Figure 51. Rubik's cube photographs

4.1 Dense point cloud and mesh with Metashape

Once the photographs were obtained, they were imported into the Metashape software where the alignment of the photographs was carried out first and then the mesh and the dense point cloud were generated which are the three fundamental outputs that must be obtained to then import the cube. by Rubik in Revit.

The alignment of the images is the first process where calculations are made, based on certain parameters that must be selected that cause the software to make choices or analyse the images that make up the dataset in a more or less thorough way. The choice of these parameters then affects the output that occurs at the end of the alignment, that is the scattered point cloud.

The alignment of the images is the first step of the whole structure from motion process which is a cascade process, so each step is linked to the previous one, which is why the parameters that are chosen during the alignment phase also affect all other outputs

In this phase, the Metashape software performs an image-by-image analysis and, depending on the degree of detail, finds characteristic points which are then compared with the other images. When there is a correspondence between the points identified in different images, these characteristic points go from being points in two-dimensional space within each image to becoming points in three-dimensional space. These points make up the scattered cloud in Metashape.

As the level of detail increases, the characteristic points identified for each image increase, so when the software compares them with the characteristic points identified for the other images, many matches are obtained. If instead I set a low level of detail, then the characteristic points identified for each image will be few, consequently I will get a scattered cloud with little identification. If you increase the level of detail, the processing times increase, so to carry out a preliminary test it is possible to set low levels, if everything goes back then I subsequently perform a more accurate alignment.

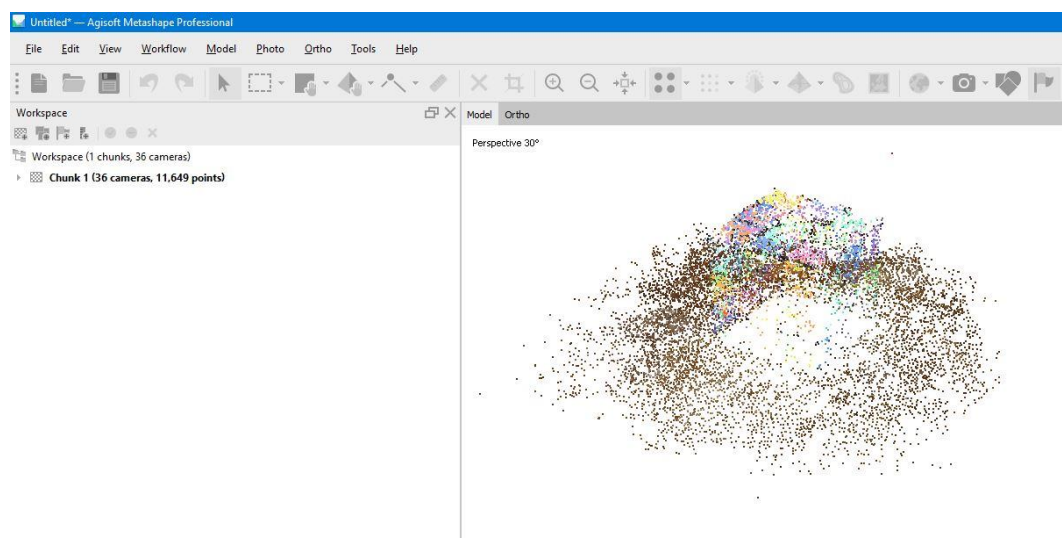


Figure 52. Point alignment

After generating the scattered cloud of the cube, the next step was to generate the dense cloud of the same. Also in this case there are several parameters that must be set, on which the final output then depends. In particular, the main parameter is the quality or resolution and you have five possibilities ranging from low quality to ultra high quality. By passing from a high to a low quality, the software performs a subsampling, in the sense that the pixels of the base and the pixels of the image height are divided by two and therefore the new subsampled image will be characterized by a quarter of the pixels of the image. departure. The final number of points that characterize the dense point cloud and also the processing time depend on this.

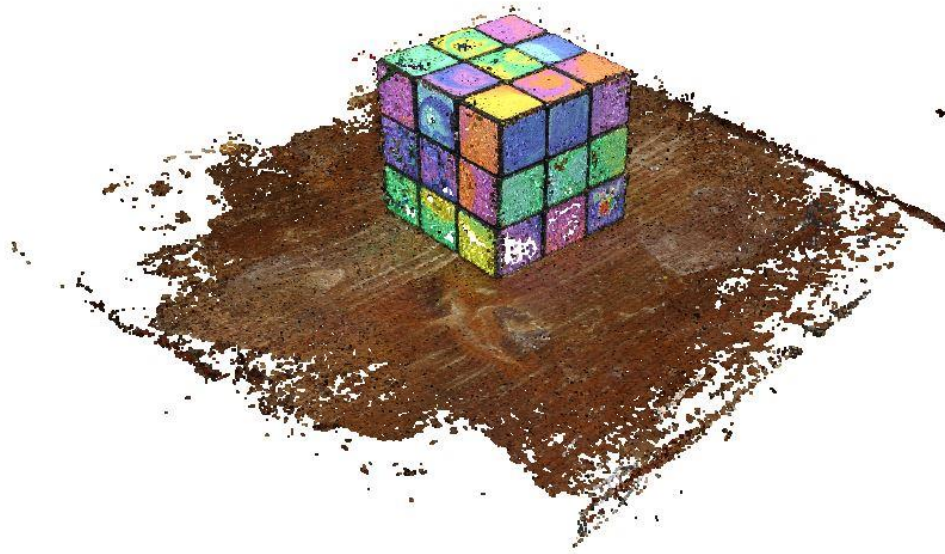


Figure 53. Dense cloud.

Then this dense cloud has been cleaned.

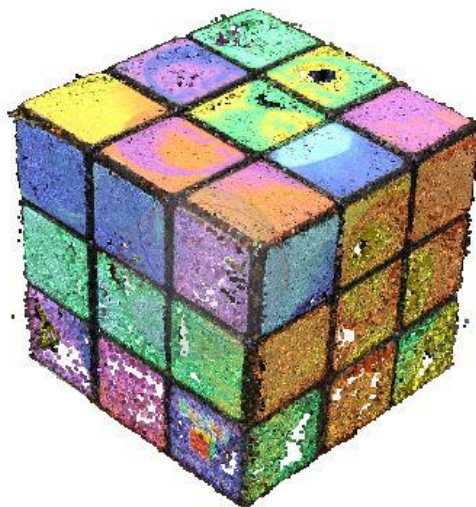


Figure 54. Dense cloud cleaned.

The next step was to generate a mesh starting from the dense point cloud by connecting the discrete elements of the point cloud that become the vertices of triangles, creating a surface. The main difference between a point cloud and a mesh is that the point cloud is discontinuous, so if someone gets too close to the model he will see discontinuous points, while however close someone can get to a mesh, will always be visible a continue surface.

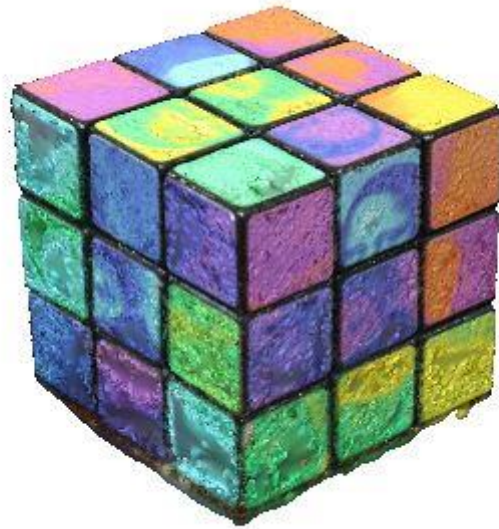


Figure 55. Mesh.

4.2 Eliminate distortions and separate faces with Meshmixer and Meshlab

Once we obtained the dense point cloud from the Metashape software and subsequently the 3D mesh of the Rubik's cube it was possible to observe that since the software was provided with only the photographic data and there were no natural points or markers detected, the mesh obtained was characterized by distortions. There were some uncalibrated chambers and not enough information had been provided to the software.

To eliminate these distortions and restore the geometry of the cube, for example by finishing the edges of the cube and correcting any distortions, the Meshmixer software was used, within which there are tools that allow you to select the surface in order to cut it, refine it or decrease the number of triangles.

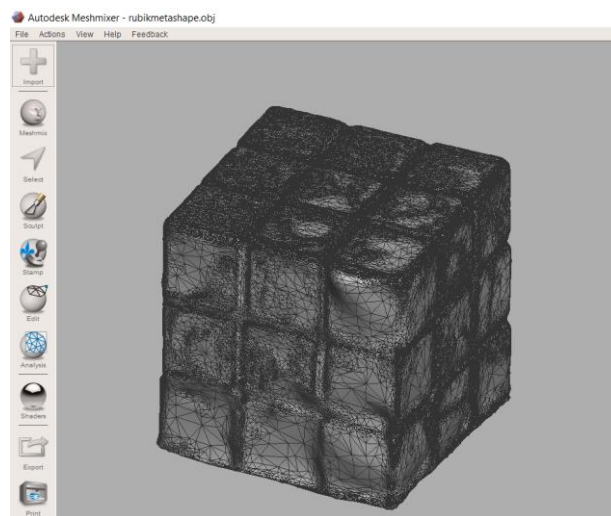


Figure 56. Imported cube with distortions.

The final result obtained through the Meshmixer software was the following.

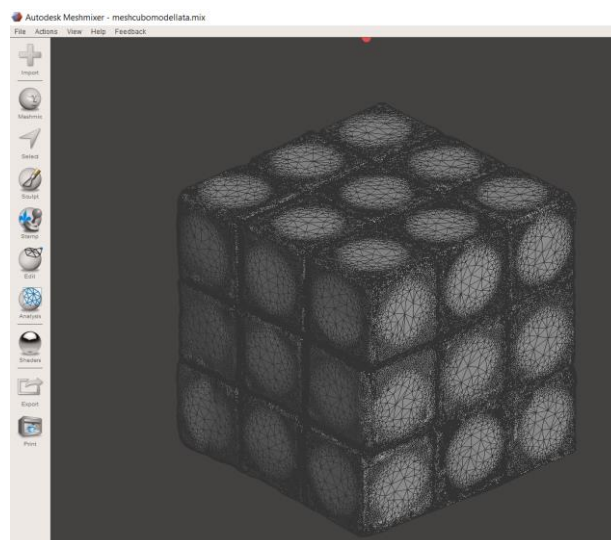


Figure 57. Reshaped cube in Meshmixer.

Then, to import this remodelled Rubik's cube into Revit it was necessary to use another software, namely Meshlab.

The Meshlab software was needed to select the faces of the cube to separate them and then import them into Revit in order to apply the orthophotos as an image in Revit.

For example, the following image shows a cube face selected and duplicated in a new layer.

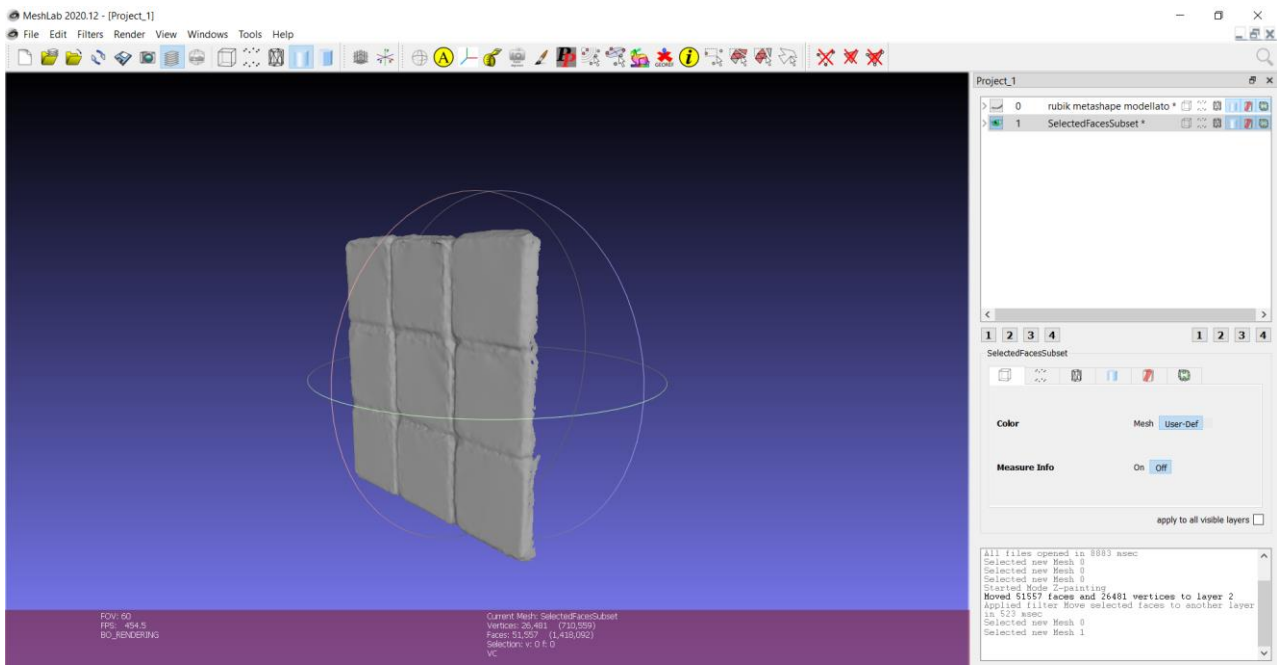


Figure 58. Cube's face in Meshlab.

4.4 Import into Revit

Subsequently the 5 faces were exported separately in .dxf format, and imported into Revit.

It was essential to separate the faces and not import the whole cube because to apply the texture you have to create a new material and assign the various orthophotos of the cube individually.



Figure 59. orthophotos of the model.

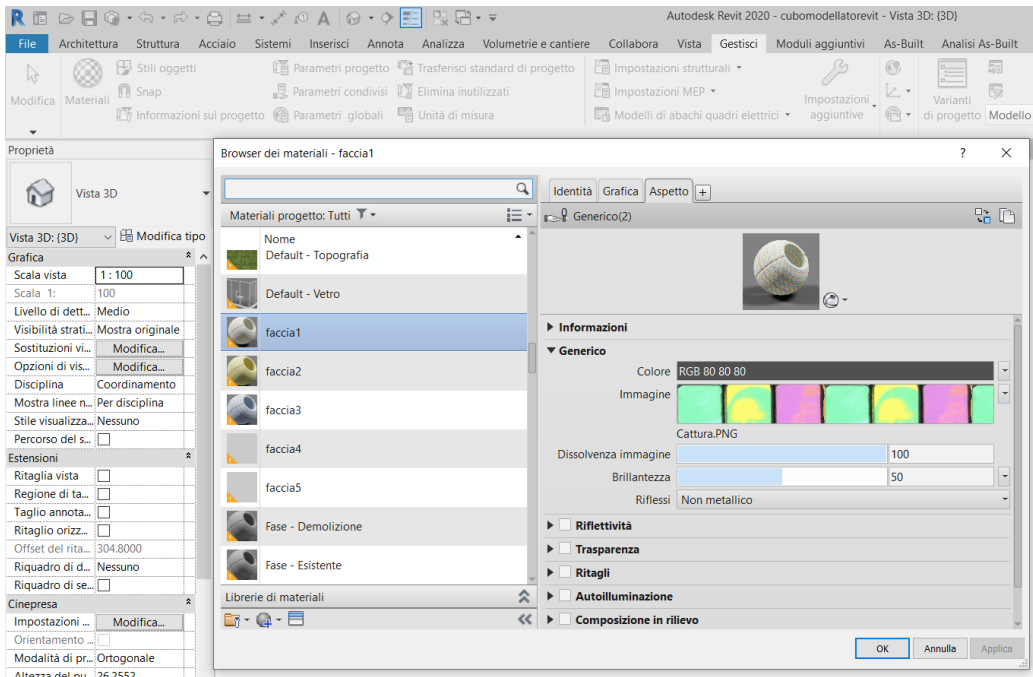


Figure 60. Creation of new materials with orthophotos in Revit.

After assigning the orthophotos as material for the various separate layers in Meshlab, the final result was quite satisfactory, even if this procedure was not actually used which allows to obtain the texture associated with the 3D object directly in Revit, because it is not a automatic and time-consuming procedure.

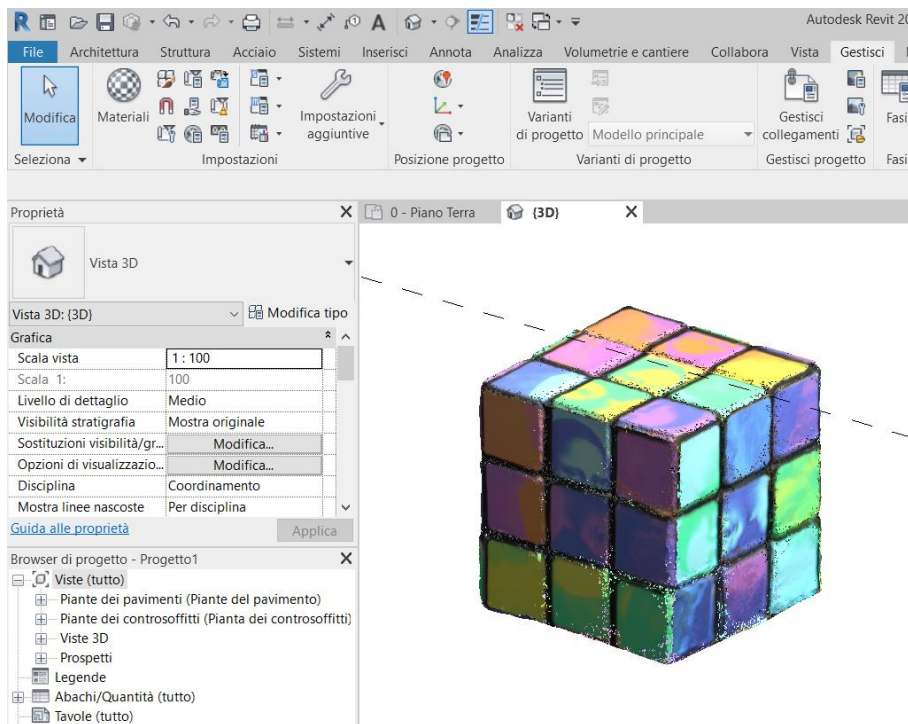


Figure 61. Rubik's cube imported into Revit.

5 PIER CAP: Mesh and Scan to BIM

The pier cap in question comes from an urban bridge located in Largo Grosseto in Turin, designed, and built in 1960. The bridge, after operating for over 50 years, was dismantled in 2019 in order to build a new underground passage.



Figure 62. Largo grosseto overpass during its useful life.



Figure 63. Grosseto overpass during demolition.

In this case it was decided to follow both the mesh-to-BIM procedure and the scan-to-BIM methodology and carry out the necessary assessments on the two methodologies, in order to then choose the most advantageous and fastest methodology.

In the following thesis work, the point cloud of the pier cap obtained through the Recap-photo software was already available. The cloud was exported both in .e57 format, a format compatible with various software such as CloudCompare and Meshlab, and in .rcs format to load it in Revit.

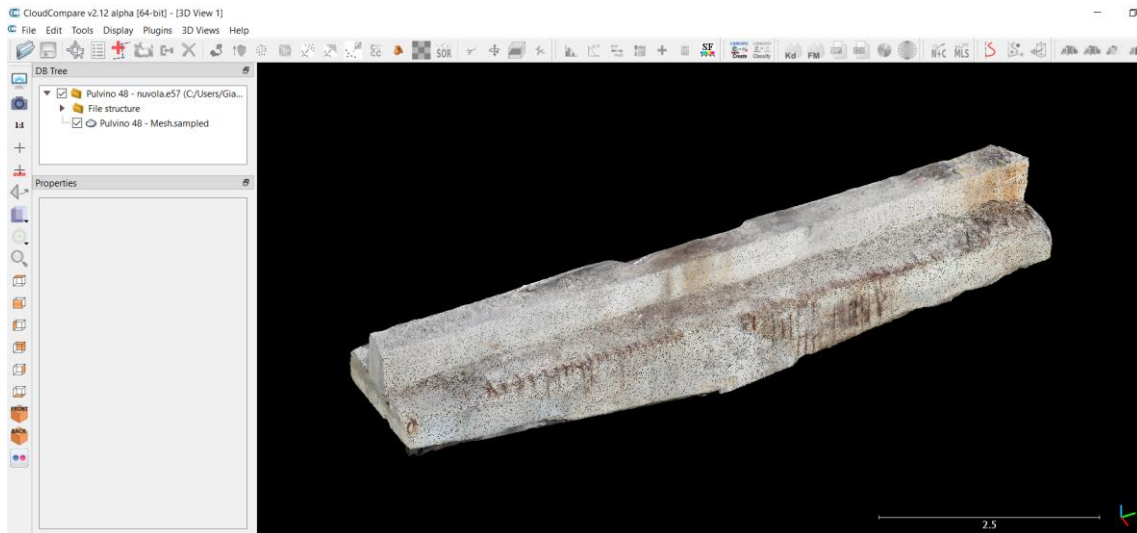


Figure 64. Dense point cloud of the pier cap in CloudCompare.

Subsequently, the generation of the mesh in CloudCompare will be addressed starting from the point cloud, but in this case the mesh obtained through the ReCap software was already available and it was simply imported into CloudCompare. This procedure can be done through different formats such as .ply and .obj.

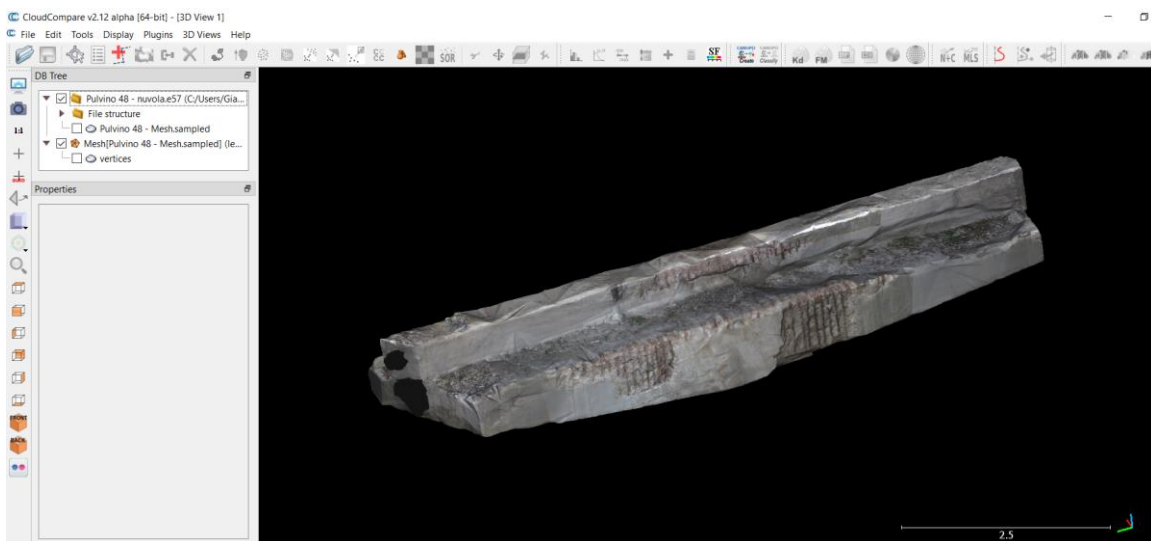


Figure 65. Mesh of the pier cap in CloudCompare.

After obtaining these outputs, first the mesh-to-BIM process was carried out as had already been done for the Rubik's cube, then the scan-to-BIM process was carried out.

5.1 Mesh to BIM:

Regarding this process, the first step is to obtain the orthophotos of each face of the pier cap in order to import them into Revit.

To obtain the orthophotos of each face of the pier cap, the 3D model was first turned in order to show all the various faces which can then be exported through the CloudCompare tool “Render to file”, in .png format.



Figure 66. Back view in CloudCompare



Figure 67. Bottom view in CloudCompare.



Figure 68. Left side view in CloudCompare.



Figure 69. Right side view in CloudCompare.



Figure 70. Top View in CloudCompare.

After exporting the orthophotos from CloudCompare it was necessary to remove the background and to do this we used the Paint3D software.

We start by importing the .png image exported from CloudCompare into Paint3D and using the "magic selection" tool to distinguish the real image that must be imported into Revit as a material, from the background that must not be imported because it is irrelevant.

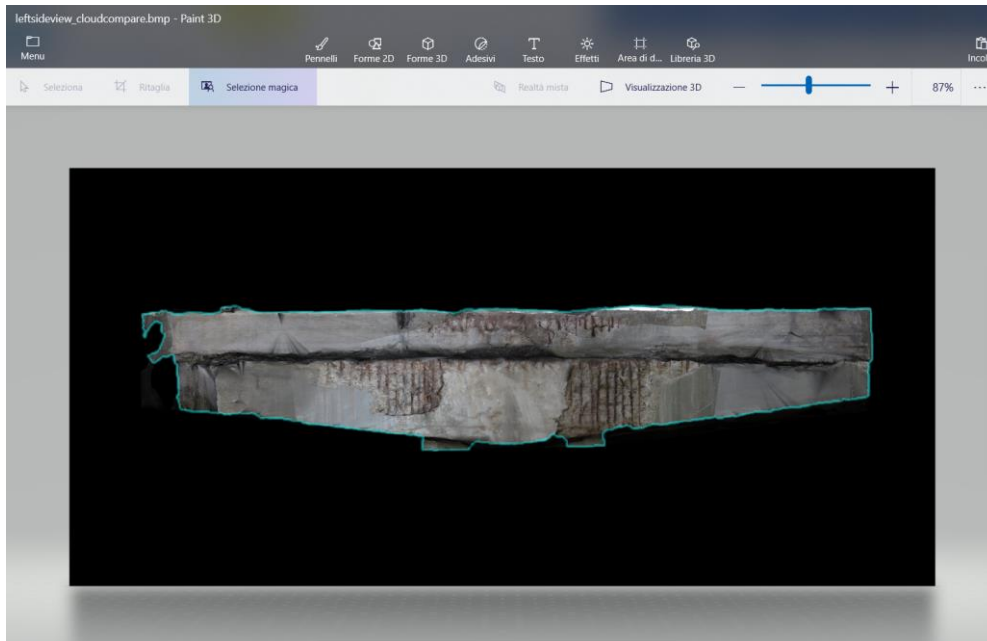


Figure 71. "Magic selection" tool in Paint3D.

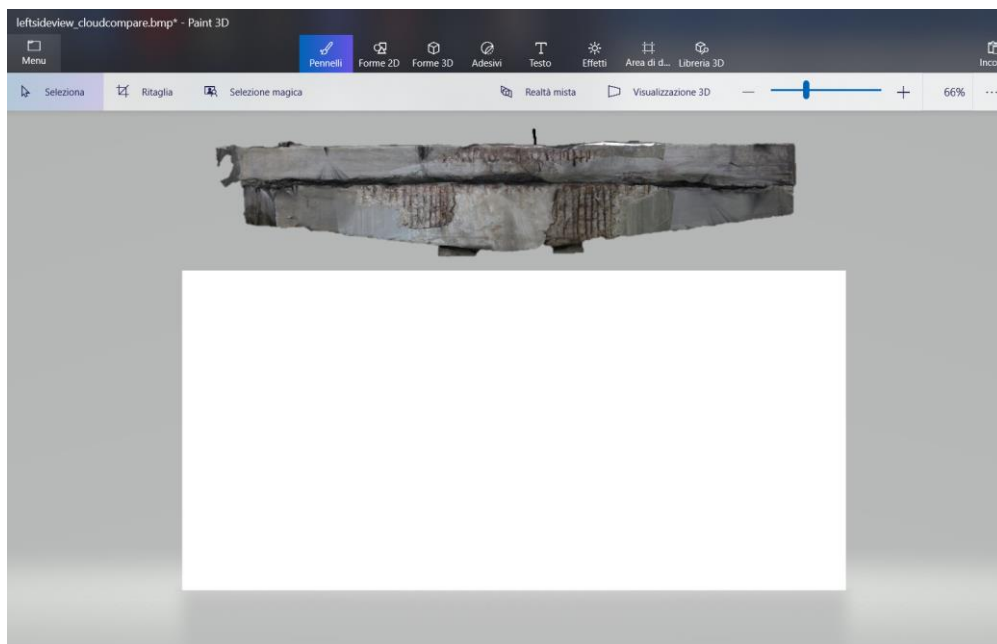


Figure 72. Cleaning the background in Paint3D.

Subsequently, drag the cropped image again with the "magic selection" tool inside the new white sheet.

The process ends by saving the image in .png by activating the transparency option that makes the white background invisible, leaving only the necessary part of the orthophoto.



Figure 73. Exporting the left side view without background.

This operation was carried out for all the faces of the pier cap, thus obtaining the various clean orthophotos.



Figure 74. back view without background.



Figure 75. Bottom view without background.



Figure 76. Front view without background.



Figure 77. Left view without background.



Figure 78. Right view without background.



Figure 79. Top view without background.

After obtaining the orthophotos, the work continued by carrying out the same procedure as for the Rubik's cube. Then in Meshlab the various layers were separated and subsequently imported individually into Revit as .dxf

The fundamental problem of the mesh-to-BIM process is that the mesh can be safely imported into Revit in .dxf format, while the texture can't be imported, so all information regarding the real colour of the object is lost.

In a first phase, the mesh from CloudCompare was exported in .ply format and imported into Meshlab.

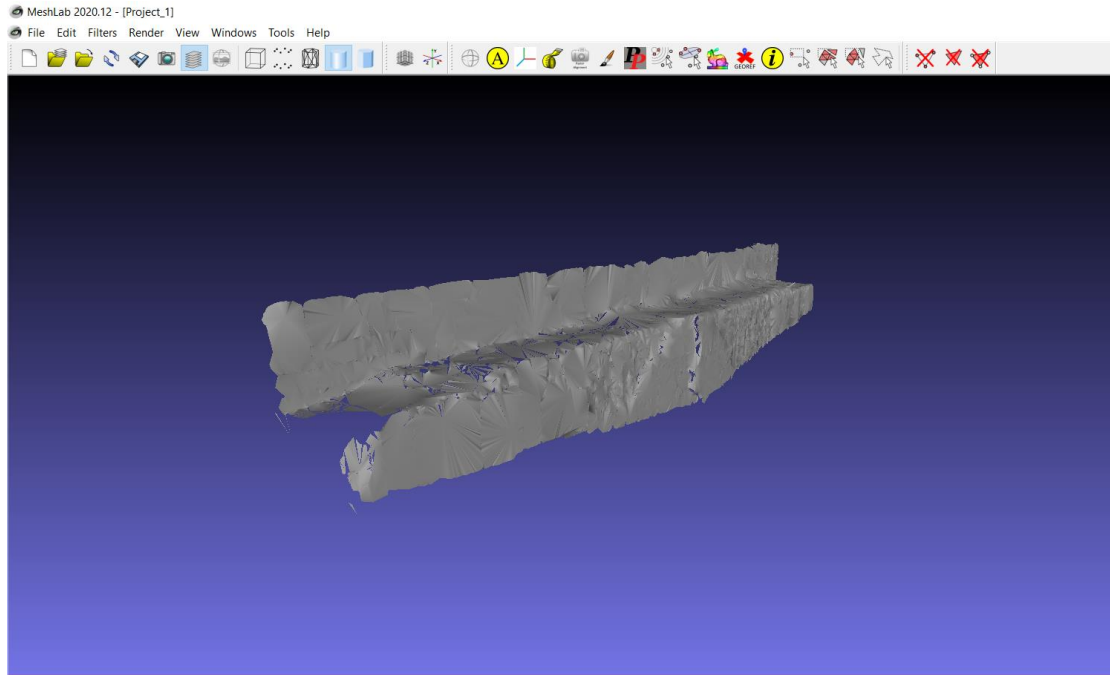


Figure 80. Pier cup's face selected in Meshlab.

After carrying out this discretization operation of the faces, they were exported individually in .dxf and imported into Revit, in order to assign the orthophotos of all the faces as done for the rubik's cube, i.e. creating new materials to assign to each layer in order to complete the mesh-to-BIM process.

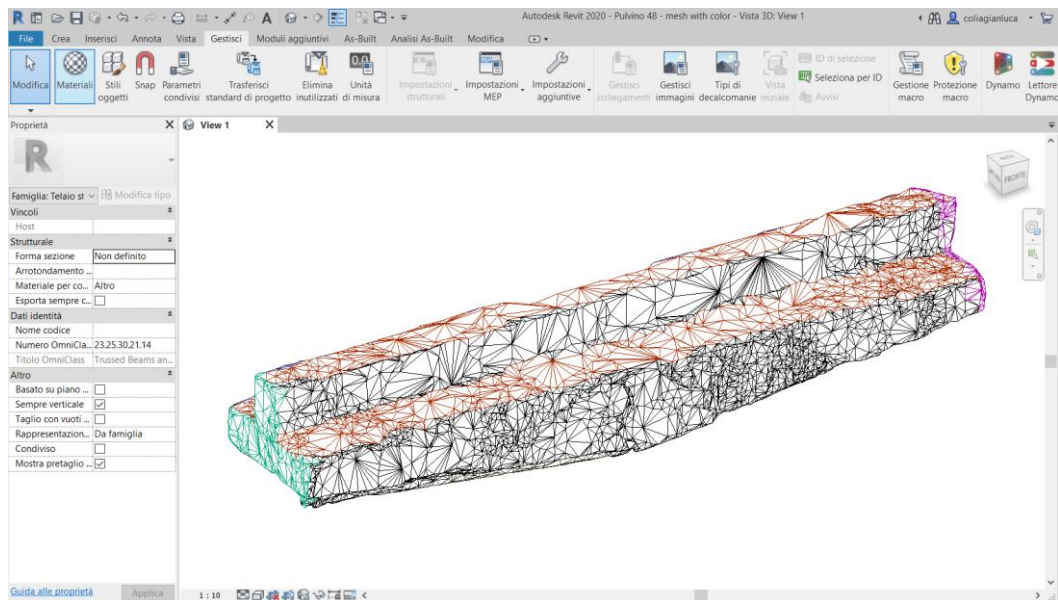


Figure 81. Pier cup's wireframe in Revit.

Therefore, again in the materials section, the various orthophotos have been assigned to the layers of the pier cap.

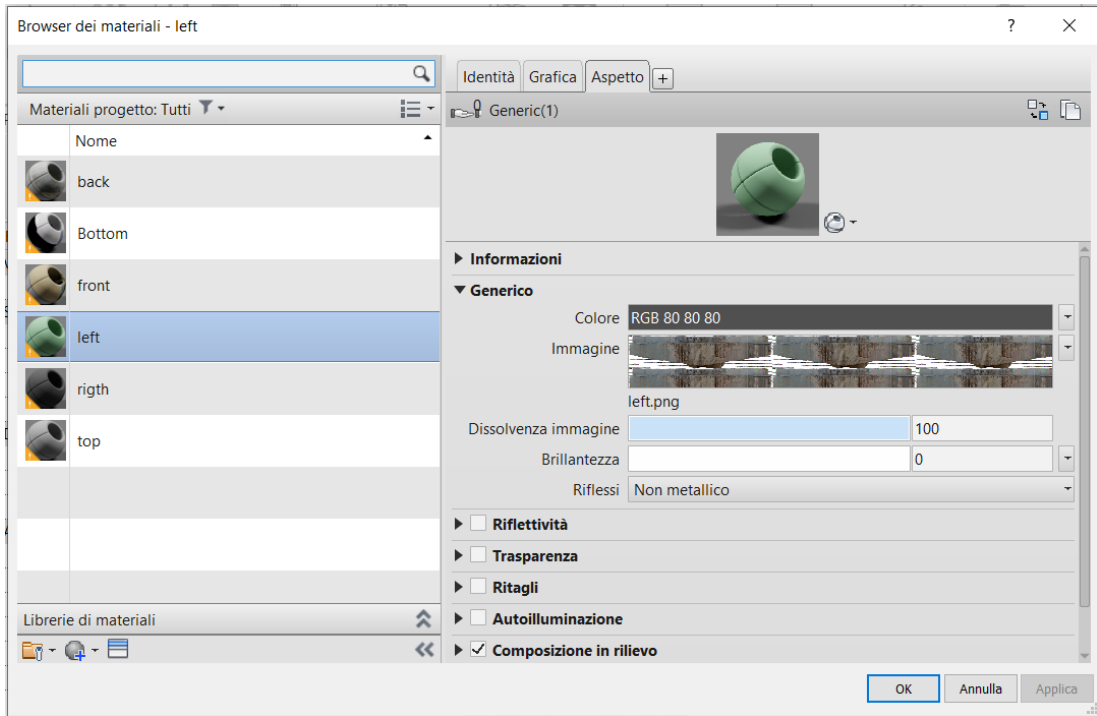


Figure 82. Creation of new materials with orthophotos

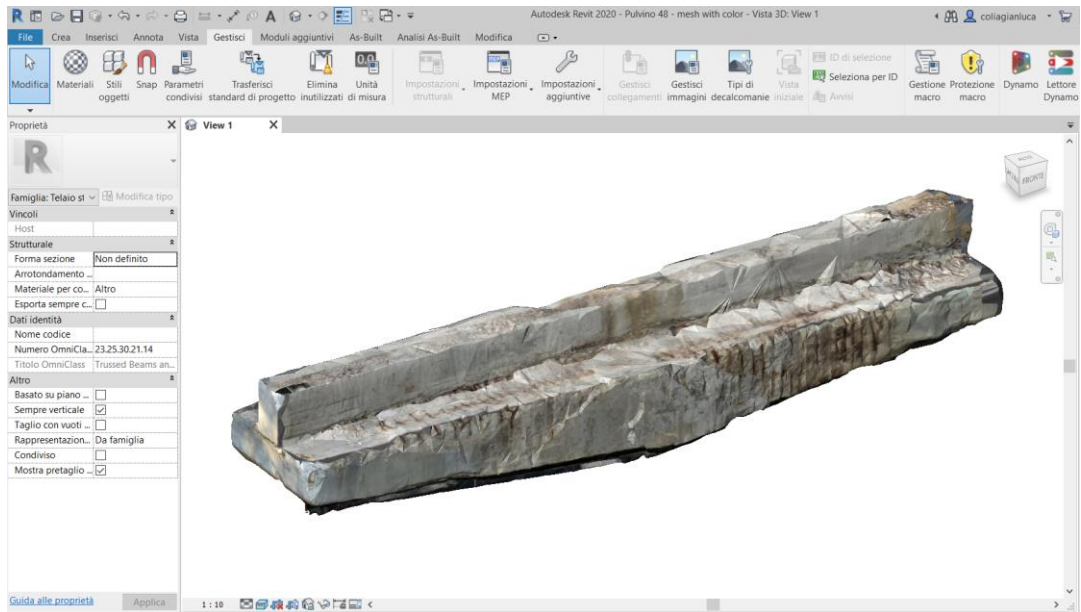


Figure 83. Pier cup imported in Revit.

5.2 Solid Family

Until now we have seen that it is possible to import a mesh with the texture in Revit, but once we have the 3D model with the texture associated at each face.

The textured mesh in the Revit environment is certainly useful for identifying and characterizing damage, but after carrying out this operation it would not be possible to import the mesh geometry into a calculation software, because the formats are not compatible and because the calculation software is not currently able to read such geometries. In fact, the geometry is not solid, but is made up of many triangles, which joined together to generate a surface.

In this phase, a procedure was searched that always falls in the mesh-to-BIM methodology, but solves this problem.

This process, have the advantage of being able to identify damage directly in Revit, and has also the advantage of being exported as solid geometry in other software, such as calculation software, without having to reconstruct the model.

This procedure with respect to the one analysed previously has the difference that the support geometry for the orthophotos imported as material, is no longer the mesh made up of triangles, but is a solid geometry of the pier cap model modelled in Revit.

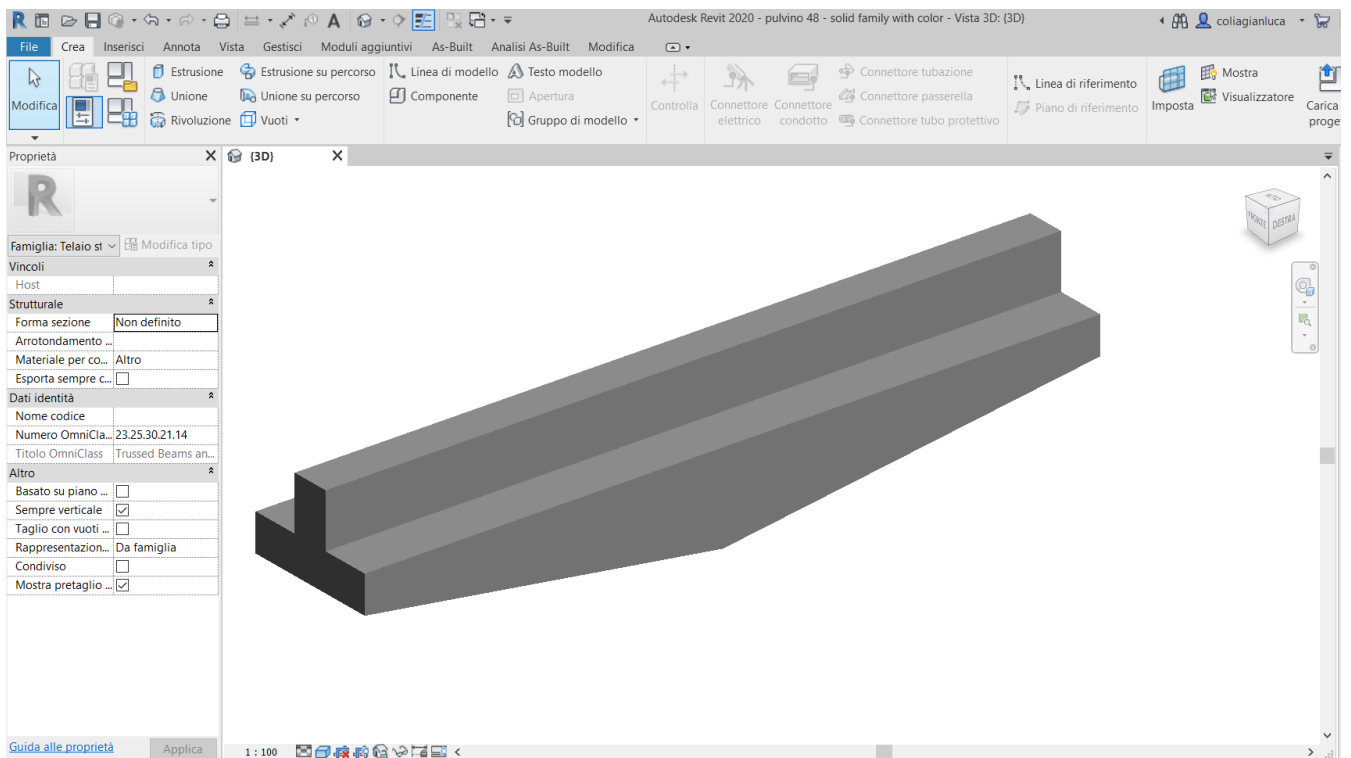


Figure 84. Solid geometry modelled in Revit.

After modelling the pier cap in Revit, the same material assignment operation was carried out, obtaining the following final output.

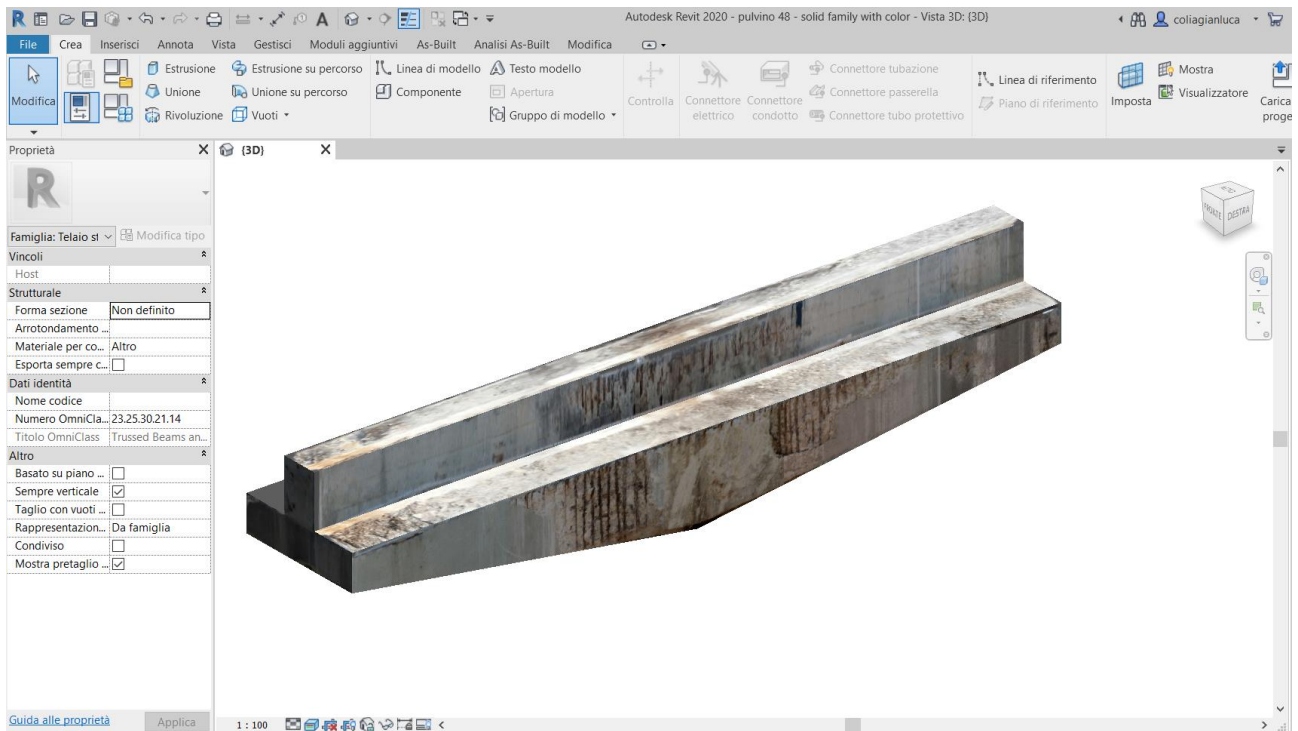


Figure 85. Solid Family with orthophotos.

An advantage of the mesh-to-BIM methodology is to have the structural element directly in the Revit environment with all the graphic information imported as orthophotos, sufficient to identify the damage. However, despite being able to obtain high resolutions, the information related to the depth of the crack or even any swelling is still lost.

On the other hand, the mesh-to-BIM methodology turns out to be completely manual and not automatic, so the processes to follow in order to import the mesh, but also the texture in Revit turn out to be time-consuming.

5.3 Scan to Bim

In this methodology, not the mesh but the dense point cloud was imported into Revit. So in the Revit environment we don't have a surface made up of triangles, but we have a set of points that represent the object, but not through a surface.

Damage determination and classification depends on the quality of the dense point cloud imported into Revit which may or may not allow you to identify a certain damage. The size of the object whose damage must be identified is also fundamental, because as the size increases, the points of the dense cloud will increase, consequently the accuracy of the dense cloud in accurately representing the object will decrease.

In terms of size, the difference between a pier cup that constitutes a bridge and the bridge itself is considerable.

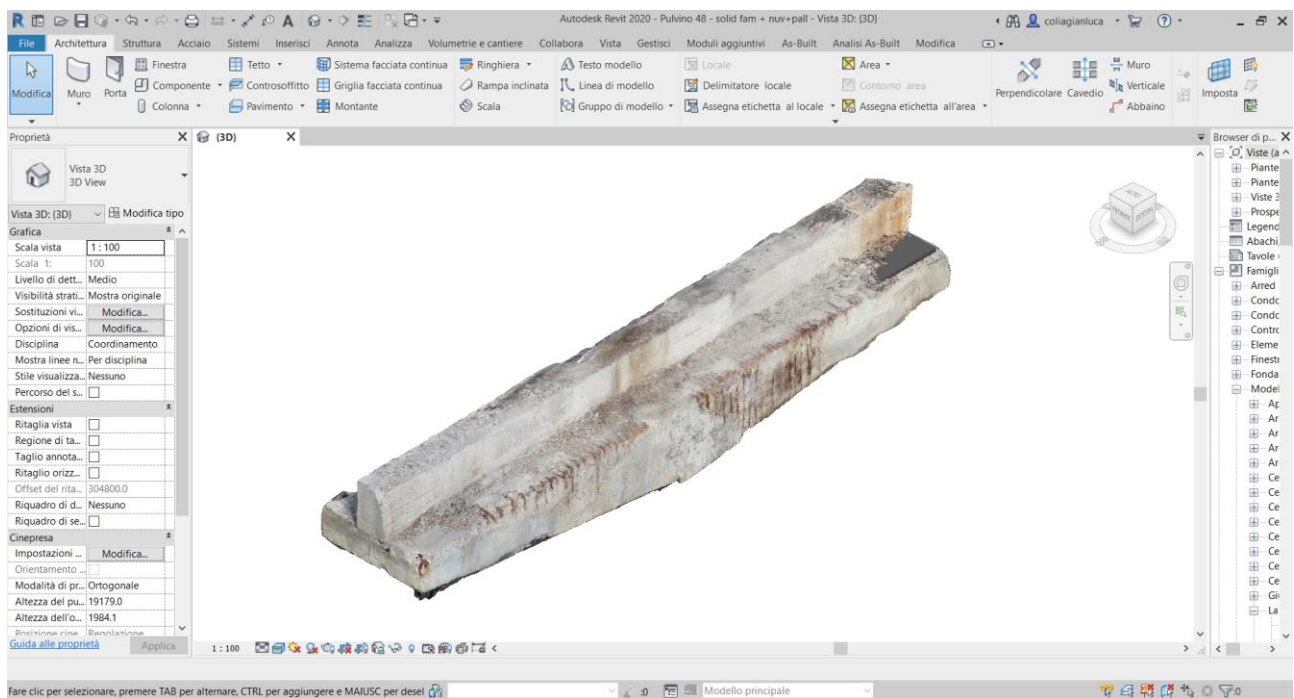


Figure 86. Pier cap with dense point cloud in Revit.

The main problem of having a 3D model on which a point cloud is superimposed is that no matter how dense this point cloud is, it will never be similar to a surface.

In reality, if the zoom level is low enough then it is possible to confuse a dense point cloud with a contiguous surface, but if the zoom level increases then it is possible to observe that there will be many points close together, that do not constitute a surface.

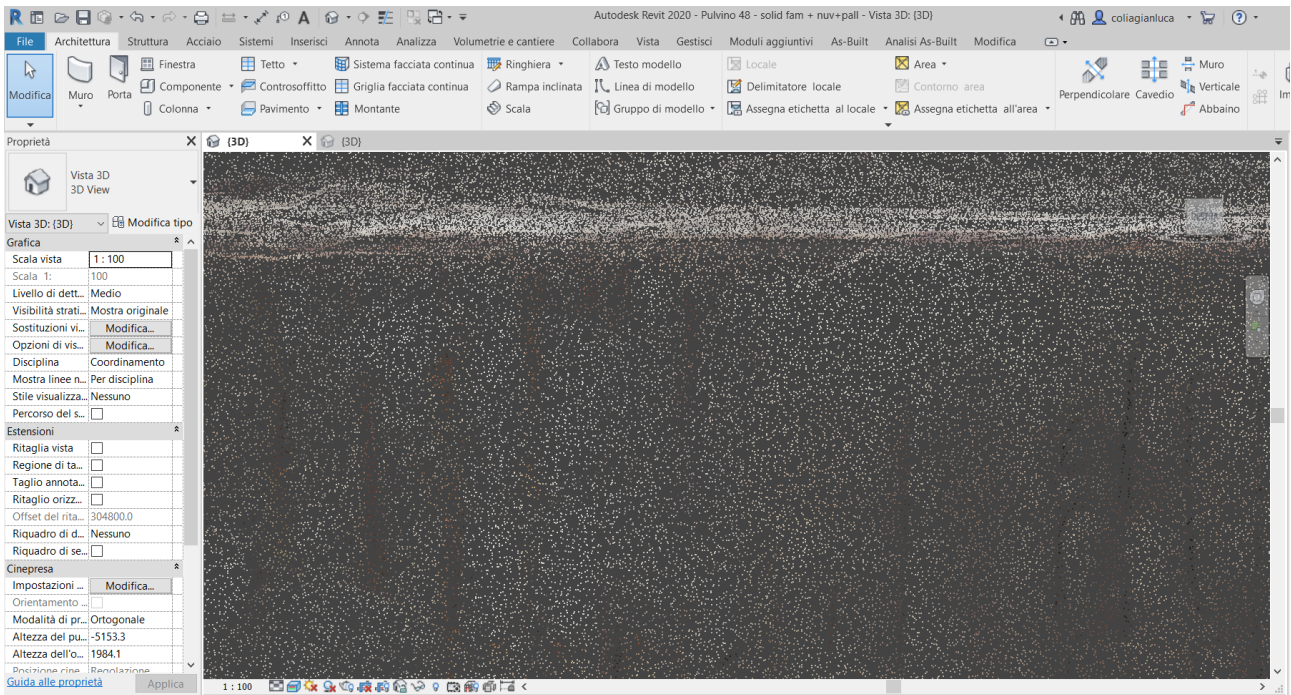


Figure 87. High zoom level.

So if you have to monitor damages that have a reduced extension, such as micro-cracks or micro-areas of humidity, and you want to do it simply by viewing a dense cloud, you could making relevant errors and there is also the possibility that the damage would not be possible to detect.

With this in mind, the research work focused on identifying a workflow through which the identification of damage can be carried out automatically and quickly with respect to the mesh-to-BIM methodology.

The workflow is characterized by the use of CloudCompare software, in which we have the mesh of the 3D object and where it is possible to do a damage inspection and identify points that can be exported in .txt format. In the Revit software, on the other hand, we have the pier cap model modelled in Revit in which the point cloud has been superimposed. the two software communicate through the use of Dynamo, where through a code based on the Python programming language, it is possible to import the points from the mesh into CloudCompare and through a user interface, position them on the pier cap model in Revit.

5.3.1 Mesh generation in CloudCompare

After importing the pier cap point cloud from the Agisoft Metashape software with .e57 format into CloudCompare, it is possible to reconstruct the mesh through the use of some tools in the software.

In particular, the “compute normals” tool was used which is a new algorithm through which it is possible to calculate the normals based on the scanning grids, thus estimating the local surface represented by a point and adjacent points. The noise level, in number and distance of neighbouring points affects the appearance of this surface and in this case 2D triangulation was chosen as the modelling of the local surface.

Subsequently, to generate the surface, the “PoissonRecon” plug-in was used. This plug-in consists of an interface where there are several clear parameters that have a precise definition. The main parameter is "octree depth", so as the depth increases, the resolution of the result increases, with an increase in the size of the mesh file but also in computational time.

Finally, after generating the mesh, it is possible, through the use of a scalar field filter, to reduce the extensions of the output mesh in order to obtain a surface as similar as possible to the shape and size of the input cloud.

The final output is the generation of the following mesh.

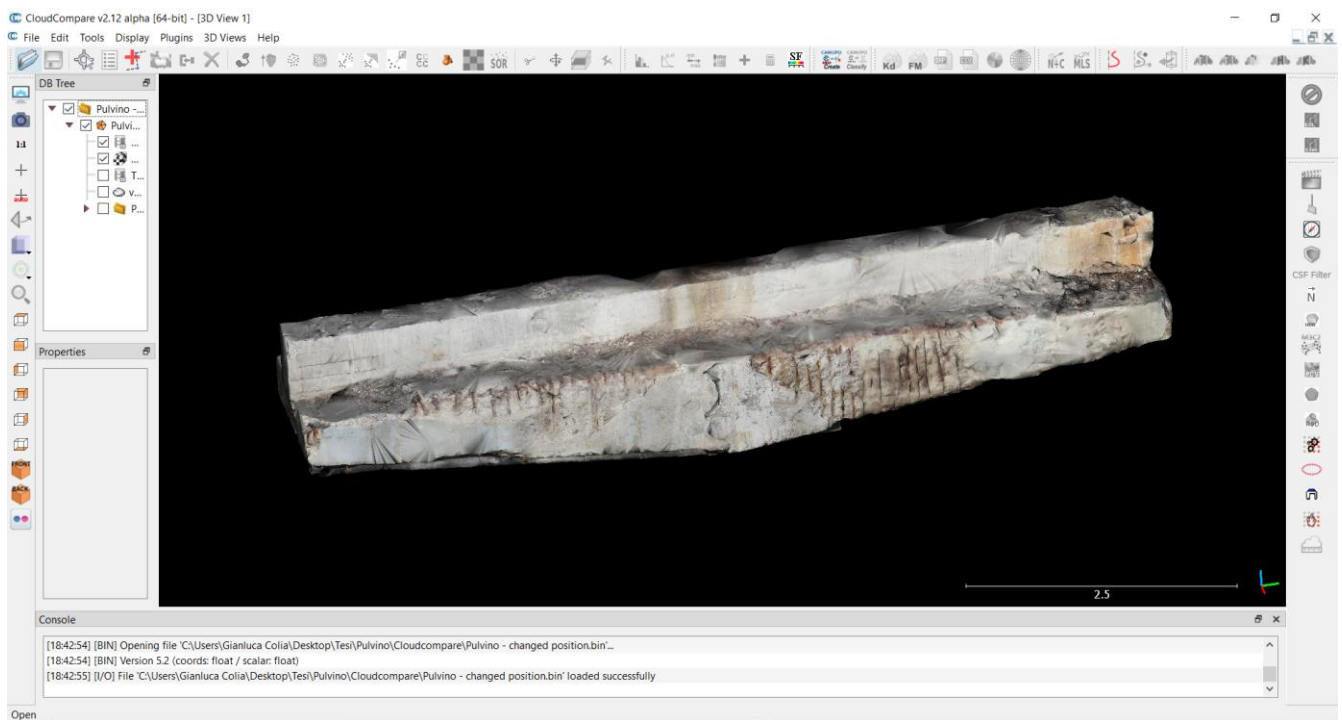


Figure 88. Mesh generated in CloudCompare.

After generating the mesh, we moved on to identifying the damage present on the pier cap by inserting points with the "Point list picking" tool. This tool allows you to select different points on a point cloud or mesh in order to generate a list of points that can be exported as a file, a new cloud or a polyline connecting the points.

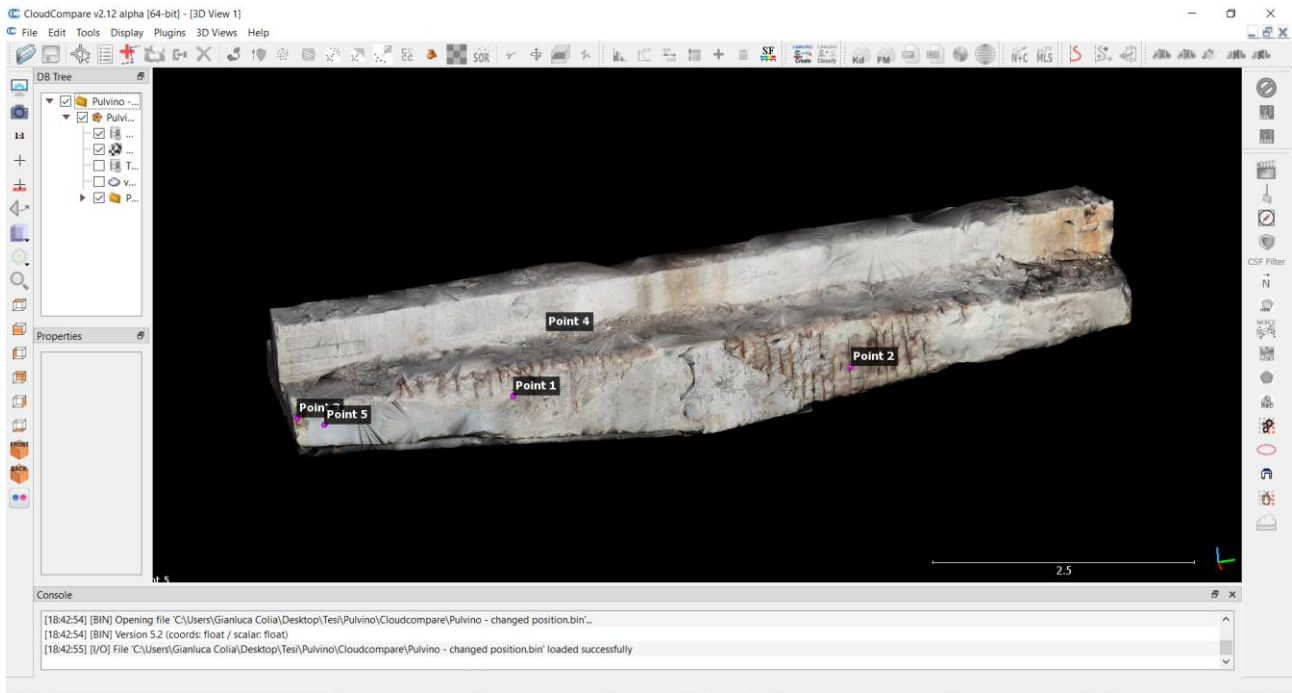


Figure 89. Mesh with selected points.

The list can then be exported as a file:

- x,y,z
- local index, x, y, z
- global index, x, y, z
- label name, x, y, z
- new cloud
- new polyline

In this case, the identified points are exported as label name, x, y, z, in .txt format because it is necessary to have the information linked to the numbering of the various points identified as well as their spatial coordinates, and then place them in automatic way in Revit through the use of Dynamo.

The exported points are as follows:

- Point 1, -9.266113281250,8.202177047729, -0.101557590067
- Point 2, -9.304108619690,11.468873977661, -0.347780972719
- Point 3, -9.295166015625,6.116762638092, -0.008361082524
- Point 4, -10.773661613464,8.785569190979, -0.274550259113
- Point 5, -9.225783348083,6.363213539124, -0.085119478405

5.3.2 Dynamo Code

Dynamo is an open-source programming software, based on the Python programming language, which can be started directly from the Revit software.

It is a tool based on visual programming, better recognized as Visual programming Language (VPL), which has the purpose of carrying out analyses or generating algorithms to represent a logical workflow.

Through visual programming it is possible to establish visual, systematic but also geometric relationships between the different parts of a project. These relationships are also called workflows, which translate into algorithms developed by ourselves, obtaining a useful result in the subsequent phases of the project.

Basically, a Dynamo code consists of two entities, the nodes and the threads. Nodes are the objects connected to form a visual program and therefore each node contains within it a Python code that performs a certain function. A node can represent a simple function such as storing a number or it can also be a more complex action such as creating geometry.

There are several nodes in dynamo and there is also the possibility of creating new ones, being an open-source software. In particular, except for the input nodes, most of the nodes present in dynamo consist of five parts:

- Name: The node name with a category. Name naming convention.
- Main: the main body of the node
- Doors: are the receivers of incoming or outgoing files that provide the node input or output data.
- Link icon: indicates the link option specified for the corresponding list inputs.
- Default value: some nodes have default values that can be used or not.

The main function of the wires is to calculate the nodes by establishing a workflow of the visual program, in fact you can think of the wires literally as electrical wires that transmit impulses of data from one object to the next.

They connect an output from a node, also called a port on the right of the node, with an input, also called a port on the left, of another node, thus generating a workflow that generally moves from left to right.

In the following research work, a dynamo code has been written which, starting from the .txt file exported by CloudCompare, generates user interfaces thanks to which, in addition to positioning the various points, attributes information to them, thus making a classification of the damage.

The first step to be carried out was to import the points identified in Dynamo. In this piece of code, the following nodes were used:

- File path: allows you to select a file within a memory, importing it into dynamo.
- FileSystem.ReadText: Reads a text file and returns the contents as a string
- String.Split: Splits a single string into a list of strings, at a separator, such as a comma.
- List.count: returns the number of items stored in the given list
- List.GetItemAtIndex: returns an item from the given list, located at the specified index.
- String.ToNumber: Converts a string to an integer or a Double value
- Point.ByCoordinates: defines a point consisting of three coordinates, that is the coordinates coming from the CloudCompare software.

The Group has been renamed "IMPORT POINTS", and is the following part of the code:

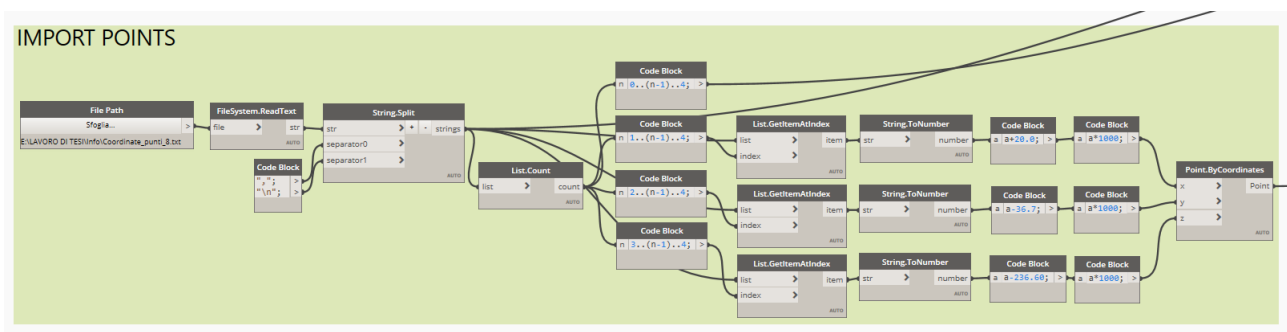


Figure 90. Import points code.

After importing the points into dynamo, a code was written that would create a user interface that would allow the user to indicate detailed information at each point, in order to carry out a real classification. In this part of the code, the following nodes were used:

- DropDown Data: this node allows the creation of a dropdown input which can then be selected by the user
- Textbox Data: add a text box by inserting a form. This creation method allows you to set the text box label, defining the default value.
- Damage Inteface: this node ultimately generates the first interface

The group has been renamed "FIRST DAMAGE INTERACE", and is the following piece of code

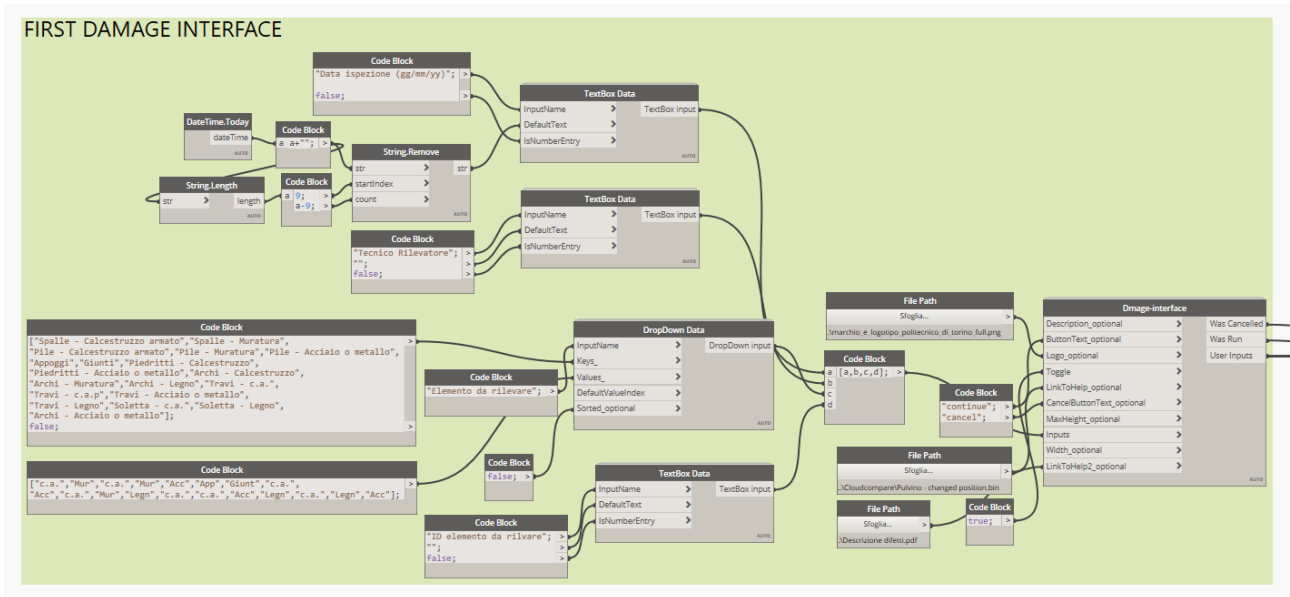


Figure 91. First damage interface code.

The screenshot shows the 'Damage Interface' dialog box with the following elements:

- Title Bar:** 'Damage Interface' with a close button (X).
- Input Fields:**
 - 'Data ispezione (gg/mm/yy)': A text input field.
 - 'Tecnico Rilevatore': A text input field.
 - 'Elemento da rilevare': A dropdown menu with a downward arrow.
 - 'ID elemento da rilevare': A text input field.
- Footer:**
 - Logo of Politecnico di Torino (1859).
 - 'cancel' and 'continue' buttons.
 - Two blue hyperlinks: [See CloudCompare model](#) and [See Defects description](#).

Figure 92. First damage interface.

It is possible to observe that in this interface it is necessary to fill in the boxes where the following data must be entered:

- Inspection date
- Detector Technician
- Element to be detected: Shoulders - Reinforced concrete, Shoulders - Masonry, Piles - Reinforced concrete, Piles - Masonry, Piles - Steel or metal, Bearings, Joints, Abutments - Concrete, Abutments - Steel or metal, Arches - Concrete, Arches - Masonry "
- Item ID to be detected.

Furthermore, it is possible to observe that there are two links:

- See CloudCompare model: allows you to open meshes of the element to be monitored directly in CloudCompare. The link is based on a Filepath node.
- See Defects description: allows you to open the pdf attached to the guidelines for monitoring existing bridges, or the defect sheets that report the description of the degradation phenomena to be detected during the inspection and the criteria for identifying the parameters to be assigned.

After indicating this information, we proceed with writing a code that generates a second interface where the user must enter additional parameters. In this part of the code, the following nodes were used:

- DropDown Data: its description has already been made previously
- List.Flatten: This node transforms a list of lists into a one-dimensional list.
- Damage: node that ultimately generates the second interface.

As input for the List.Flatten node a Code Block was used where through a string all the inputs that are supplied to the Damage-interface node are summarized, that is:

- Point in the cloud appears
- Damage to be detected
- Extension - K1: It can have values of 0.2, 0.5 or 1. Generally, 0.2 is applied if the defect is weakly present, 0.5 if it is present in more than 50% of the surface or 1 if on the complete surface, but its meaning can change depending on the type of damage.
- Intensity - K2: Can have values of 0.2, 0.5 or 1. Its values change based on the size of the damage from 0.2 being the smallest and 1 being the largest. Its meaning varies according to the type of damage.
- Static Prejudice: yes / no
- Comments
- Face: it is necessary to indicate on which face the point to be inserted is located in a manner congruent with the cube present in Revit, therefore right, left, back, front, top, bottom.

The group has been renamed "SECOND DAMAGE INTERACE", and is the following piece of code

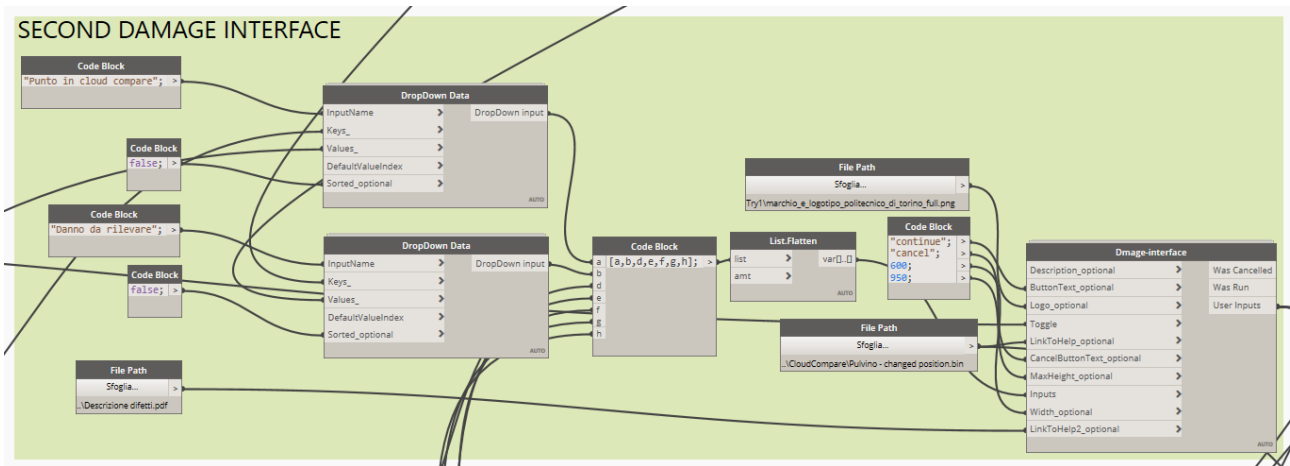


Figure 93. Second damage interface code.

Figure 94. Second damage interface.

Also, in this interface the two links “See CloudCompare model” and “See deflection description” have been inserted.

The points were then imported into revit and are identified by a line and a dot created as a Revit family.

Describe the label family and how the radii and color changes depending on the parameters

By clicking on the label, all the various information entered in the step-by-step interface are then shown in the properties.

The code in its entirety looks like this, and the highlighted parts are the relevant code groups discussed above.

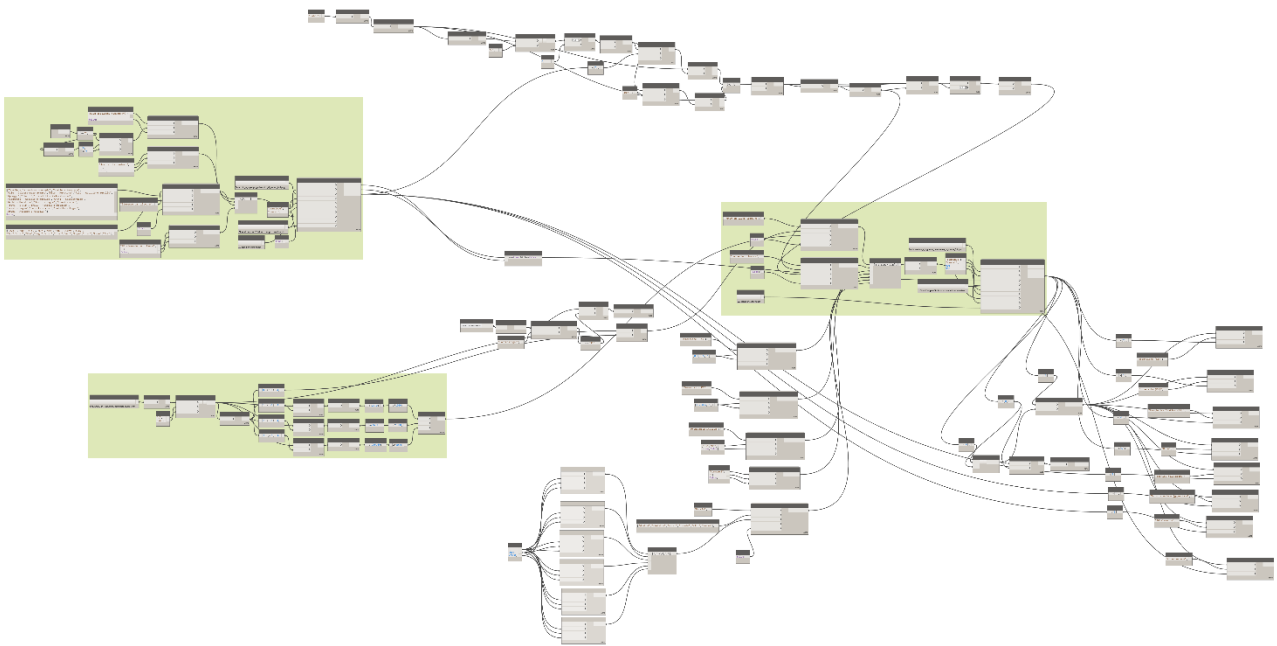


Figure 95. Full dynamo code.

Once the code has been started and the process of placing the points with damage classification has been completed, the final output of the 3D model is as follows.

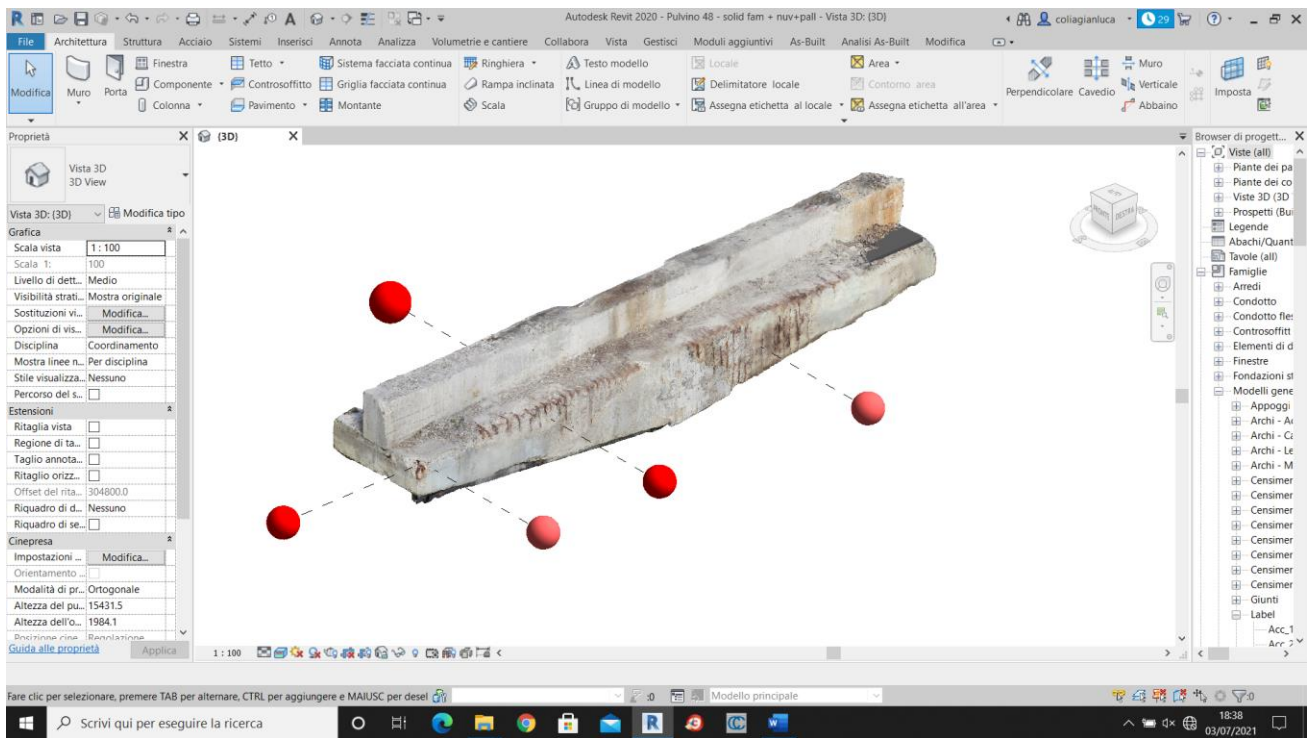


Figure 96. Pier cap with imported points.

Then it is possible to observe the 3D model of the pier cap, on which the corresponding cloud of points has been superimposed, from which lines emerge that connect the points to dots that vary their size and their color, of more or less intense red, based on the severity of the damage.

At the end of this operation done for a pier cap, it was decided to use the same workflow to identify the damage to a bridge span, which will be discussed in the next chapter.

6 STURA BRIDGE

The RA10 km motorway junction connects the city of Turin and the Caselle international airport and has a length of 10.7 km. The Stura bridge is located at the progressive K2 + 800m from the beginning of the road towards Turin - Caselle airport.

The road platform consists of a double carriageway with two lanes for each direction of travel, separated by a central “New Jersey” barrier and laterally confined by a system of flexible barriers.

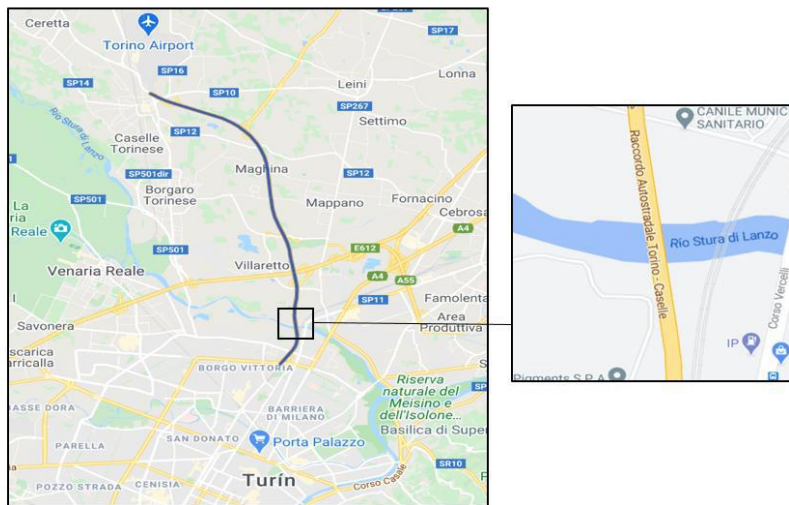


Figure 97. Location of Ponte Stura on the RA10 motorway junction

The Stura bridge has a length of 150 meters and is made up of two separate structures next to each other that support the two carriageways made up of two lanes for both directions.

The bridge has been the subject of various monitoring activities during its useful life, given its strategic importance as it connects the city of Turin with the airport. In 2018, nine wireless multisensors were installed on the bridge pillars, which measure deformations, displacements, inclinations, and temperature in real time.



Figure 98. Sensors installed in 2018. Source: ANAS S.p.A. and SYSDEV – Monitoraggio strutturale di ponti e viadotti.

The goal of the thesis work is to create a database with the information of the damage exposed on the surface, following the level 1 of the new guidelines for existing bridges, through the use of Lidar and photogrammetric techniques.

In particular, for this thesis work we had a dense point cloud in .e57 format coming from a laser scanner survey performed for the first span of the bridge, combined with the dense cloud of points obtained from a survey carried out with a drone of the second span. This data is already available because it was used for a previous thesis work in 2020.

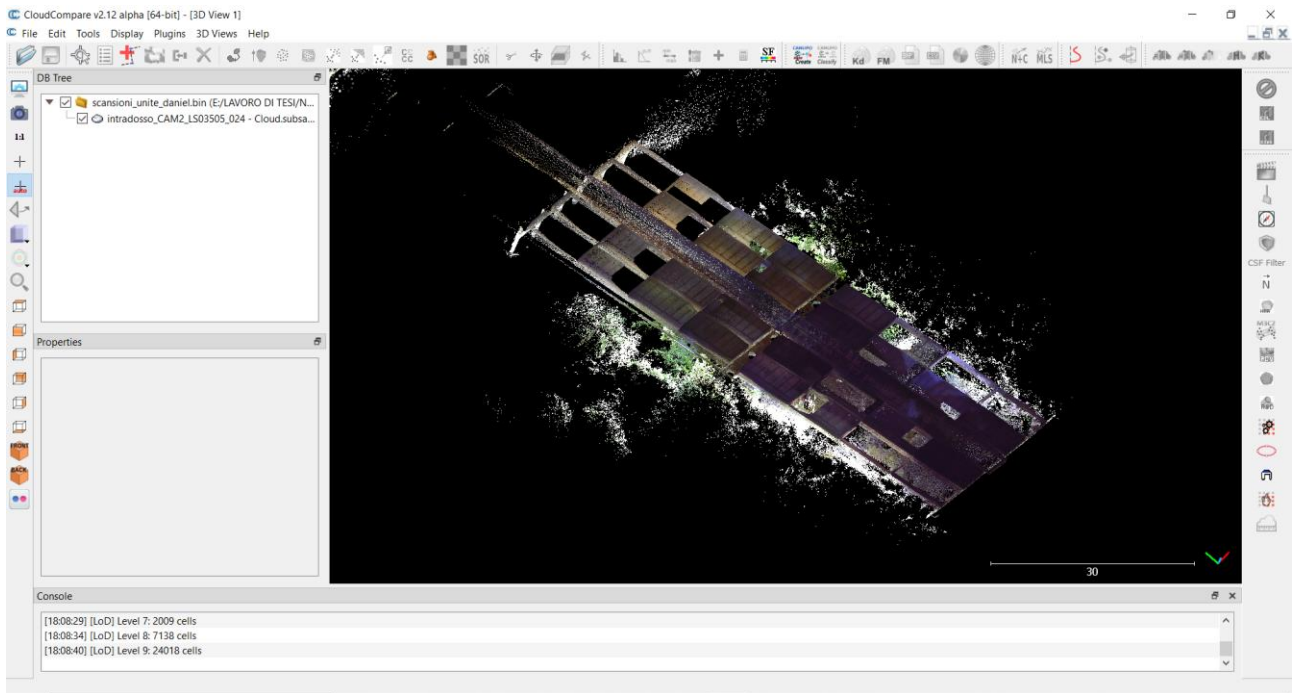


Figure 99. dense point cloud of the span 1 and 2.

The subsequent survey carried out in collaboration with the geomatics team of Politecnico di Torino concerns all the other spans of the bridge, thus carrying out a laser scanner survey for 3 spans of the bridge and a UAV survey for the same number of spans.

In particular, the following surveys were carried out for the different spans of the bridge:

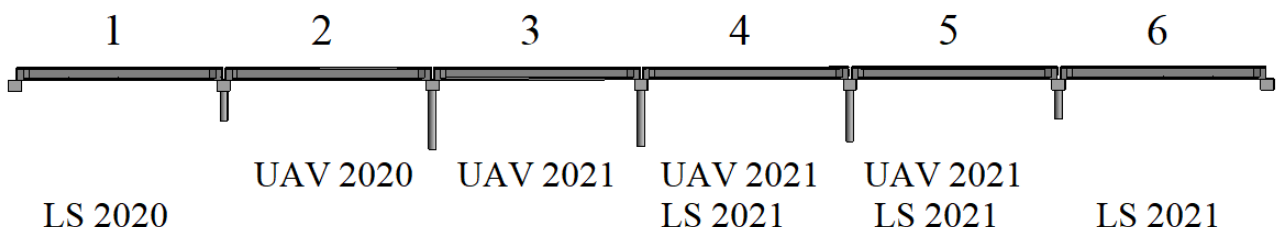


Figure 100. surveys carried out in the years 2020/21.

6.1 Linee guida per la classificazione e gestione del rischio, la valutazione della sicurezza ed il monitoraggio dei ponti esistenti

The guidelines represent a procedure to control the risk related to the safety management of existing bridges and consist of three parts: The census and classification of the risk, the verification of safety and the surveillance and monitoring of bridges.

The risk classification is carried out through a multilevel approach, justified by the number of infrastructures present in the area, which starts from the census of the works and arrives at the determination of a class of attention, on the basis of which the safety check will be carried out.

The levels of analysis that make up the following approach are equal to six and as the level of analysis increases, the degree of depth and complexity increases.

Level 0

A zero-level classification consists in carrying out a census of all the works in the area, describing their main characteristics in geometric, structural and geolocation terms, indicating the road network and the site in which it is inserted.

It is essential to carry out this operation because to create a database of the bridges present in the Italian territory, in order to update the various data following their evolution over time.

In order to carry out the level 0 classification, Annex A "level 0 census forms" is provided through which it is possible to collect the various information.

Schede di censimento ponti di Livello 0



Codice IOP _____

Strada di appartenenza: _____

Nome Ponte/Viadotto _____

Progressiva km iniziale: _____ Progressiva km finale: _____

Localizzazione

Provincia/Regione: _____ Comune: _____ Località: _____ Sismicità dell'area [a _g] (Suolo A, TR = 475 ann) _____	Coordinate Geografiche <input type="radio"/> ETRF2000 <input type="radio"/> WGS84		<table border="1" style="width: 100%; border-collapse: collapse;"> <tr> <td style="width: 10%;">Centro</td> <td>Quota s.l.m. [m]: _____ Longitudine: _____ Latitudine: _____</td> </tr> <tr> <td>Iniziale</td> <td>Quota s.l.m. [m]: _____ Longitudine: _____ Latitudine: _____</td> </tr> <tr> <td>Finale</td> <td>Quota s.l.m. [m]: _____ Longitudine: _____ Latitudine: _____</td> </tr> </table>	Centro	Quota s.l.m. [m]: _____ Longitudine: _____ Latitudine: _____	Iniziale	Quota s.l.m. [m]: _____ Longitudine: _____ Latitudine: _____	Finale	Quota s.l.m. [m]: _____ Longitudine: _____ Latitudine: _____
Centro	Quota s.l.m. [m]: _____ Longitudine: _____ Latitudine: _____								
Iniziale	Quota s.l.m. [m]: _____ Longitudine: _____ Latitudine: _____								
Finale	Quota s.l.m. [m]: _____ Longitudine: _____ Latitudine: _____								

Fenomeni erosivi e di alluvionamento Assenti

Fenomeni franosi Assenti

Già valutati

Già valutati

Da verificare

Da verificare

Informazioni generali

Proprietario _____ Concessionario _____ Ente vigilante _____	Anno di costruzione/ristrutturazione		<table border="1" style="width: 100%; border-collapse: collapse;"> <tr> <th style="font-size: small;">Ultimazione costruzione (collaudo)</th> <th style="font-size: small;">Eventuali interventi sostanziali</th> </tr> <tr> <td><input type="radio"/> Effettivo</td> <td><input type="radio"/> Effettivo</td> </tr> <tr> <td><input type="radio"/> Presunto</td> <td><input type="radio"/> Presunto</td> </tr> </table>	Ultimazione costruzione (collaudo)	Eventuali interventi sostanziali	<input type="radio"/> Effettivo	<input type="radio"/> Effettivo	<input type="radio"/> Presunto	<input type="radio"/> Presunto
Ultimazione costruzione (collaudo)	Eventuali interventi sostanziali								
<input type="radio"/> Effettivo	<input type="radio"/> Effettivo								
<input type="radio"/> Presunto	<input type="radio"/> Presunto								

Figure 101. Pag 1/11 "bridges census cards" ATTACHMENT A. Source: (Linee guida per la classificazione e gestione della sicurezza e il monitoraggio dei ponti esistenti, 2020).

Level 1

A level 1 classification consists in carrying out visual inspections on site of both the extrados and the intrados of the bridge in order to identify the presence of specific degradation phenomena, providing the intensity and extent with which they occur.

To cope with any accessibility or limited inspection of the bridge, it is possible to use geometric measurement instruments or photographic instruments, such as UAVs, in order to carry out remote photographic surveys.

"Defect cards" are provided (ATTACHMENT B) which must be filled in to classify the damage, based on the "defect cards guide" (ATTACHMENT C) where the typical defects of a particular element are reported.

In addition to the defect survey sheets, for each bridge, the inspection description sheet (Annex B) must be filled in with the main characteristics of the structure detected during the visual inspection, such as structural type, type and material of the structural elements, hydro- geomorphological features of the territory, general geometric schemes.

Scheda Ispezione Ponti di Livello 1

1													Spalle N _____ Strada di appartenenza: _____ Progressiva km: _____				
Calcestruzzo													Tecnico rilevatore: _____ Data ispezione: __/__/__				
Codice difetto	Descrizione difetto	visto	G	Estensione K1			Intensità K2			N° foto	PS	NA	NR	NP	Note		
				0,2	0,5	1	0,2	0,5	1								
c.a./c.a.p._1	Macchie di umidità passiva	<input type="checkbox"/>	1	<input type="checkbox"/>			<input type="checkbox"/>	<input type="checkbox"/>	<input type="checkbox"/>								
c.a./c.a.p._2	Macchie di umidità attiva	<input type="checkbox"/>	3	<input type="checkbox"/>			<input type="checkbox"/>	<input type="checkbox"/>	<input type="checkbox"/>								
Dif. Gen_1	Tracce di scolo	<input type="checkbox"/>	3	<input type="checkbox"/>			<input type="checkbox"/>	<input type="checkbox"/>	<input type="checkbox"/>								
c.a./c.a.p._3	Cis dilavato / ammalorato	<input type="checkbox"/>	3	<input type="checkbox"/>			<input type="checkbox"/>	<input type="checkbox"/>	<input type="checkbox"/>								
Dif. Gen_2	Ristagni d'acqua	<input type="checkbox"/>	2	<input type="checkbox"/>			<input type="checkbox"/>	<input type="checkbox"/>	<input type="checkbox"/>								
c.a./c.a.p._4	Vespai	<input type="checkbox"/>	2	<input type="checkbox"/>			<input type="checkbox"/>	<input type="checkbox"/>	<input type="checkbox"/>								
c.a./c.a.p._5	Distacco del copriferro	<input type="checkbox"/>	2	<input type="checkbox"/>			<input type="checkbox"/>	<input type="checkbox"/>	<input type="checkbox"/>								
c.a./c.a.p._6	Armatura ossidata/corrosiva	<input type="checkbox"/>	5	<input type="checkbox"/>		<input type="checkbox"/>	<input type="checkbox"/>	<input type="checkbox"/>	<input type="checkbox"/>								
c.a./c.a.p._7	Lesioni a ragnatela modeste	<input type="checkbox"/>	1	<input type="checkbox"/>			<input type="checkbox"/>	<input type="checkbox"/>	<input type="checkbox"/>								
c.a./c.a.p._8	Fessure orizzontali	<input type="checkbox"/>	2	<input type="checkbox"/>			<input type="checkbox"/>	<input type="checkbox"/>	<input type="checkbox"/>								
c.a./c.a.p._9	Fessure verticali	<input type="checkbox"/>	2	<input type="checkbox"/>			<input type="checkbox"/>	<input type="checkbox"/>	<input type="checkbox"/>								
c.a./c.a.p._10	Fessure diagonali	<input type="checkbox"/>	5	<input type="checkbox"/>		<input type="checkbox"/>	<input type="checkbox"/>	<input type="checkbox"/>	<input type="checkbox"/>								
c.a./c.a.p._11	Lesioni attacco pilastri (spalle a telaio)	<input type="checkbox"/>	3	<input type="checkbox"/>			<input type="checkbox"/>	<input type="checkbox"/>	<input type="checkbox"/>								
c.a./c.a.p._12	Riprese successive deteriorate	<input type="checkbox"/>	1	<input type="checkbox"/>			<input type="checkbox"/>	<input type="checkbox"/>	<input type="checkbox"/>								
Dif. Gen_3	Danni da urto	<input type="checkbox"/>	4	<input type="checkbox"/>		<input type="checkbox"/>	<input type="checkbox"/>	<input type="checkbox"/>	<input type="checkbox"/>								
Dif. Gen_6	Fuori piombo	<input type="checkbox"/>	5	<input type="checkbox"/>		<input type="checkbox"/>	<input type="checkbox"/>	<input type="checkbox"/>	<input type="checkbox"/>								
Ril/Fond_1	Scalzamento	<input type="checkbox"/>	5	<input type="checkbox"/>		<input type="checkbox"/>	<input type="checkbox"/>	<input type="checkbox"/>	<input type="checkbox"/>								
Ril/Fond_2	Dilavamento del rilevato	<input type="checkbox"/>	1	<input type="checkbox"/>			<input type="checkbox"/>	<input type="checkbox"/>	<input type="checkbox"/>								
Ril/Fond_3	Dissesto del rilevato - deformazioni	<input type="checkbox"/>	2	<input type="checkbox"/>			<input type="checkbox"/>	<input type="checkbox"/>	<input type="checkbox"/>								
Ril/Fond_4	Dissesto del rilevato - stabilità	<input type="checkbox"/>	4	<input type="checkbox"/>		<input type="checkbox"/>	<input type="checkbox"/>	<input type="checkbox"/>	<input type="checkbox"/>								
Ril/Fond_5	Movimenti di fondazione	<input type="checkbox"/>	5	<input type="checkbox"/>		<input type="checkbox"/>	<input type="checkbox"/>	<input type="checkbox"/>	<input type="checkbox"/>								
c.a./c.a.p._13	Lesioni da schiacciamento	<input type="checkbox"/>	4	<input type="checkbox"/>			<input type="checkbox"/>	<input type="checkbox"/>	<input type="checkbox"/>								
Dif. Gen_4	Lesioni caratteristiche zone appoggio	<input type="checkbox"/>	3	<input type="checkbox"/>			<input type="checkbox"/>	<input type="checkbox"/>	<input type="checkbox"/>								
Eventuali note																	

Figure 102. Page 2/24 "defect cards" ATTACHMENT B. Source: (Linee guida per la classificazione e gestione della sicurezza e il monitoraggio dei ponti esistenti, 2020).

If the defect in the list has not been identified in the structure then it must be reported using the box:

- NA if the defect is not applicable to the type of artifact to the element under examination
- NR if the defect is not detectable by visual inspection
- NP if the defect is not present

In the column "N ° photos" it is necessary to report the number of photos taken to the specific defect that must be catalogued and numbered. Each sheet also contains a space to indicate any notes and observations.

Schede difettologiche					N° difetto: c.a./c.a.p._1			
Macchie di umidità passiva								
Peso del difetto								
G = 1	G = 2	G = 3	G = 4	G = 5	Estensione k ₁	0,2 (appena presente)	0,5 (~50% superficie)	1 (~tutta la superficie)
					Intensità k ₂	Sempre = 1		
Descrizione								
<p>Il difetto si presenta con aree di colorazione diversa dal materiale integro. In particolare, si tratta di tracce di calcio rilasciate sulla superficie dall'umidità penetrata attraverso il calcestruzzo. Si parla di macchie di umidità passiva qualora il fenomeno si intende estinto e del quale restano macchie di colore biancastro.</p>								
Cause								
<p>La penetrazione di umidità e di acqua meteorica attraverso il materiale è favorita in presenza di:</p> <ul style="list-style-type: none"> - materiali caratterizzati da elevata porosità - mancanza o carenze nel sistema di impermeabilizzazione - sistemi di convogliamento delle acque assenti, inadeguati o danneggiati - Imperfetta tenuta dei giunti - Scossaline assenti o deteriorate 								
Fenomeni di degrado correlati								
<p>Il progredire di tale fenomeno di degrado potrebbe comportare l'innescarsi di fenomeni di dilavamento e di ammaloramento del calcestruzzo. Tale difetto è diverso da altri fenomeni, quali le tracce di scolo, dovuti a scorrimenti superficiali di acqua.</p>								

Figure 103. Page 31/131 "defect cards" ATTACHMENT C. Source: (Linee guida per la classificazione e gestione della sicurezza e il monitoraggio dei ponti esistenti, 2020).

The various damages are reported in the defect cards guide and each of them is associated with a G weight ranging from 1 to 5, as the G weight increases, the severity of the defect increases. For defects that have a weight of G = 4 or G = 5, it is necessary to report whether this defect involves the static damage of the work (box PS).

After identifying the defect, two coefficients must be assigned to it:

- K1: represents the extension and is between 0.2 and 1
- K2: represents the intensity and is between 0.2 and 1.

Level 2:

A level 2 classification consists in the analysis of relevant risks, through the Attention Class (BoD), based on the information obtained at the previous levels.

The classes of attention are identified based on the simplified assessment of the hazard, exposure and vulnerability of the single bridge taking into account the information from level 0 and level 1.

In particular, the guideline provides for 5 classes of attention:

- High Class
- Upper-middle class
- Middle Class
- Lower-Middle Class
- Low Class

On the basis of the attention class, the actions to be taken are identified following the following table.

This level is not further described as its application does not take part in this thesis work.

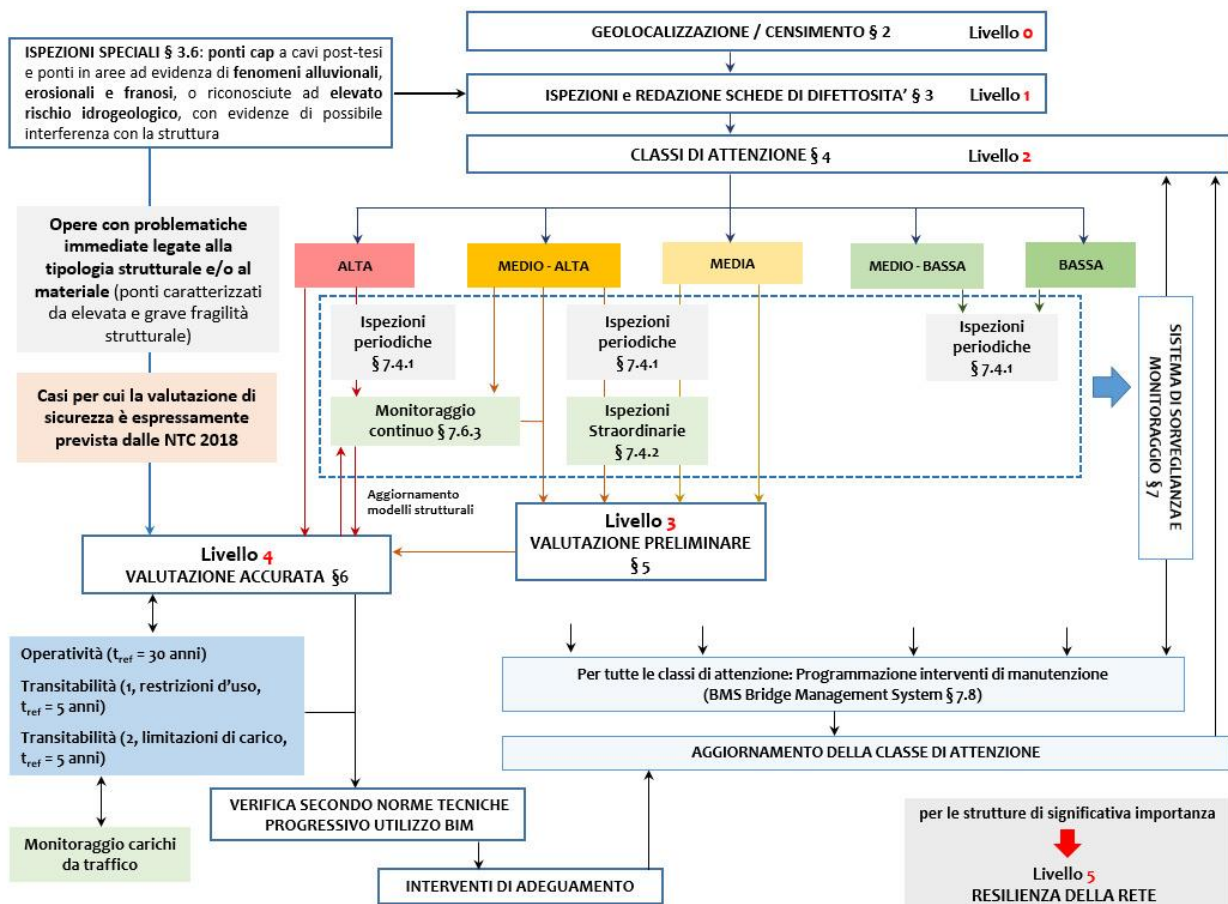


Figure 104. Multilevel approach and relationships between levels of analysis. Source: (Linee guida per la classificazione e gestione della sicurezza e il monitoraggio dei ponti esistenti, 2020).

Level 3

A level 3 classification consists of a more accurate assessment of the defects identified in the level 1 classification, analysing them in greater detail and identifying the possible causes.

Subsequently, it is necessary to preliminary estimate the resources guaranteed by the standards used at the time of the design of the work with respect to the current regulations.

This operation can be carried out by comparing the demand induced on the various structural elements that make up the bridge based on the traffic loads provided for by the regulations of the time, with the demand obtained using the traffic loads provided for by the regulations in force.

By making the relationship between the stresses induced by the design loads and those induced by the loads envisaged by current regulations, it is possible to make a preliminary estimate of the minimum resources guaranteed by the bridge, on the basis of which accurate level 4 assessments must then be performed.

This level is not further described as its application does not take part in this thesis work.

$M_{max,1933}$	$M_{max,2018}$	$M_{max,1933}/ M_{max,2018}$
1319 kNm	2217 kNm	0.59

Figure 105. Example of bending stress relationship calculated with the Normale n.8 of 1933 and the D.M. 17.01.2018. Source: (Linee guida per la classificazione e gestione della sicurezza e il monitoraggio dei ponti esistenti, 2020).

Level 4

A level 4 classification must be carried out for bridges that received a high BOD during the level 2 classification, or for bridges whose level 3 analysis highlighted certain criticalities

In this phase, a more complete analysis is carried out by carrying out more accurate structural checks on the basis of the existing NTC18 legislation, as is the case with any existing building or structure.

The role of knowledge in this phase is fundamental because as the knowledge of the building increases, the uncertainty related to the evaluation of loads, behaviour of materials and structures decreases. To increase the level of knowledge it is necessary to increase the diagnostic campaign, in order to create more accurate structural models.

This level is not further described as its application does not take part in this thesis work.

Level 5

It is not covered in the current guidelines as it refers to bridges of particular importance on the road network and a more refined specific study should be applied.

6.2 Laser scanner data processing with FARO SCENE

The point clouds acquired by laser scanner technology have been processed and georeferenced through the FARO SCENE software, which is a program associated with the laser scanner used.

Starting from the acquired point clouds, a complete point cloud of the 3 spans detected by this technology was obtained, in particular the following scans in .fls format were processed:

- Sixth span: Stura_scan003 - Stura_scan004 - Stura_scan005 - Stura_scan006 - Stura_scan007 - Stura_scan008 - Stura_scan009 - Stura_scan010 - Stura_scan011
- Fifth span: Stura_scan012 - Stura_scan013 - Stura_scan014 - Stura_scan015 - Stura_scan016 - Stura_scan017 - Stura_scan018 - Stura_scan019
- fourth span: - Stura_scan020 - Stura_scan021 - Stura_scan022 - Stura_scan023

The FARO SCENE software provides various functions, such as the positioning and registration of scans, the creation of colour scans and the export of point clouds in different formats, a fundamental function to then join the point cloud generated through this software, with the point cloud coming from the drone data processing.



Figure 106. laser scanner used for the survey of the Stura bridge

6.2.1 Creating a project and importing scans

After starting the software, you can create a new project by selecting the destination folder and the name of the project.

After having generated a new project, which in this thesis work was referred to as "first4scansions", the scans acquired with the laser scanner must be imported by dragging and dropping the .fls files into the work area.

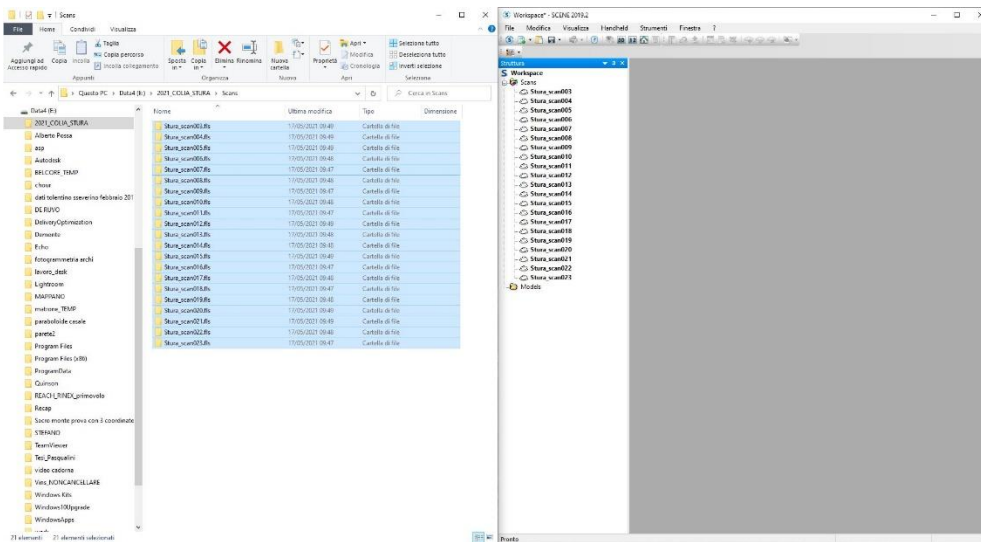


Figure 107. Drag & Drop

After importing the scans, you need to load the scans by clicking the "load all scans" option, or by selecting the "quick view" option, which in addition to loading the points also allows us to view the image.

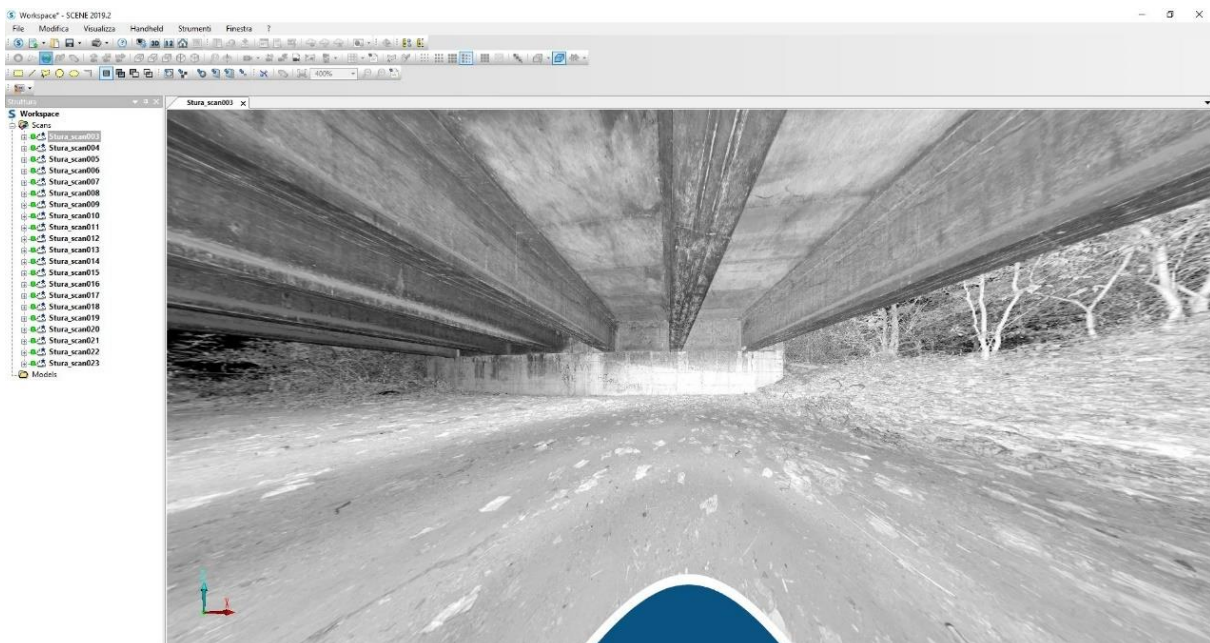


Figure 108. quick view Stura_scan003

6.2.2 Registration of scans

Once the scans have been imported into the software, they must be georeferenced, that is, their position in the global reference system must be found.

Each scan is carried out in a different point than the others, so each scan corresponds to a local reference system that originates at the point where the laser pulse hits the internal mirror of the instrument.

Consequently, the first step to be carried out is to pass from a local reference system, relative to the single scan, to a global reference system, therefore relative to the earth's surface.

To carry out this operation, the coordinates of all the points in .csv format that make up the detail network, equal to 327 points, renamed by the software as "References", were imported into Scenes via Drag & Drop.

N001	397401,03459	4996434,41641	223,81919
N002	397395,88078	4996434,71767	221,91613
N003	397392,39196	4996436,02167	225,72966
N004	397400,08260	4996434,83446	228,02229
N005	397388,26378	4996436,20062	222,86293
N006	397386,31766	4996436,81650	224,42211
N007	397385,76351	4996436,85348	226,84638
N008	397381,27358	4996437,63834	225,17554

.....

N319	397386,76474	4996544,93384	226,48995
N320	397382,29154	4996545,45394	224,97908
N321	397377,40920	4996546,12944	225,73556
N322	397376,47966	4996546,25214	225,20431
N323	397370,03457	4996547,16775	224,45212
N324	397368,47177	4996524,52763	226,42066
N325	397374,67801	4996520,43670	226,73950
N326	397376,69990	4996546,21697	224,58506
N327	397370,55879	4996547,08519	224,93561

Figure 109. References imported.

Two methodologies were followed to place the scans, namely placement by shape and placement based on markers or natural points.

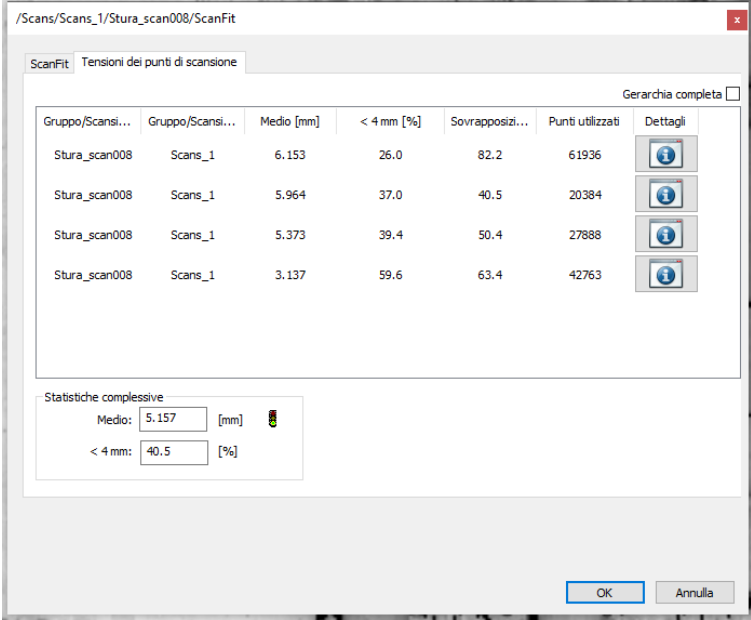
Placement of scans by shape

The software automatically places the scans in space according to the shape of the point clouds coming from the different scans, which will be similar in the common points of the different scans. To carry out this operation, it is necessary to set the scan mode "from cloud to cloud", assigning further parameters.

In a first phase it is advisable to carry out this operation for the scans that are actually close in space and which consequently have points in common such as to be able to overlap them in shape.

After carrying out this operation, it is possible to check the quality of the alignment by analysing the properties of the ScanManager which reports the discrepancy in mm of positioning between two adjacent scans.

For example, the following shows this operation, however, carried out for the first four scans, with the related errors which are of the order of 5 mm.



The screenshot shows the ScanFit software interface with a table titled "Tensioni dei punti di scansione". The table has the following columns: Gruppo/Scansi..., Gruppo/Scansi..., Medio [mm], < 4 mm [%], Sovrapposizi..., Punti utilizzati, and Dettagli. There are four rows of data, each representing a scan. Below the table, there is a section for "Statistiche complessive" with input fields for "Medio" (5.157 [mm]) and "< 4 mm" (40,5 [%]).

Gruppo/Scansi...	Gruppo/Scansi...	Medio [mm]	< 4 mm [%]	Sovrapposizi...	Punti utilizzati	Dettagli
Stura_scan008	Scans_1	6.153	26.0	82.2	61936	[Info]
Stura_scan008	Scans_1	5.964	37.0	40.5	20384	[Info]
Stura_scan008	Scans_1	5.373	39.4	50.4	27888	[Info]
Stura_scan008	Scans_1	3.137	59.6	63.4	42763	[Info]

Statistiche complessive
Medio: 5.157 [mm]
< 4 mm: 40,5 [%]

Figure 110. cloud-to-cloud point errors

Placement of scans based on natural points

To carry out the alignment, natural points, that are part of a detailed network of a georeferenced topographic survey, were used. The global reference system used is WGS 84 / UTM zone 32N (EPSG :: 326332)

By assigning their coordinates in the global reference system to natural points, it is possible to roto-translate scans from the local reference system to the global reference system.

To place a georeferenced point, the "Rectangular selector" command was used and its center was subsequently recorded as the "midpoint".



Figure 111. natural point 5/327

For each scan it is necessary to identify at least 3 natural points, because it is necessary to perform a roto-translation in space. To improve the accuracy of the placement of scans in space in this thesis work, the following natural points were placed for the different scans:

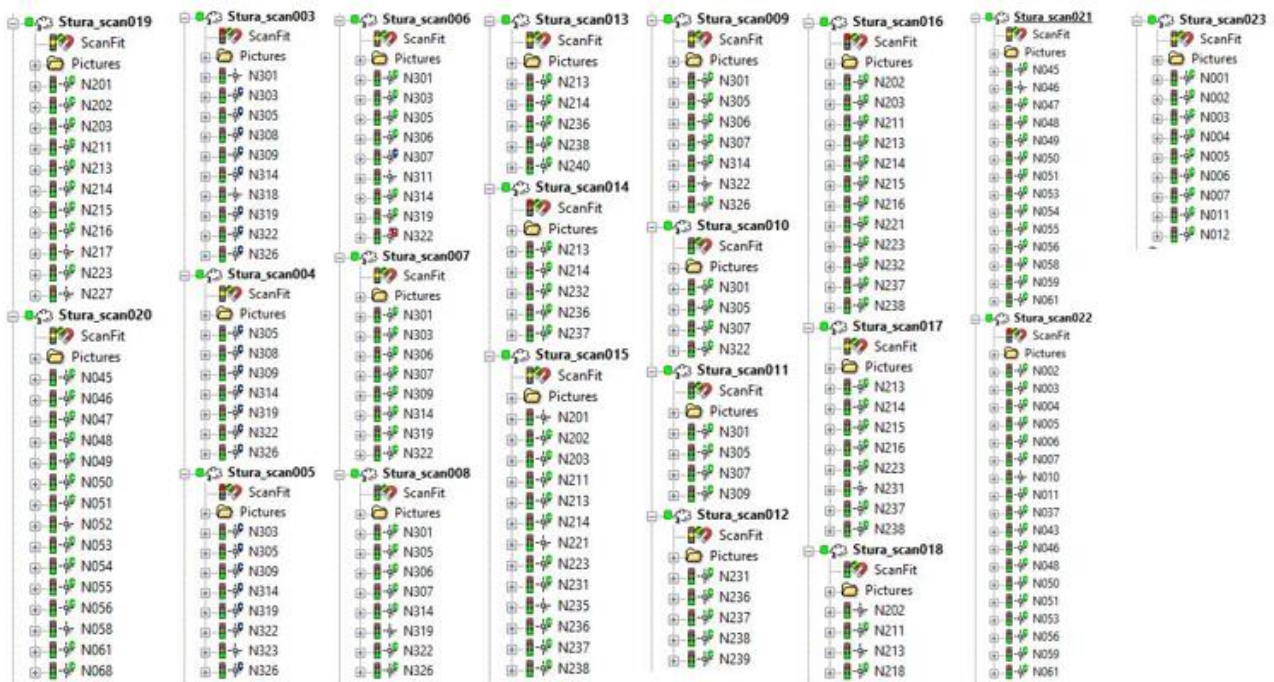


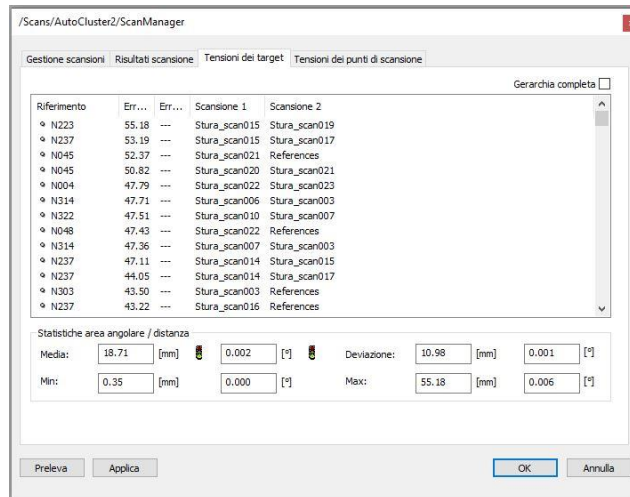
Figure 112. Natural points collimated for each scan

After placing by shape and placing the natural points, a placement of the scans with “Target Based” Placement Mode was also performed.

6.2.3 Results obtained and target error

To check the correct positioning of the scans, it is necessary to analyse the “Scan Results” tab, where it is possible to check the error of the Targets and eliminate those that have distances greater than the pre-set tolerance.

The following average error of 1.8 cm was obtained after several iterations.



The screenshot shows the 'Tensioni dei target' tab in the ScanManager software. It displays a table of target data and statistical values.

Riferimento	Err...	Err...	Scansione 1	Scansione 2
N223	55.18	---	Stura_scan015	Stura_scan019
N237	53.19	---	Stura_scan015	Stura_scan017
N045	52.37	---	Stura_scan021	References
N045	50.82	---	Stura_scan020	Stura_scan021
N004	47.79	---	Stura_scan022	Stura_scan023
N314	47.71	---	Stura_scan006	Stura_scan003
N322	47.51	---	Stura_scan010	Stura_scan007
N048	47.43	---	Stura_scan022	References
N314	47.36	---	Stura_scan007	Stura_scan003
N237	47.11	---	Stura_scan014	Stura_scan015
N237	44.05	---	Stura_scan014	Stura_scan017
N303	43.50	---	Stura_scan003	References
N237	43.22	---	Stura_scan016	References

Statistiche area angolare / distanze					
Media:	18.71 [mm]	0.002 [°]	Deviazione:	10.98 [mm]	0.001 [°]
Min:	0.35 [mm]	0.000 [°]	Max:	55.18 [mm]	0.006 [°]

Figure 113. Tension of the target.

After verifying that the target errors were below the predetermined tolerance values, it was possible to merge the point clouds from the different scans.

The images below show the 3 bridge spans detected through laser scans, in particular the following scans were performed for the three spans:

- Sixth span: Stura_scan003 - Stura_scan004 - Stura_scan005 - Stura_scan006 - Stura_scan007 - Stura_scan008 - Stura_scan009 - Stura_scan010 - Stura_scan011

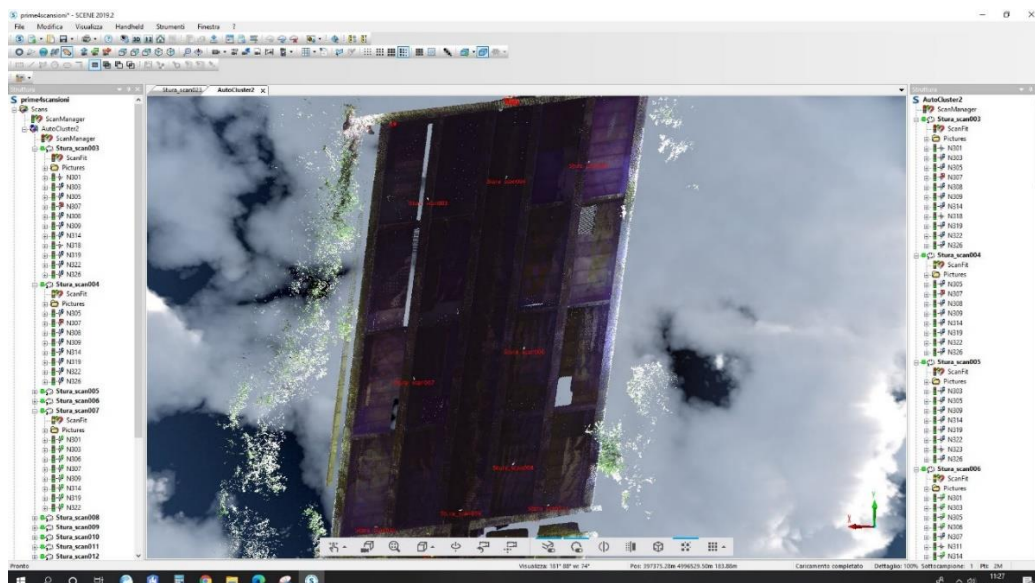


Figure 114. first span scans

- Fifth span: Stura_scan012 - Stura_scan013 - Stura_scan014 - Stura_scan015 - Stura_scan016 - Stura_scan017 - Stura_scan018 - Stura_scan019

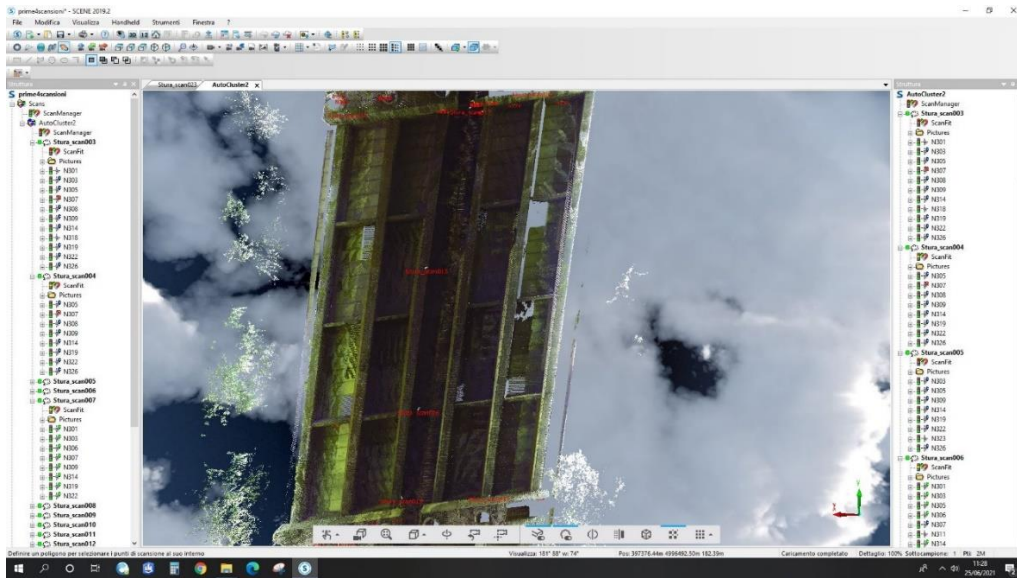


Figure 115. second span scans

- fourth span: - Stura_scan020 - Stura_scan021 - Stura_scan022 - Stura_scan023

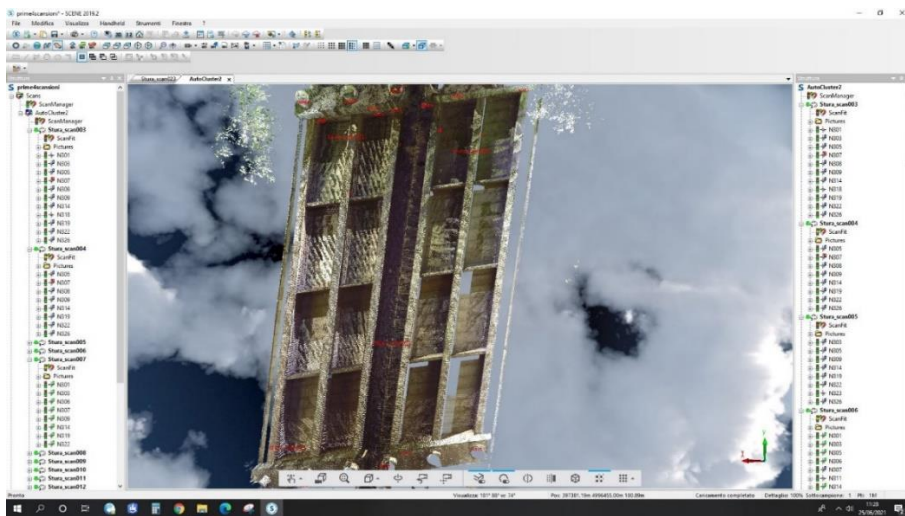


Figure 116. Third span scans

In the following image it is also possible to observe the points in which the laser scanners were placed and therefore from which the scans were made.

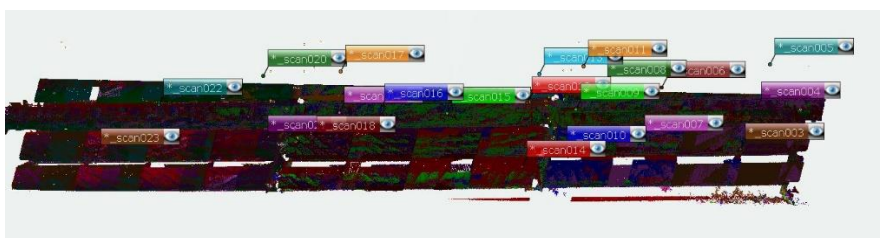


Figure 117. laser scanner's positions

6.2.4 Colouring of scans and export of point clouds

After placing the scans, within the structure of each one of them there is a "pictures" folder containing the images taken by the instrument with the "colour" option. Through these frames it is possible to associate RGB information to all the points of the scans and carry out the so-called "Coloration of the scans" activity.

This operation is carried out at the end of the process in order to not weigh down the files and to avoid lengthening processing times.

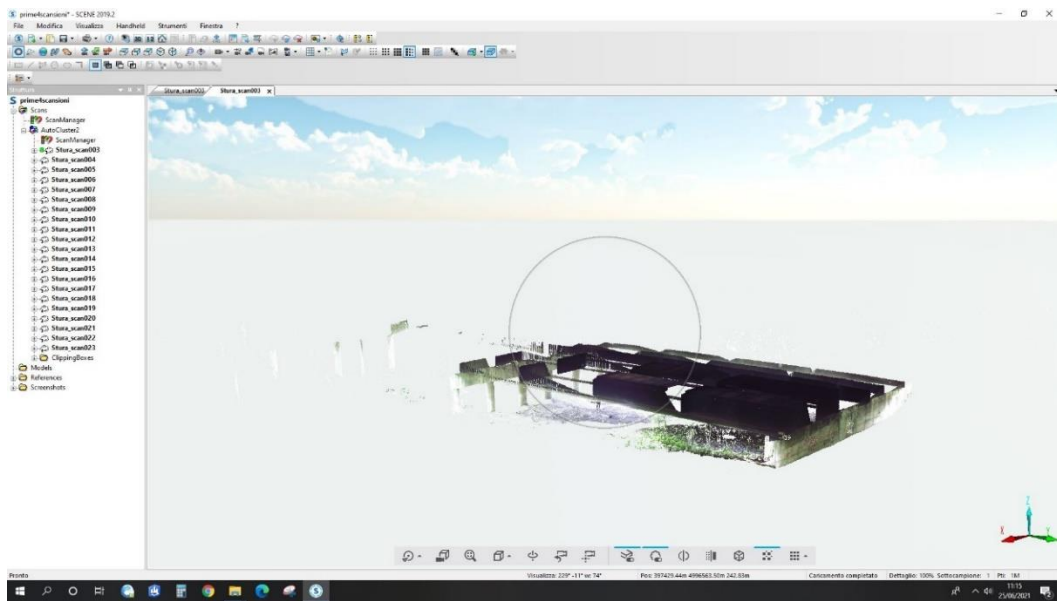


Figure 118. 3D view stura_scan003

Once the scans were placed first with the "cloud to cloud" method and then with the "target based" method, the following final output was obtained, in the 3D view.

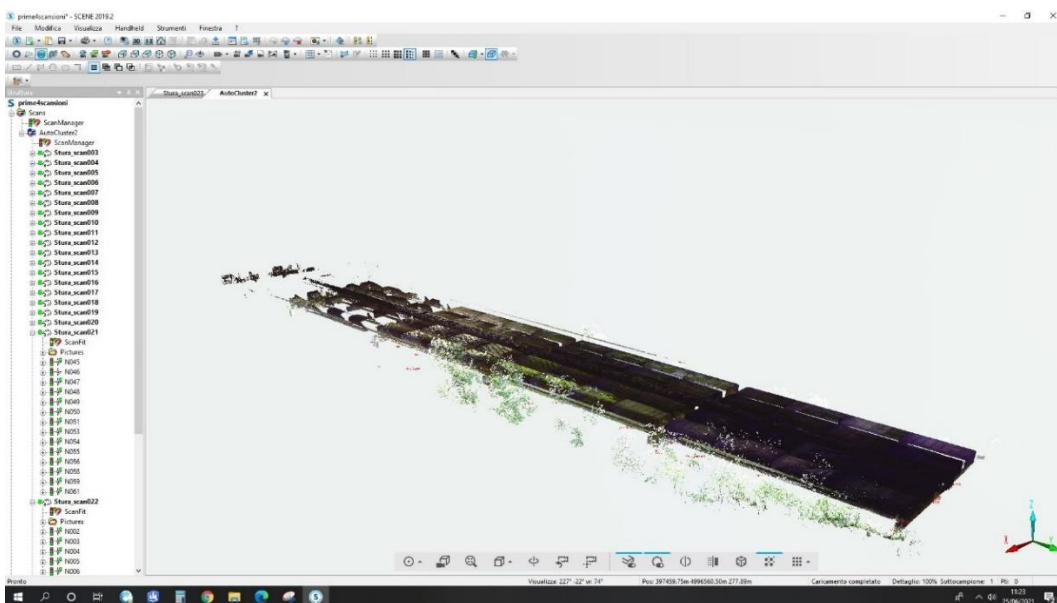


Figure 119. Full 3D dense cloud view

The last step carried out in the Faro scene software was to export the resulting point cloud.

The dense cloud can be exported in different formats and to do this you need to right click on the group of scans and then select "export sorted scans"

The scans were then exported in .e57 format which is a very versatile format that is compatible with many software, such as CloudCompare.

The exported scans, which mainly concern the first 3 spans of the bridge, are the following and have a total weight of 3.68 GB

scansioni_esportate_ordinate_Stura_scan003.e57	16/06/2021 14:50	File E57	218 349 KB
scansioni_esportate_ordinate_Stura_scan004.e57	16/06/2021 14:50	File E57	224 765 KB
scansioni_esportate_ordinate_Stura_scan005.e57	16/06/2021 14:50	File E57	217 687 KB
scansioni_esportate_ordinate_Stura_scan006.e57	16/06/2021 14:50	File E57	202 872 KB
scansioni_esportate_ordinate_Stura_scan007.e57	16/06/2021 14:50	File E57	208 116 KB
scansioni_esportate_ordinate_Stura_scan008.e57	16/06/2021 14:50	File E57	213 035 KB
scansioni_esportate_ordinate_Stura_scan009.e57	16/06/2021 14:50	File E57	214 269 KB
scansioni_esportate_ordinate_Stura_scan010.e57	16/06/2021 14:50	File E57	198 641 KB
scansioni_esportate_ordinate_Stura_scan011.e57	16/06/2021 14:50	File E57	194 984 KB
scansioni_esportate_ordinate_Stura_scan012.e57	16/06/2021 14:49	File E57	168 337 KB
scansioni_esportate_ordinate_Stura_scan013.e57	16/06/2021 14:50	File E57	172 158 KB
scansioni_esportate_ordinate_Stura_scan014.e57	16/06/2021 14:50	File E57	166 461 KB
scansioni_esportate_ordinate_Stura_scan015.e57	16/06/2021 14:50	File E57	157 598 KB
scansioni_esportate_ordinate_Stura_scan016.e57	16/06/2021 14:50	File E57	154 914 KB
scansioni_esportate_ordinate_Stura_scan017.e57	16/06/2021 14:51	File E57	149 648 KB
scansioni_esportate_ordinate_Stura_scan018.e57	16/06/2021 14:51	File E57	172 538 KB
scansioni_esportate_ordinate_Stura_scan019.e57	16/06/2021 14:51	File E57	178 966 KB
scansioni_esportate_ordinate_Stura_scan020.e57	16/06/2021 14:51	File E57	137 596 KB
scansioni_esportate_ordinate_Stura_scan021.e57	16/06/2021 14:51	File E57	156 278 KB
scansioni_esportate_ordinate_Stura_scan022.e57	16/06/2021 14:51	File E57	179 602 KB
scansioni_esportate_ordinate_Stura_scan023.e57	16/06/2021 14:51	File E57	179 158 KB

Figure 120. Exported scans sorted in .e57 format

6.3 UAV data processing with AGISOFT METASHAPE

The photogrammetric data used in this thesis work to reconstruct the dense point cloud and the mesh of a bridge span comes from the flight performed with the Anafi-work drone, the characteristics of which have been discussed in chapter 3.6.

In particular, three flights were carried out by the drone, one for each span (3,4,5), and in each flight videos were recorded from which photographs were extracted through the VLC program.

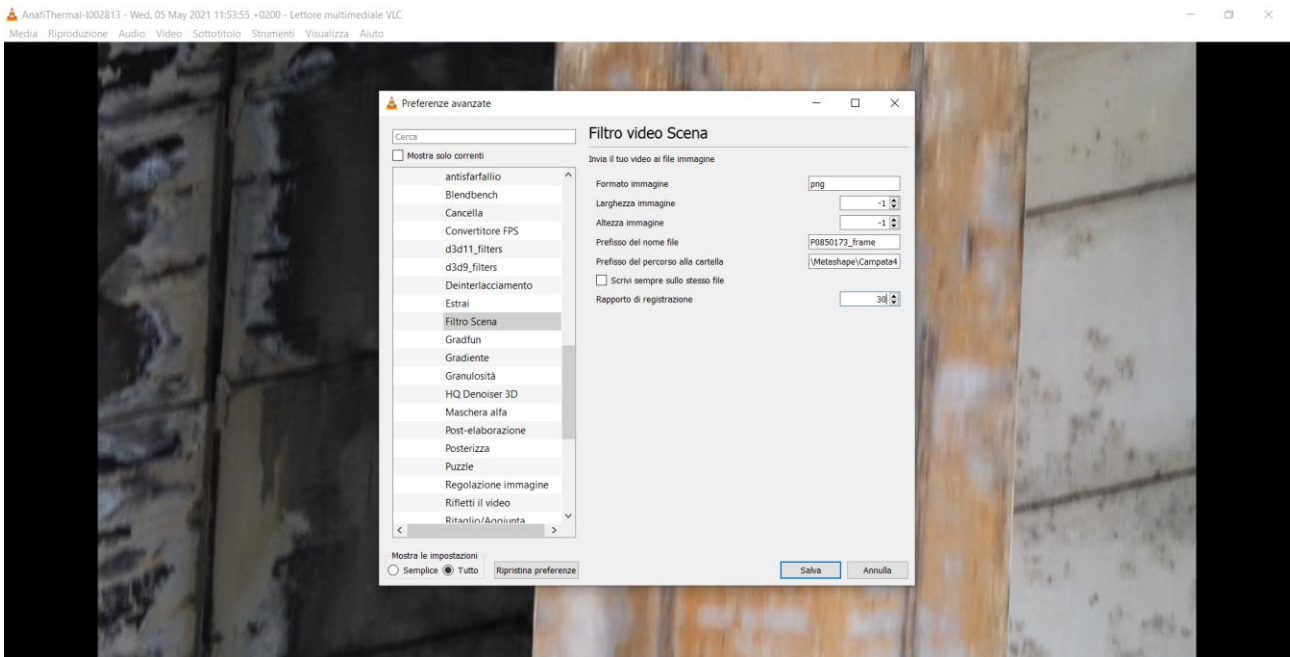


Figure 121. Extraction of 1/30 images with VLC

The images were sampled at a ratio of 1 in 30, so one image was captured for every 30 frames.

For the third span, 382 photos with an overall size of 693 MB were extracted

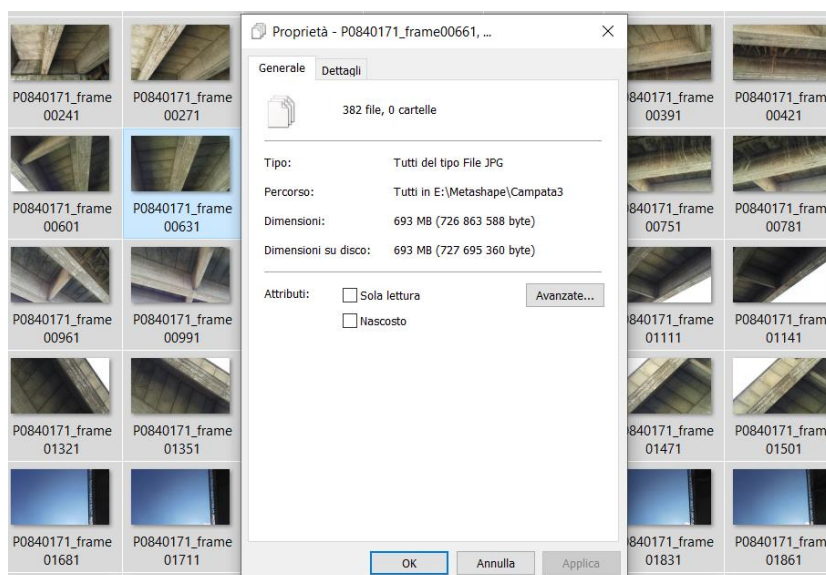


Figure 122. photos extracted for the third span

For the fourth span, 858 photos with an overall size of 9.42 GB were extracted

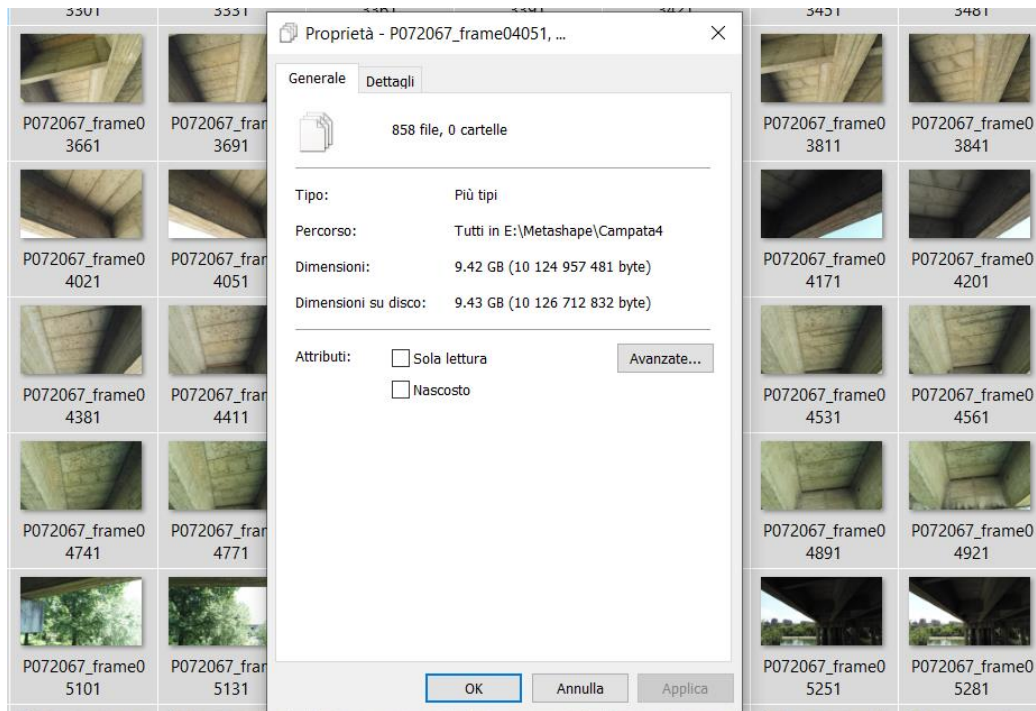


Figure 123. photos extracted for the fourth span

For the fifth span, 377 photos with a total size of 713 MB were extracted.

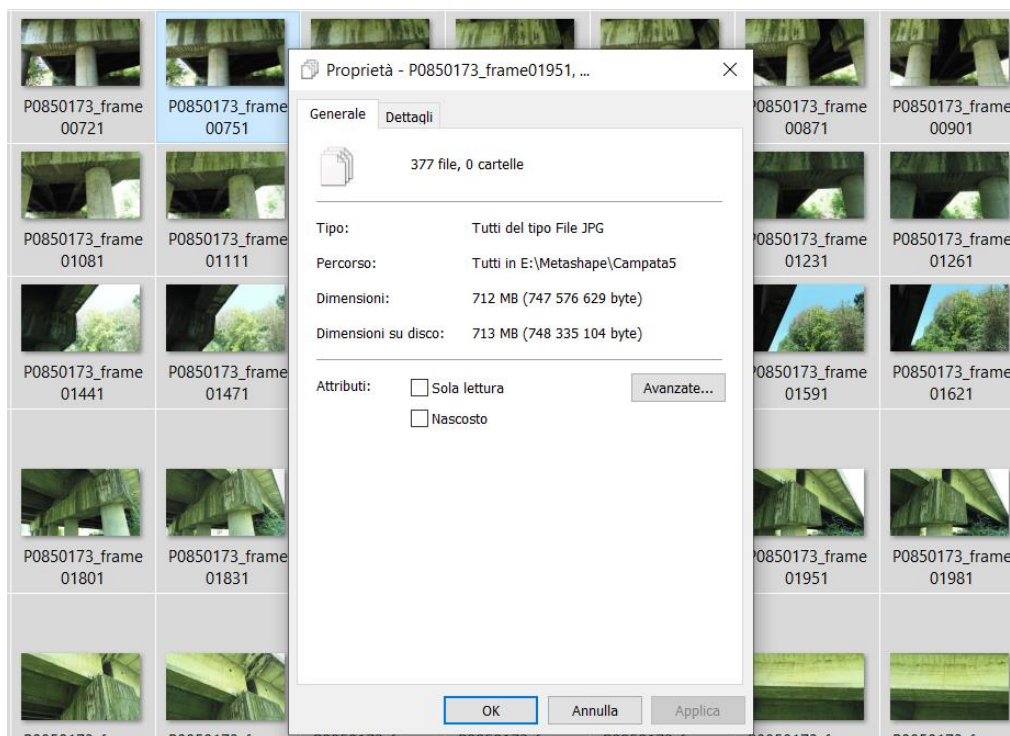


Figure 124. photos extracted for the fifth span

6.3.1 Upload and align photos to generate sparse point cloud

After obtaining the photos relating to the three spans, they must be loaded into a new project of the Agisoft Metashape software. This operation can be carried out using the “Workflow-add photos” menu or, alternatively, the images can be drag from the folder in which they are contained in the project screen.

The uploaded images must have at least 60% overlap to be processed by the software, otherwise they can be deleted. Various actions can be performed in the work area for this operation, such as enabling, disabling or removing the cameras.

After uploading them, the images the images must be aligned using the “Workflow-align photos” command. In this phase the software automatically detects the homologous points between the images that make up the photogrammetric block and builds a scattered cloud of points.

When aligning the photos, the alignment parameters have to be entered, the most important is the "Accuracy", on the basis of which the resolution of the analysed images is calibrated:

- Highest: images at a scale increased by a factor of 4 (2 per side);
- High: original scale images;
- Medium: images down scaled by a factor of 4;
- Low: Down images scaled by a factor of 16 (4 per side).

Going from Low to Highest increases the time required for processing because the resolution of the analysed images increases.

Then it was obtained the following clouds scattered over the 3 spans.

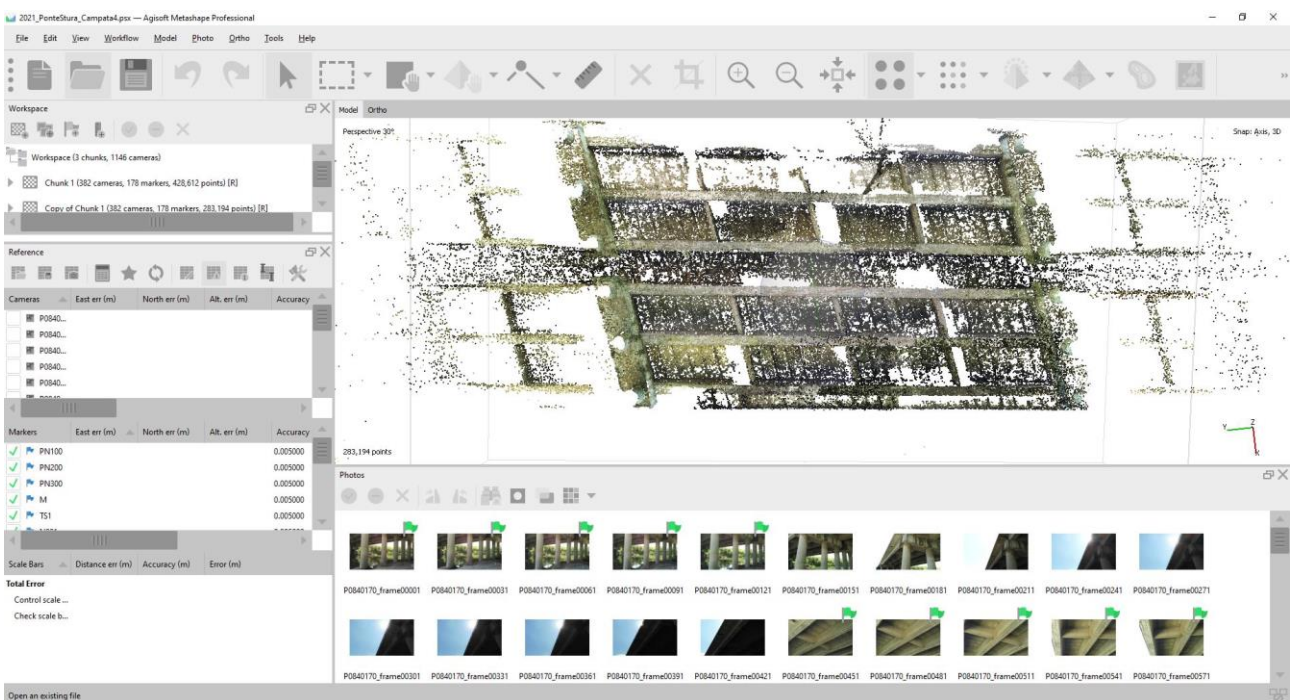


Figure 125. sparse cloud span 3

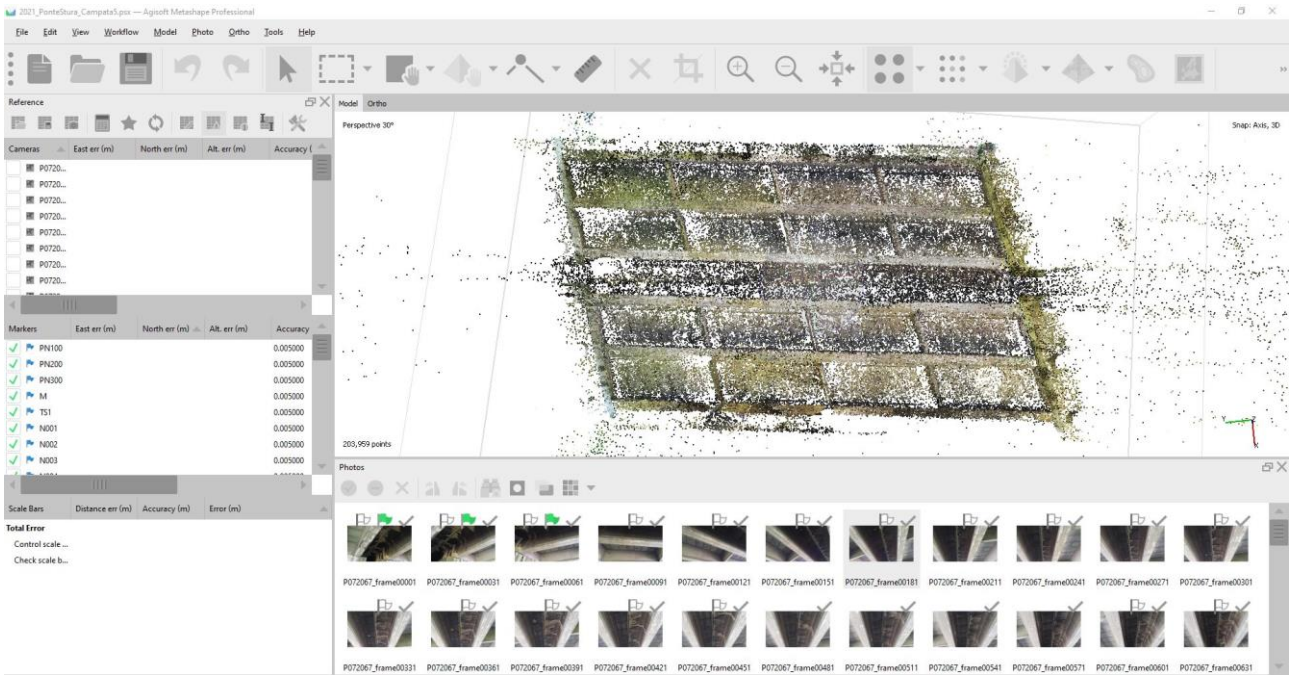


Figure 126. sparse cloud span 4

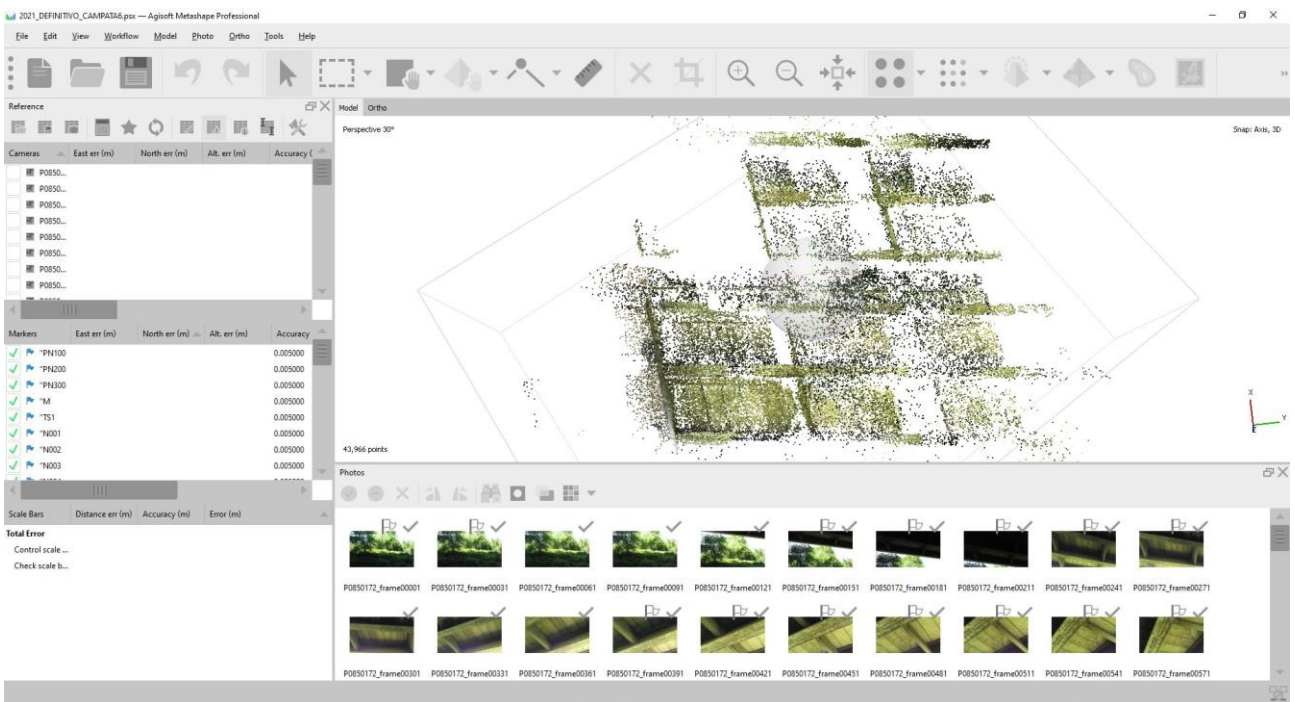
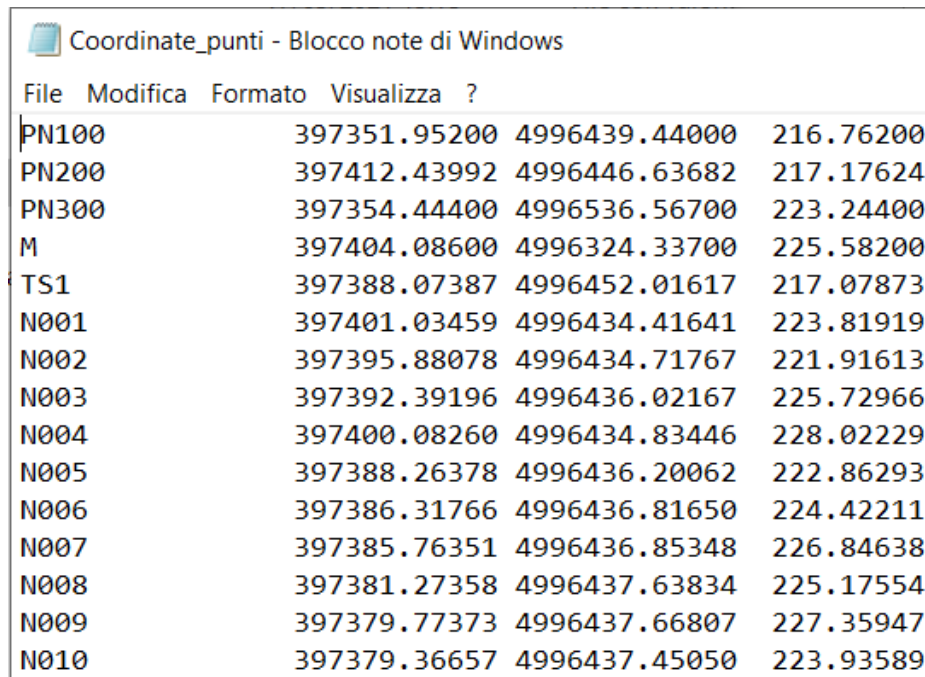


Figure 127. sparse cloud span 5

6.3.2 Upload and align photos to generate sparse point cloud

To georeference the model it is necessary to specify the coordinates in a reference system, in this case WGS 84 / UTM zone 32N (EPSG :: 326332).

The coordinates can be written manually or in the “Reference” box it is possible to load the coordinates of the markers in .txt format.



File	Modifica	Formato	Visualizza	?
PN100		397351.95200	4996439.44000	216.76200
PN200		397412.43992	4996446.63682	217.17624
PN300		397354.44400	4996536.56700	223.24400
M		397404.08600	4996324.33700	225.58200
TS1		397388.07387	4996452.01617	217.07873
N001		397401.03459	4996434.41641	223.81919
N002		397395.88078	4996434.71767	221.91613
N003		397392.39196	4996436.02167	225.72966
N004		397400.08260	4996434.83446	228.02229
N005		397388.26378	4996436.20062	222.86293
N006		397386.31766	4996436.81650	224.42211
N007		397385.76351	4996436.85348	226.84638
N008		397381.27358	4996437.63834	225.17554
N009		397379.77373	4996437.66807	227.35947
N010		397379.36657	4996437.45050	223.93589

Figure 128. coordinates of natural points in .txt format

After loading the coordinates, it is necessary to place the markers which are used to set a coordinate reference system, optimize the alignment of photos, measure distances and volumes within the scene and align different projects characterized by markers in the same system. of reference.

The more photos are used to specify the position of the marker, the greater the accuracy of the positioning of the marker. To define the position of the marker within a scene, it should be placed on at least two photos.

The marker can be positioned in a guided or manual way.

Manual approach.

The manual approach implies that the marker projections must be manually indicated on each photo, in fact this approach does not require a 3D model and can be performed even before aligning the photos. To position the marker, a click with the right mouse button on the point of the photo where it is to be positioned, then select “add marker” by selecting the corresponding instance. This adds the marker projection to the current photo. After placing the first marker, it is necessary to repeat the previous step to place the markers on the other photos.

Guided approach

The surface of the reconstructed 3D model is required for the guided approach. The positioning of the markers is quick because Metashape automatically projects the corresponding radius on the surface of the model and calculates the projections of the marker on the rest of the photos where it is visible. To position the marker, right click on the photo in the point where Metashape estimated the marker position, then select “place marker”.

In the thesis work both approaches were followed, starting from a first alignment carried out by the software, the markers were positioned and the model was updated from time to time to obtain errors that were within the tolerance limits. Below is an example of marker 69/327.

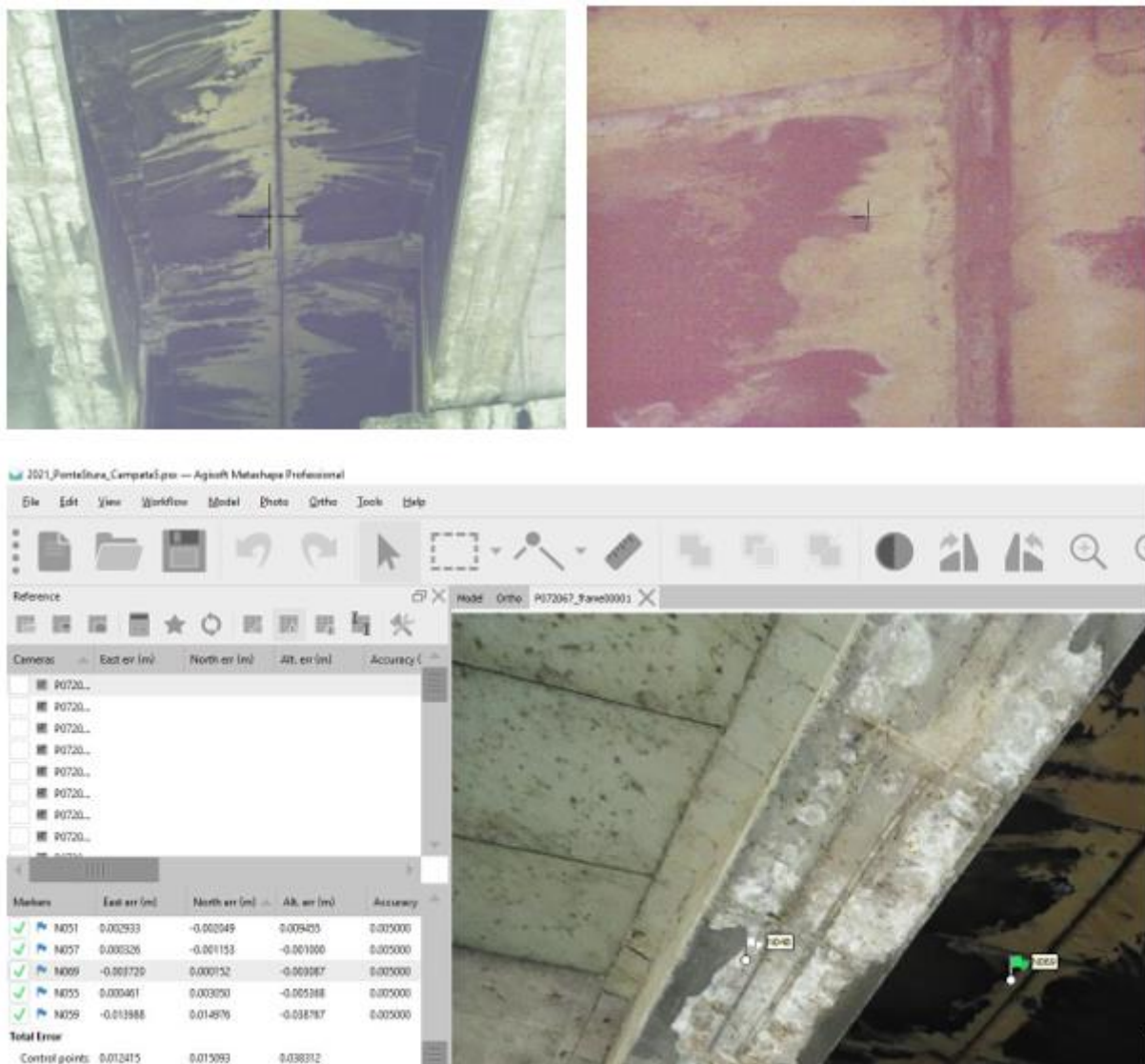


Figure 129. marker 69/327

After inserting the markers, click on “optimize cameras” in order to finish the georeferencing process of the model.

6.3.3 Build dense cloud

After having georeferenced the model, the photos are aligned again in order to obtain a scattered cloud again, but this time georeferenced.

In this phase it is possible to observe the residual error, which indicates the distance between the input and the subsequently estimated position of the marker.

After several tests and iterations, the following errors were obtained for the scattered and consequently dense clouds of the three spans.

For the third span, a residual error of 1.3 cm was obtained.

✓	🚩	N028	-0.001989	-0.003083	-0.000233
✓	🚩	N019	0.000526	-0.001531	0.005890
✓	🚩	N017	-0.002462	-0.000329	-0.006162
✓	🚩	N018	0.003337	0.000894	0.009828
✓	🚩	N027	0.000587	0.004050	-0.009323
✓	🚩	N014	-0.031926	0.041246	0.026483
Total Error					
		Control points	0.013172	0.016982	0.012633

Figure 130. third span residual error

For the fourth span, a residual error of 1.2 cm was obtained.

✓	🚩	N044	0.025282	-0.029752	0.054202
✓	🚩	N043	0.016235	-0.024674	0.081775
✓	🚩	N049	-0.010577	-0.009443	0.022047
✓	🚩	N051	0.002933	-0.002049	0.009455
✓	🚩	N057	0.000326	-0.001153	-0.001000
✓	🚩	N069	-0.003720	0.000152	-0.003087
✓	🚩	N055	0.000461	0.003050	-0.005368
✓	🚩	N059	-0.013988	0.014976	-0.038767
Total Error					
		Control points	0.012415	0.015093	0.038312

Figure 131. residual error fourth span

For the fifth span, a residual error of 1 cm was obtained.

✓	🚩	"N216	0.013228	-0.007798	0.003426
✓	🚩	"N069	-0.001909	0.000399	-0.000880
✓	🚩	"N203	-0.001885	0.002413	-0.000900
✓	🚩	"N223	-0.009435	0.004986	-0.001646
Total Error					
		Control points	0.008234	0.004786	0.002002

Figure 132. fifth span residual error

After making sure that the errors obtained were well within the tolerance limits that for a bridge structure had been set at 5 cm, we proceeded to create the dense clouds.

As happens for the generation of scattered clouds, also in this case as for the generation of the scattered cloud it is necessary to choose the "Accuracy", which for this phase has been set as "Highest", so the images are at a scale increased by a factor of 4(2 per side).

The final outputs obtained are the following:

- Dense cloud span 3

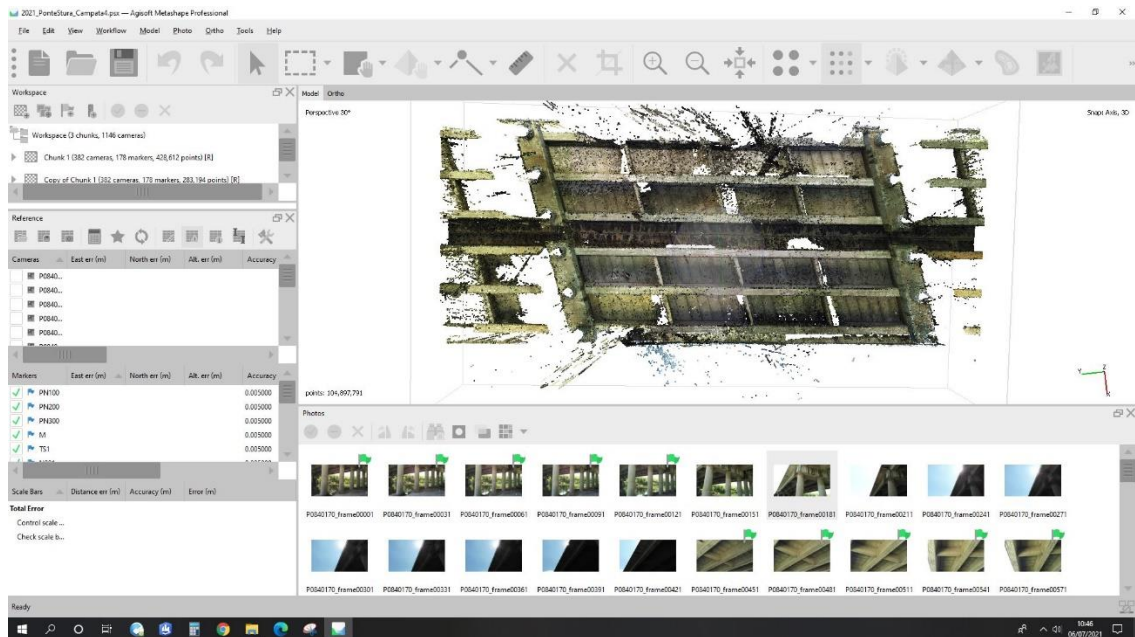


Figure 133. dense cloud span 3

- Dense cloud span 4

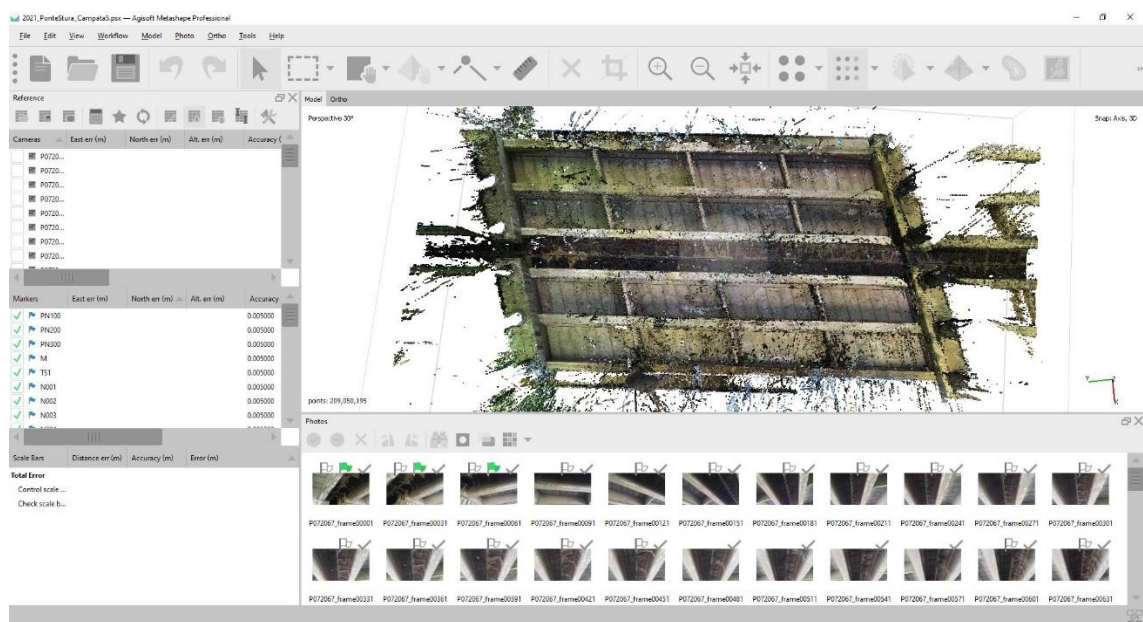


Figure 134. Dense cloud span 4.

- Dense cloud span 5

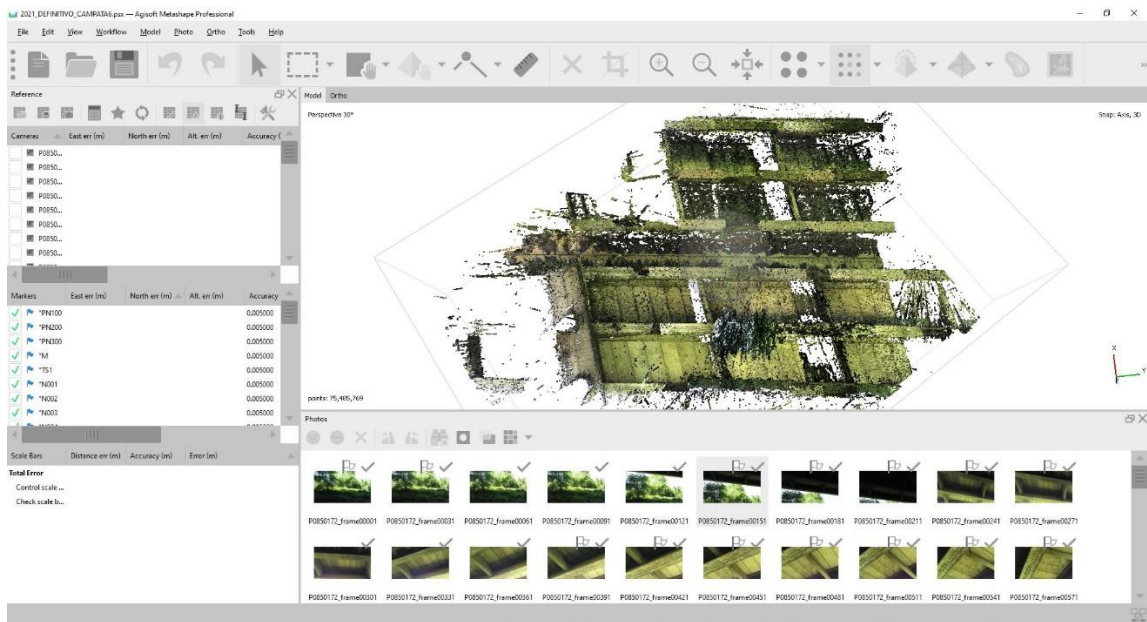


Figure 135. Dense cloud span 5

After obtaining the dense clouds relating to the 3 spans detected with the drone, they were exported in .e57 format, in order to subsequently import them into CloudCompare to clean them and join them to the dense point cloud obtained from the laser scanner.

6.4 Generating the full dense cloud with CloudCompare

The open-source software CloudCompare allows the editing and processing of 3D point clouds and triangular meshes. In this thesis work the software has already been described in chapter 5.3 concerning the pier cap.

In this phase activities of fundamental importance were performed. Both to clean and subsequently join the different dense clouds of points of different spans of the bridge, and also to generate the mesh of span 4 (the one with better quality) and finally localize the damage through points and polylines that were later imported into Revit.

6.4.1 Importing, cleaning and merging point clouds

As previously mentioned, the spans 1, 4, 5, 6 of the bridge were detected by laser scans, while the spans 2, 3, 4, 5 were detected by UAVs.

In particular, span 1 and span 2 were detected and processed by laser scanner and drone survey respectively in a previous thesis work, so for these two spans of the bridge the dense point cloud was already available and joined, but there were still points to be eliminated due to noise and vegetation.

The first step was to import the dense point cloud of the first and second span into CloudCompare, in .e57 format through a "Drag & Drop", and the result of this operation is visible in fig.3.

After carrying out this operation, the single scans from the laser scanner, in .e57 format processed with the FaroScene software visible in fig. 98., were imported always through a "Drag & Drop".

When importing the scans, the software allows me to perform a "Global Shift / scale", which is proposed when entities characterized by very large coordinates are imported.

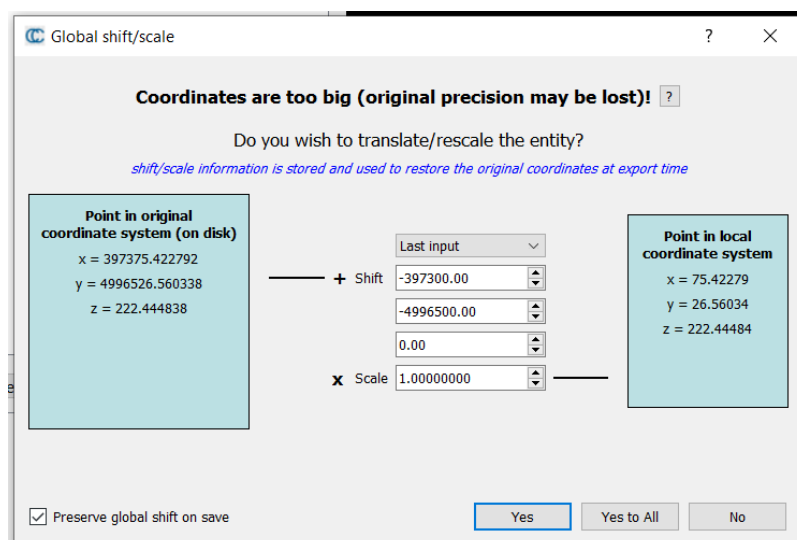


Figure 136. Global Shift & Scale proposed by CloudCompare

The interface shows on the left the point expressed in the global reference system, while on the right the same point is expressed in the local coordinate system. The software proposes a shift for the x, y, z coordinates which, however, can be modified by the user.

If one select a local reference system then the software will modify the global coordinate system, however once exported the entity may not be in the same place as the original one.

If one keep the global coordinate system, then the coordinate system remains unchanged, and after exporting it the point cloud will be in the same original position.

For this thesis work it was decided to operate with a local coordinate system, since the point cloud characterized by not too high coordinates is lighter and easier to manage, so we clicked on the "Yes to All" option .

After carrying out this operation it was necessary to merge the different scans together, through the CloudCompare tool "Merge Multiple Clouds", and the following result was obtained.

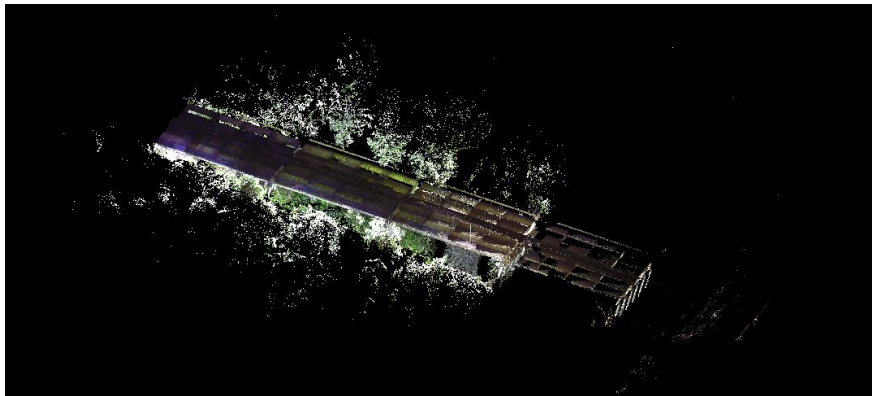


Figure 137. Scans span 4, 5, 6 joined (2021)

After having combined the scans of spans 4, 5, 6 carried out by laser scanner survey in 2021, the dense point cloud obtained by laser scanners and UAVs of the first and second spans, in 2020, were also joined.

The following operation is to clean the dense point cloud of the bridge coming from the Lidar survey, in particular this operation was carried out by segmenting the cloud through the tool "Cross section - Export multiple slices by repeating the process along one or several dimension"



Figure 138. Dense cloud from laser scanner cleaned

Finally, the dense clouds obtained starting from the photogrammetric data were imported individually into CloudCompare, in order to clean them from noise and vegetation:

- span 3 imported in .e57 format and subsequently cleaned.

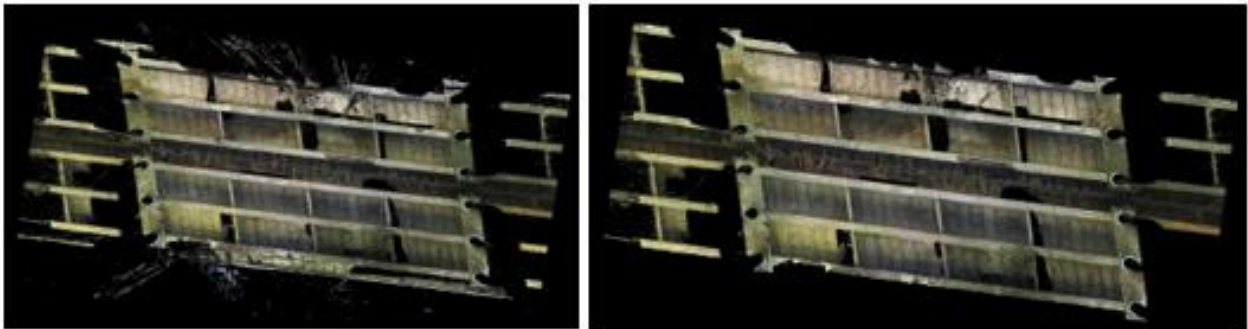


Figure 139. dense cloud of span 3

- span 4 imported in .e57 format and subsequently cleaned.



Figure 140. dense cloud of span 4

- span 5 imported in .e57 format and subsequently cleaned.

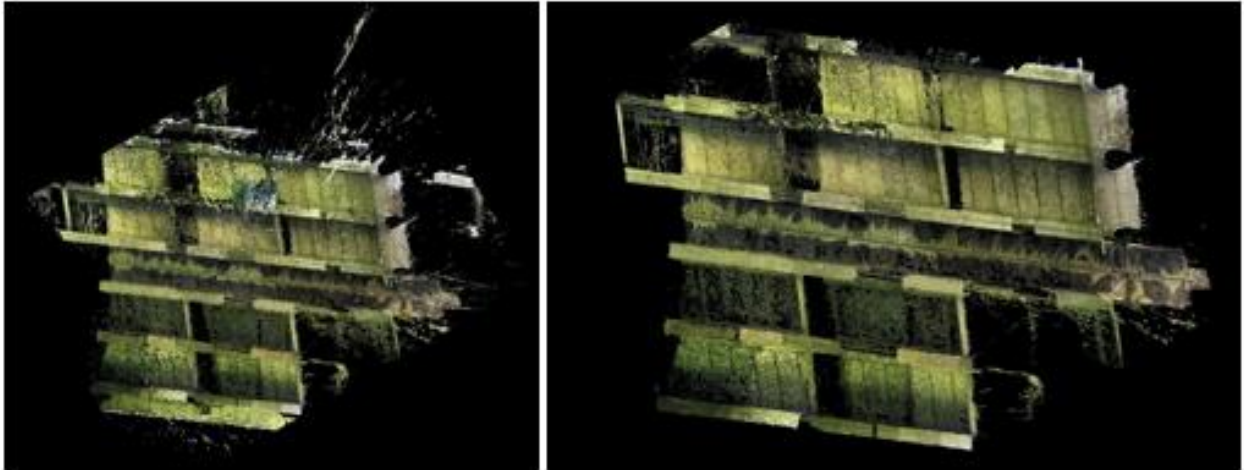


Figure 141. dense cloude of span 5

At the end of the process, the point clouds coming from the Lidar data were joined with the point clouds coming from the photogrammetric data, obtaining the following result:



Figure 142. Final dense cloud

6.4.2 Span 4 mesh generation and damage detection

The workflow to follow to generate a mesh in CloudCompare has already been described in chapter 5.3, where some tools such as “compute normals” and “PoissonRecon” have been used.

In this phase, therefore, it has begun from the point cloud of span 4 which was also extrapolated through the "Cross section" tool and was divided into 3 parts in order to individually generate the mesh of the piers with the pier cups and of the deck, to then join them.

It is realized only the fourth span because it is the span that overpass the bridge, and so it is the most difficult span to monitor in situ. Obviously, the process done for this span can be carried out for every span of the bridge.

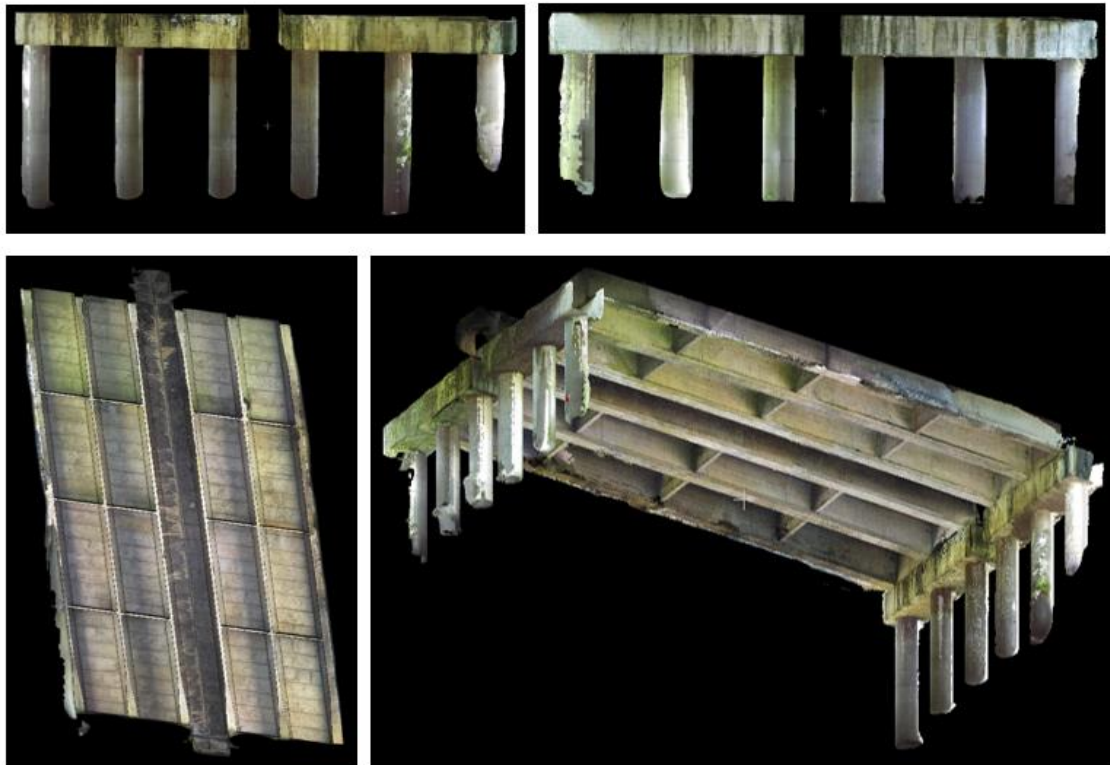


Figure 143. Span mesh generation 4

6.4.3 Damage recognition and machine learning algorithm

After generating the mesh of span 4, the damage was identified, based on the "defect cards" of Annex C of the Italian guidelines.

The mesh obtained was satisfactory because by navigating in the 3D model reconstructed in CloudCompare it was possible to identify and recognize different damages that in situ would have been difficult to detect due to the height of the deck and because span 4 is the one that crosses the river Stura.



Figure 144. span 4 Stura bridge

However, by comparing the 3D mesh with the photos captured by the drone, it was possible to observe damage such as the cracks or micro-cracks visible in the individual photographs were not appreciable by observing the mesh model.

The following figure shows a comparison between a photo captured by the drone during the flight and the same area instead observed on the mesh in CloudCompare. It is clear that it is quite easy to distinguish an exposed rebar due to the detachment of the concrete cover, but damages such as cracks or microcracks are not noticeable.



Figure 145. Drone image VS mesh

To solve this problem, the photos extracted using the VLC software, coming from the video recorded by the drone during the survey of span 4, were analysed by a machine learning algorithm (developed by a doctoral student from the structural engineering department of Politecnico di Torino), which analysed the images of span 4 and generated the following output

name	classPred	scores_Cracked	scores_Delaminated	scores_Undamaged
.....				
P072067_frame01411	Delaminated	0.002660185	0.9921658	0.005173978
P072067_frame01441	Delaminated	0.000211218	0.9989164	0.000872429
P072067_frame01471	Delaminated	0.002949869	0.9937254	0.003324731
P072067_frame01501	Undamaged	0.2425229	0.1056925	0.6517847
P072067_frame01531	Undamaged	0.1710654	0.01967964	0.8092549
P072067_frame01561	Undamaged	0.2089802	0.008034633	0.7829851
P072067_frame01591	Undamaged	0.2129476	0.004968558	0.7820838
P072067_frame01621	Undamaged	0.1005146	0.002225287	0.8972601
P072067_frame01651	Undamaged	0.2240829	0.003343891	0.7725732
P072067_frame01681	Cracked	0.5691655	0.003182057	0.4276524
P072067_frame01711	Cracked	0.7399444	0.008344695	0.251711
P072067_frame01741	Cracked	0.8714927	0.01101082	0.1174966
.....				

Figure 146. Output of machine learning

It is possible to observe that for each photograph analysed there are 3 different outputs, which can be:

- delaminated, when delamination is present in most of the image
- cracked, when most of the image shows a crack
- undamaged, when no type of damage has been detected in the image.

Once these data were available, points were placed in CloudCompare to detect the damage through the "Point list picking" function, when the damage had a limited extent, while polylines were created through the "Trace a polyline by point picking" function, when the damage had a large enough extent.

This was done both thanks to the outputs provided by machine learning, but also for damages where it was sufficient to observe the mesh only.

For example, passive moisture spots have been identified (areas of different colour from the intact material since they are traces of calcium released on the surface by moisture penetrated through the concrete). When the phenomenon is extinguished, some whitish spots remain, identifiable by observing only the mesh. In this case the damage was identified by means of a polyline, observing the mesh and comparing it with the defect cards.

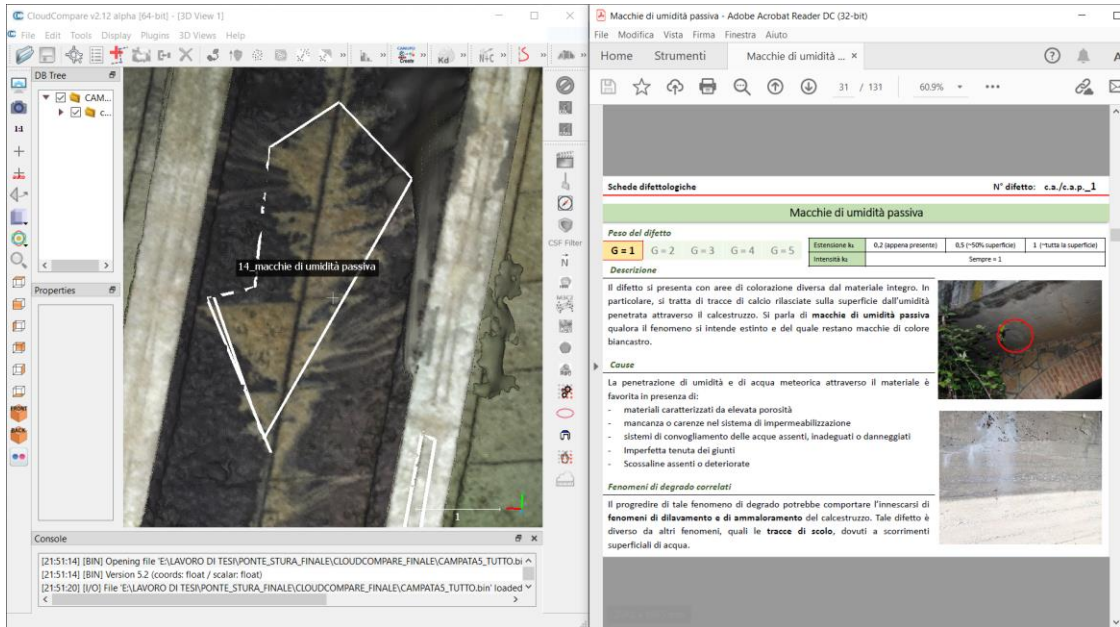


Figure 147. damage detection by polyline

Another damage identified on the pier caps are the stains of active humidity, the origin of which, unlike the stains of active humidity, is linked to the phenomena of water infiltration still in progress and presents itself with dark-coloured stains due to continuous contact with water and humidity. In this case the damage was indicated by a point since its extension was not high and as in the previous case it was identified by comparing the mesh and the defect cards.

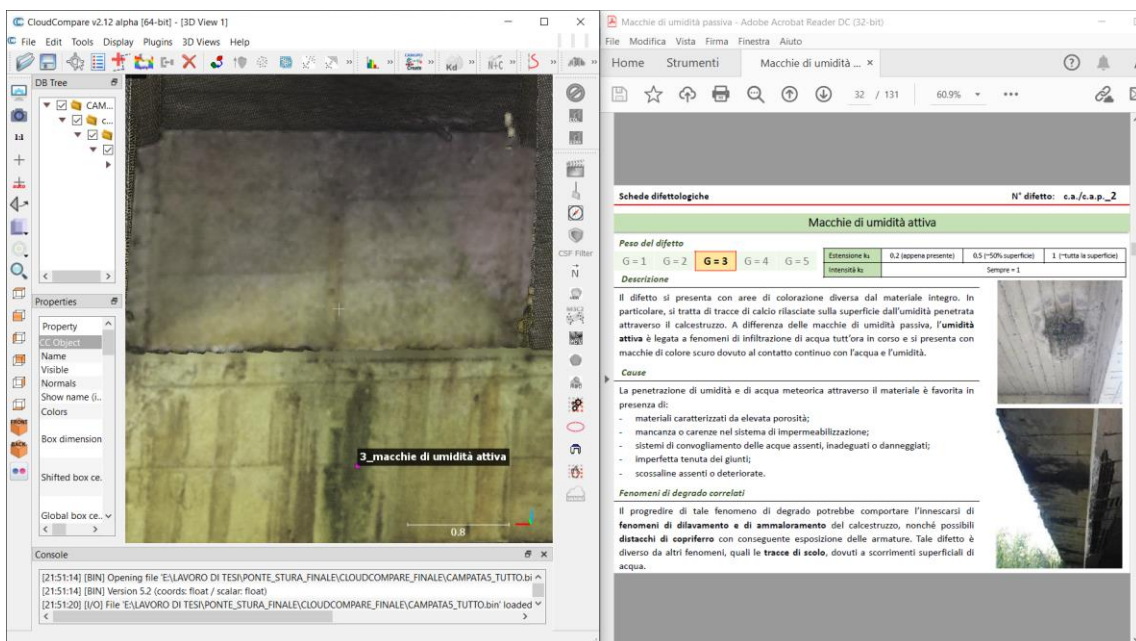


Figure 148. identification by point

As a last example, the case was reported in which it was not possible to identify the damage in a first analysis by observing only the mesh, but it was possible to do so thanks to the outputs from the machine learning analysis. In particular, cracks were identified in correspondence with the brackets, which are distributed in a regular manner, reproducing the arrangement of the brackets of the structural elements. In this case, the damage was indicated by a polyline since its extension is quite high, by comparing the mesh, the photos captured by the drone and the outputs provided by the machine learning algorithm.

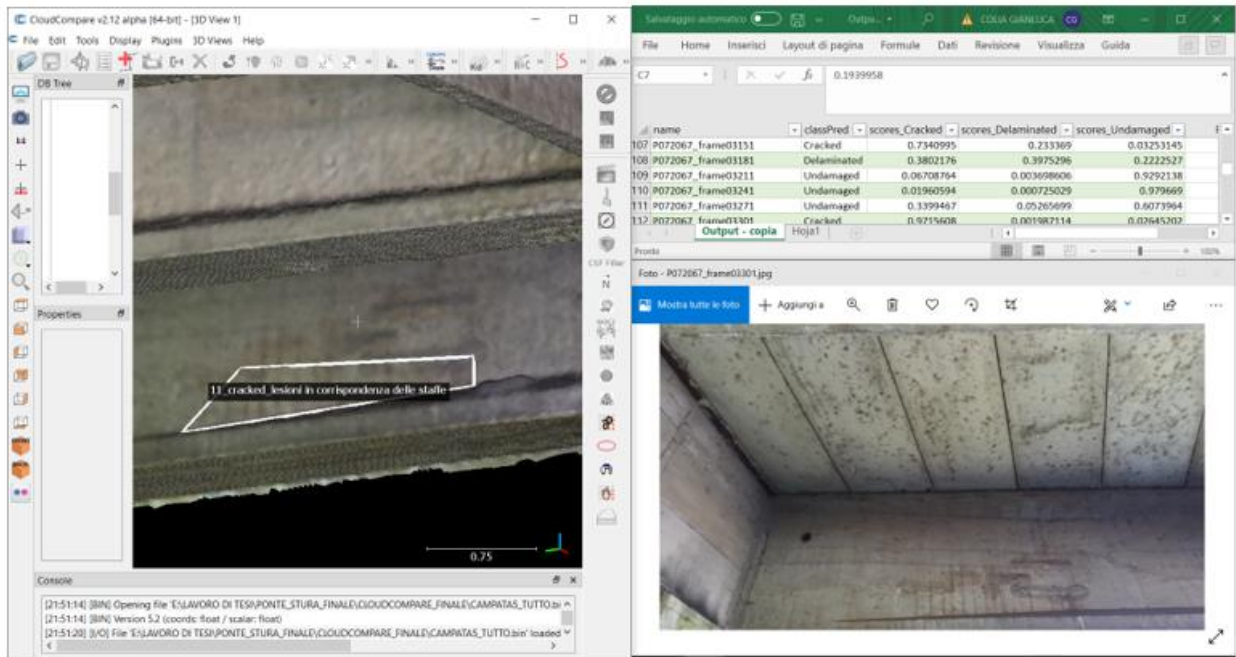


Figure 149. identification by polyline and machine learning

Following this methodology, the damages on span 4 of the bridge have been identified, and then export them in .txt format and import them into Revit through a Dynamo code.

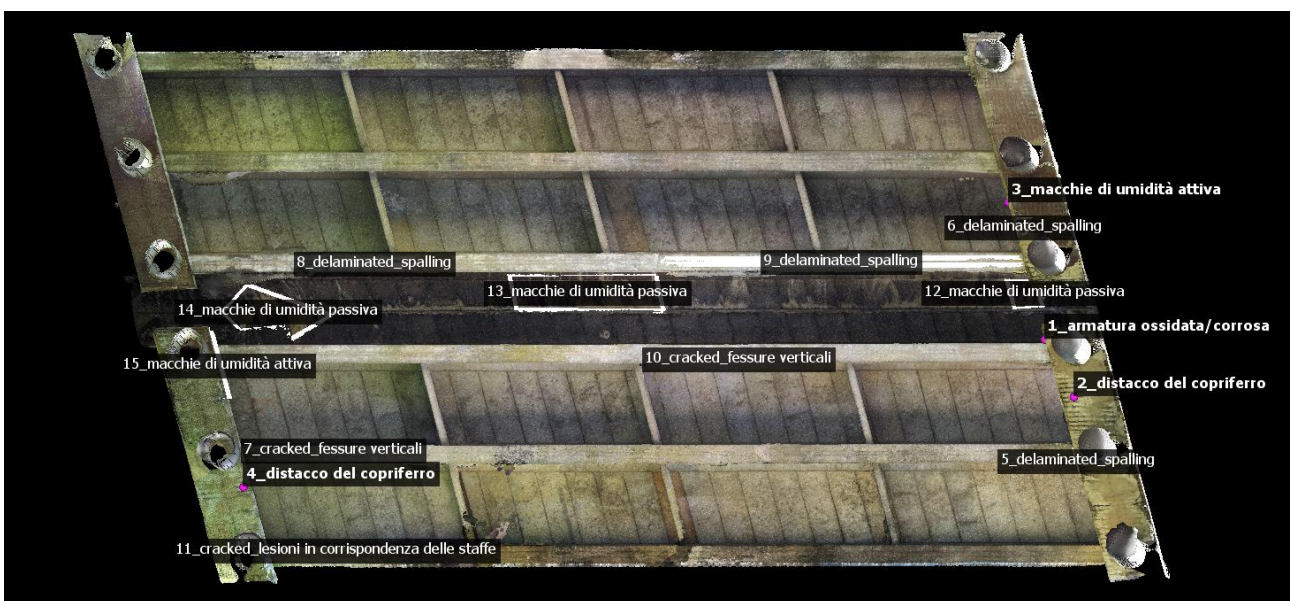


Figure 150. span damage detection 4

6.5 Scan to BIM: Recap, dynamo, Revit

For the final stage of thesis work it was necessary to carry out what has already been done in chapter 5 for the pier cap.

In particular, after obtaining the complete point cloud of the bridge in .e57 format, it was imported into Recap in order to be able to export it later in .rcp format and then import it into Revit overlapping it to an existing model of the bridge.

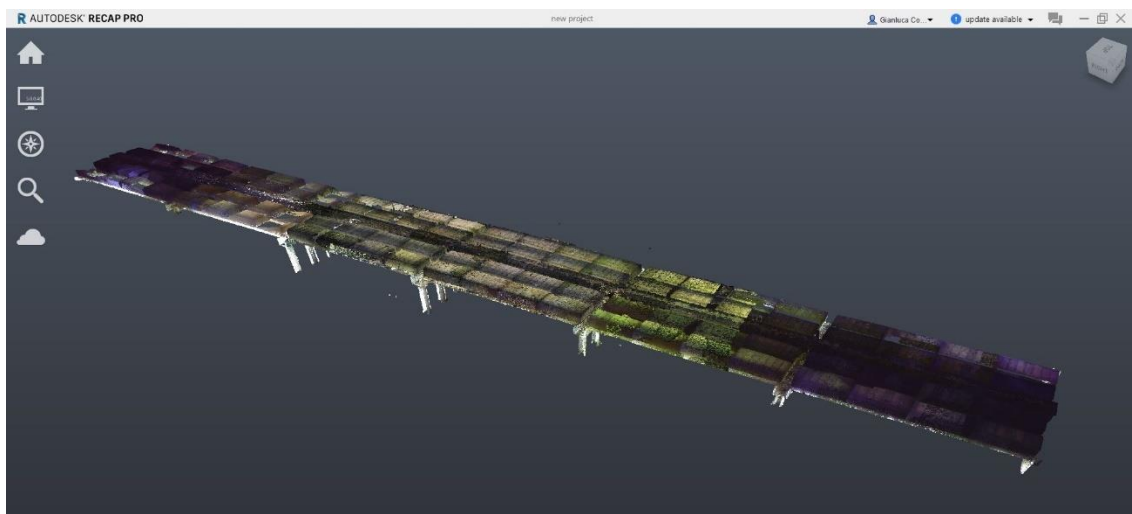


Figure 151. Final dense cloud in Recap

After exporting the point cloud from Recap, it was imported into Revit.

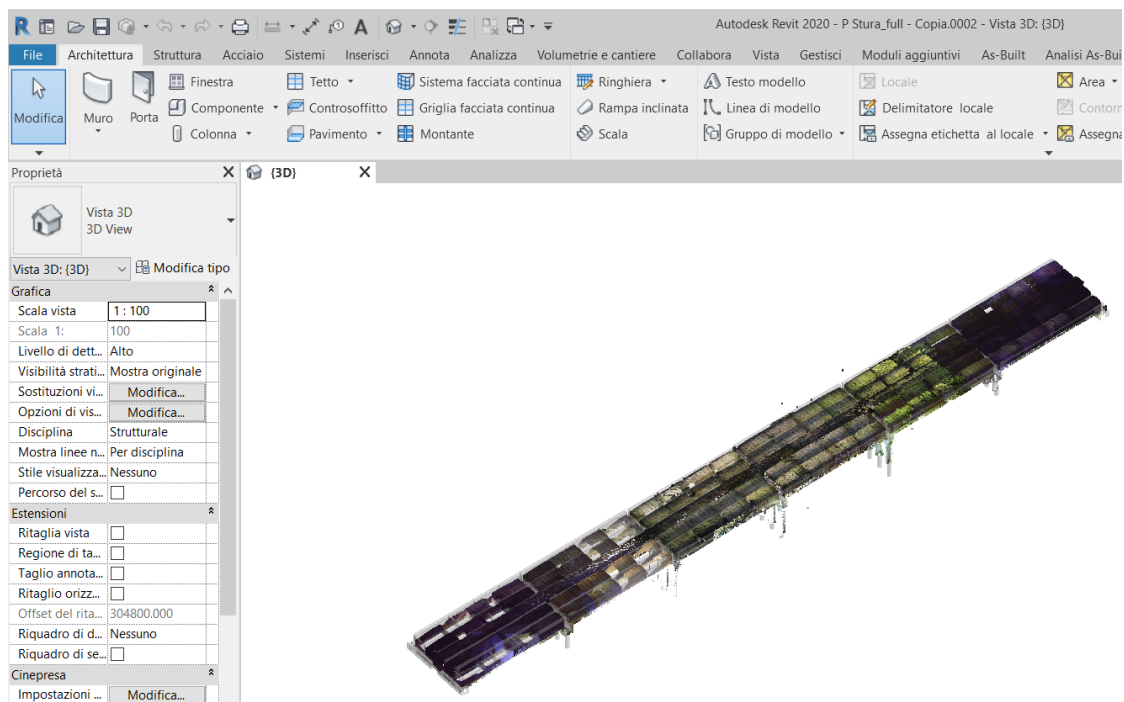


Figure 152. Final dense cloud imported in Revit

Subsequently, in Revit the family previously created for the pier cap was modified, grouping the defects into 3 macro-categories and assigning a different colour to each category.



Figure 153. spheres created in revit

The yellow sphere identifies defects that arise as an alteration of the surface colour of the structural element, and these include:

- Passive damp spots
- Stains of active humidity
- Washed out / deteriorated concrete
- Crawl spaces
- Tested washed / damaged concrete
- Humidity from inside

The green sphere identifies the defects that present in any case the exposure of the reinforcement on the surface, and these include:

- Detachment of the concrete cover
- Oxidized and / or corroded armor
- Uncovered / oxidized brackets
- Deformed longitudinal reinforcement
- Brackets break
- Unsealed anchor heads
- Sheaths in sight
- Degraded sheaths and oxidized wires
- Adherent threads in sight oxidized
- Reduction of prestressing reinforcement
- Uncovered / oxidized armour tested
- Release of anchor bars

The blue sphere identifies defects that present in horizontal, vertical, or oblique general crack or microcrack and these include:

- Moderate spider web injuries
- Horizontal cracks
- Vertical cracks
- Diagonal slots
- Pillar attachment injuries
- Subsequent shooting deteriorated
- Crushing injuries
- Injuries in correspondence of the stirrups
- Longitudinal cracks
- Transverse cracks

- Detachment of the eardrum
- Injuries detachment of beams / transoms
- Defects of Gerber saddles
- Beam-slab attachment injuries
- Capillary lesions anchors
- Detachment of head pads
- Core lesions along the cables
- Lesions along the sole of the bulb

After dividing the damages into three macro categories, the different colors have been assigned in the properties of the Revit family.

The size of the sphere is also a function of the extension -k1 parameter- and the intensity -k2 parameter- from the guideline. In particular the dot will have a radius of:

- $r = 200 \text{ mm}$, if $k1 + k2 < 0.9$
- $r = 250 \text{ mm}$, if $0.9 < k1 + k2 < 1.5$
- $r = 300 \text{ mm}$, in all remaining cases

Compared to the Scan to BIM process carried out in chapter 5 for the pier cap, in this case we also have polylines that, exported from CloudCompare, are not made up of a single spatial coordinate as is the case for points, but are characterized by an even number of spatial coordinates equal to the number of vertices of the polyline.

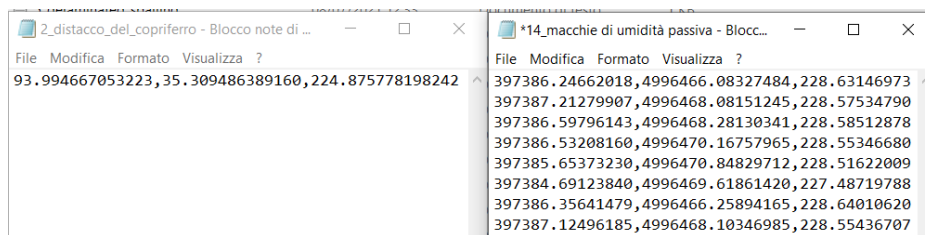


Figure 154. .txt point vs polyline

After importing the damages in Revit, identified in CloudCompare by observing only the mesh or also the outputs provided by machine learning, the final result is the following.



Figure 155. corruptions imported into Revit

7 Conclusions

In this thesis work, methods were sought to identify damage to the bridge over the river Stura on the RA10 motorway junction and implement them in a BIM context to generate a unified SHM database capable of managing the data, implementing them from time to time.

Workflows were sought to be followed for both Scan to BIM and Mesh to BIM methodologies, first applying them to simplified three-dimensional models such as the Rubik's cube or a pier cap, and then deciding, after due consideration, which methodology to follow to carry out a classification of level 1 for the stura bridge.

It has been seen that although the Mesh to BIM methodology is easier to conceive because the textured mesh of the 3D object is imported directly into Revit, it turns out to be difficult, not automatic and dispensable in terms of time.

With this in mind, it was decided to follow the Scan to BIM methodology to identify the damage to span number 4 of the bridge, that is the span overlooking the river.

Different software were used to carry out this thesis work and ultimately to carry out the survey of the bridge it was decided to use FaroScene, Agisoft Metashape, CloudCompare, Revit and dynamo, identifying an efficient and quick workflow.

As for the identification of damage to the bridge, the use of remote sensing technologies was found to be satisfactory both in practical and economic terms. Furthermore, following the Scan to BIM methodology, the speed of remote sensing is in line with the operations to be carried out to identify damage.

Starting from the data collected, excellent results were obtained. In particular, by processing the data coming from both Lidar technology and the UAV survey, outputs were obtained, therefore point cloud and mesh, characterized by an error of less than 2 cm, therefore well below the tolerance threshold set at the beginning of the work, equal to 5 cm. It is therefore possible to state that the identification of the damage can be carried out through this methodology and not directly on site if there are conditions that do not allow it.

Finally, to complete the thesis work, thus being able to identify damages that could never have been identified with the naked eye in situ due to their position and their reduced extension, an artificial intelligence algorithm, Machine learning, was used through which it was possible to first identify the damages in the photos captured by the drone and then go and locate them in the mesh in CloudCompare and finally import them into Revit through a Dynamo code.

7.1 Future developments

At the end of this thesis, it is possible to state that one of the future developments may be to generate a database in Revit that collects and manages the evolution of damage over time.

This can be done through the Revit phases where it is possible to associate the date in which a particular monitoring takes place with each phase by means of the survey techniques discussed and analysed in this thesis work.

Below an example is shown of a possible future application, as the damages identified in CloudCompare evolves with the hypothesized year in which it will have a future detection, i.e. 2030 and 2040. For the future damage, the spatial configuration has been entirely hypothesized.

After having identified the damages in the years following the first survey, they were imported into Revit following the workflow described in the following thesis work.

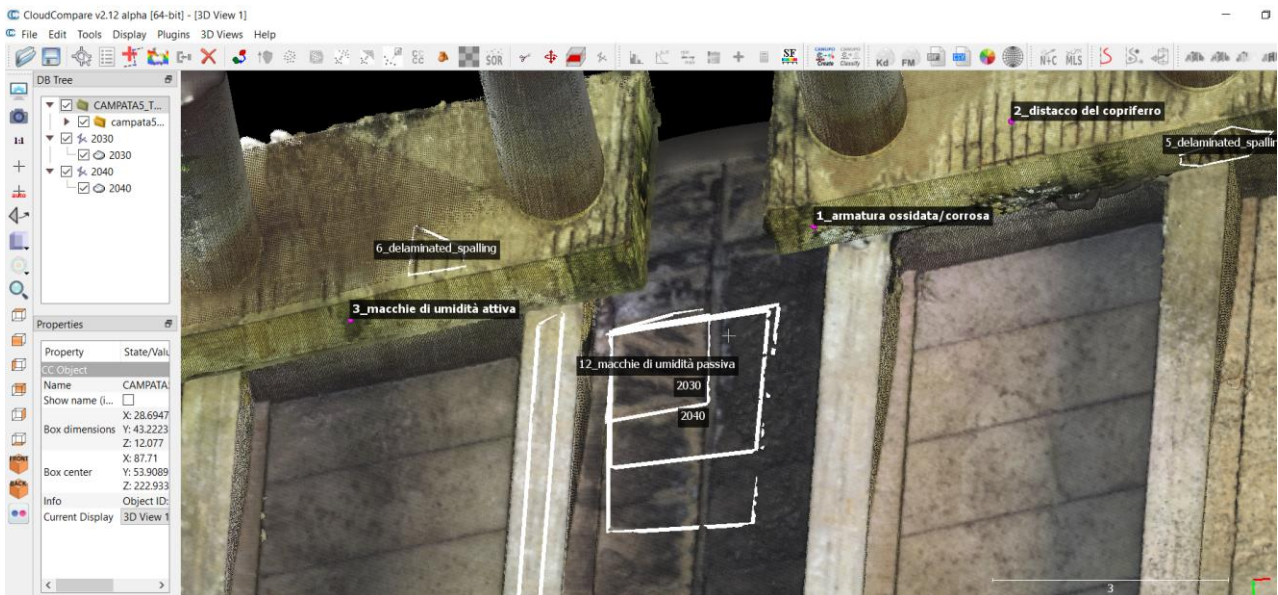


Figure 156. damages hypothesized in CloudCompare

Revit has created the phases renamed with the year in which the detection takes place, so we have 2021 where we have all the damages identified in the following thesis, while 2030 and 2040 are the years in which a new detection was assumed.

Fasi	
Fasi del progetto Filtri delle fasi di lavoro Sostituzioni grafica	
PASSATO	
	Nome
	Descrizione
1	2021
2	2030
3	2040

Figure 157. generating phases in Revit

Then new line styles were created to identify the polylines of subsequent damage with a different colour and using the phase filters it was possible to discretize the evolution of the damage for each phase.

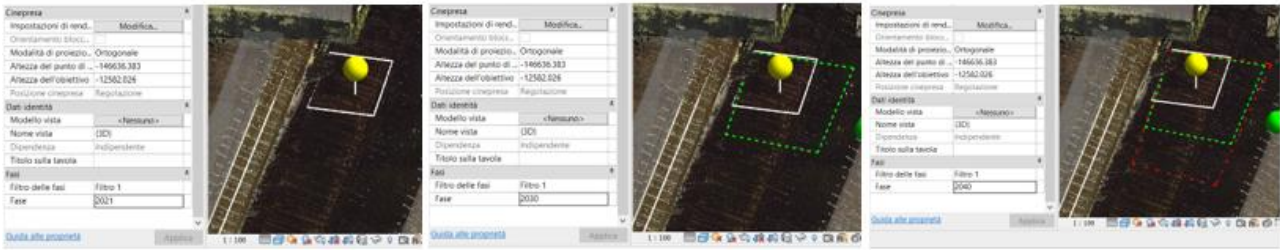


Figure 158. damage evolution 2021-2030-2040

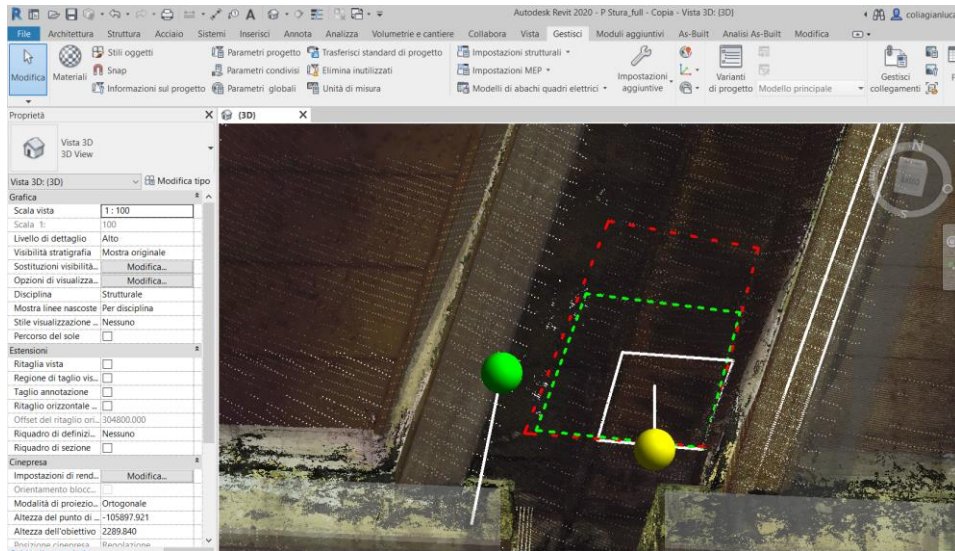


Figure 159. damage situation hypothesized in 2040

A next step could be to go to identify, thanks to this database, the most damaged areas of the bridge or in any case the areas that are undergoing a rapid evolution of damage.

Consequently, based on the database of the damages identified through the surveys carried out, in the future it will have to be possible to program the flight of the drone to detect specific areas, especially the areas that present greater criticality or an important evolution of the damage.

A further step forward that can be taken is to install a machine learning algorithm in the drone capable of automatically identifying and classifying the damage directly in situ, then implementing the model database directly in the BIM environment.

Bibliography:

- Dongming Feng*, Maria Q. Feng. Computer vision for SHM of civil infrastructure: From dynamic response measurement to damage detection – A review. Department of Civil Engineering and Engineering Mechanics, Columbia University, New York, USA
- Maria Pina Limongelli, Mehmet Celebi. Seismic Structural Health Monitoring: From Theory to Successful applications. Springer
- Ranjan Ganguli. Structural Health Monitoring: A Non-Deterministic Framework. Springer
- Dryver Roy Huston, Ali Maher: Structural sensins, health monitoring, and performance evaluation.
- M. Mollineaux, R. Rajagopal. Structural health monitoring of progressive damage. Stanford Sustainable Systems Lab (S3L), Department of Civil and Environmental Engineering, Stanford University, Stanford, CA, U.S.A.
- Mohamed Abdel, Basset Abdo. Structural Health Monitoring, History, Applications and Future. A Review Book. Open Science
- Claudia Neves. Structural Health Monitoring of Bridges Model-free damage detection method using Machine Learning. KTH ROYAL INSTITUTE OF TECHNOLOGY SCHOOL OF ARCHITECTURE AND THE BUILT ENVIRONMENT.
- Daniel Balageas, Claus-Peter Fritzen, Alfredo Güemes. Structural Health Monitoring. ISTE.
- Andre Borrmann, Christian Koch, Markus König, Jakob Beetz. Building Information Modeling: Why? What? How?: Technology Foundations and Industry Practice.
- Cettina Santagati, Despina Papacharalambous, Giulia Sanfilippo, Nikolas Bakirtzis, Carla Laurini, Sorin Hermon. HBIM approach for the knowledge and documentation of the St. John the Theologian cathedral in Nicosia (Cyprus). Journal of Archaeological Science: Reports.
- F.Banfia, L. Barazzettia, M. Previtali* a, F. Roncoroni. HISTORIC BIM: A NEW REPOSITORY FOR STRUCTURAL HEALTH MONITORING. Dept. of Architecture, Built environment and Construction engineering (ABC) Politecnico di Milano, Piazza Leonardo da Vinci 32, Milan, Italy
- Jim Bedrick, FAIA, Will Ikerd, P.E., Jan Reinhardt. LEVEL OF DEVELOPMENT (LOD) SPECIFICATION PART I & COMMENTARY For Building Information Models and Data. BIM FORUM

- Alcinia Zita Sampaio, Augusto Martins Gomes, Alberto Sánchez-Lite, Patricia Zulueta, Cristina González-Gaya 3. Analysis of BIM Methodology Applied to Practical Cases in the Preservation of Heritage Buildings.
- Bartosz Wójcik, Mateusz Żarski. ASSESSMENT OF STATE-OF-THE-ART METHODS FOR BRIDGE INSPECTION: CASE STUDY.
- Xiucheng Yang, Yi-Chou Lu, Arnadi Murtiyoso, Mathieu Koehl, Pierre Grussenmeyer. HBIM Modeling from the Surface Mesh and Its Extended Capability of Knowledge Representation.
- Bryan Hubbard, and Sarah Hubbard. Unmanned Aircraft Systems (UAS) for Bridge Inspection Safety.
- X. Yang, M. Koehl, P. Grussenmeyer. MESH-TO-BIM: FROM SEGMENTED MESH ELEMENTS TO BIM MODEL WITH LIMITED PARAMETERS. Photogrammetry and Geomatics Group, ICube Laboratory UMR 7357, INSA Strasbourg, France.
- Davide Simeone, Stefano Cursi, Ilaria Toldo, Gianfranco Carrara. B(H)IM - Built Heritage Information Modelling Extending BIM approach to historical and archaeological heritage representation.
- C. Dore, M. Murphy, S. McCarthy, F. Brechin, C. Casidy, E. Dirix. Structural Simulations and Conservation Analysis -Historic Building Information Model (HBIM). School of Surveying and Construction Management, Dublin Institute of Technology.
- Cristiana Achille, Francesco Fassi. FROM POINT CLOUD TO BIM: A MODELLING CHALLENGE IN THE CULTURAL HERITAGE FIELD.
- Gustavo Rocha, Luís Mateus, Jorge Fernández, Victor Ferreira. A Scan-to-BIM Methodology Applied to Heritage Buildings. CIAUD, Lisbon School of Architecture, University of Lisbon, 1349-063 Lisbon, Portugal.
- C. Santagati, M. Lo Turco, R. Garozzo. REVERSE INFORMATION MODELING FOR HISTORIC ARTEFACTS: TOWARDS THE DEFINITION OF A LEVEL OF ACCURACY FOR RUINED HERITAGE. Department of Civil Engineering and Architecture, University of Catania, Via Santa Sofia n.64, 95123, Catania, Italy
- C. Castagnetta, M. Dubbinib, P. C. Riccio, R. Rivolaa, M. Gianninia, A. Capra. CRITICAL ISSUES AND KEY POINTS FROM THE SURVEY TO THE CREATION OF THE HISTORICAL BUILDING INFORMATION MODEL: THE CASE OF SANTO STEFANO BASILICA. DIF Geomatics Section, University of Modena and Reggio Emilia, Via Vivarelli 10, 41125 Modena, Italy.

- Hossam El-Din Fawzy. 3D laser scanning and close-range photogrammetry for buildings documentation: A hybrid technique towards a better accuracy. Head of Civil Engineering Dep., Kafrelsheikh University, Kafr El Sheikh 33511, Egypt.
- Stuart I. GRANSHAW. PHOTOGRAMMETRIC TERMINOLOGY: THIRD EDITION. The Photogrammetric Record
- C. Tommasi, C. Achille a, F. Fassi. FROM POINT CLOUD TO BIM: A MODELLING CHALLENGE IN THE CULTURAL HERITAGE FIELD. Politecnico di Milano, 3D Survey Group, Dept. Of Architecture, Building Environment and Construction engineering, Via Ponzio 31, 20133 Milan, Italy.
- L. Barazzetti*, F. Banfi, R. Brumana, M. Previtali, F. Roncoroni. BIM FROM LASER SCANS... NOT JUST FOR BUILDINGS: NURBS-BASED PARAMETRIC MODELING OF A MEDIEVAL BRIDGE. ABC Department, Politecnico di Milano, Piazza Leonardo da Vinci 32, Milan, Italy.
- Andreas Humpe. Bridge Inspection with an Off-the-Shelf 360° Camera Drone. Campus Schachenmeierstrasse 35, University of Applied Sciences Munich, 80636 Munich, Germany.
- The center for Photogrammetric Training. History of Photogrammetry.
- Koert Sijmons. Introduction on Photogrammetry.
- C. Palestini, A. Basso, Graziani. INTEGRATED PHOTOGRAMMETRIC SURVEY AND BIM MODELLING FOR THE PROTECTION OF SCHOOL HERITAGE, APPLICATIONS ON A CASE STUDY. Dipartimento di Architettura, Università degli Studi "G. d'Annunzio" Pescara, viale Pindaro 42, 65127 Italia.
- D. Ph. Pocobelli, J. Boehm, P. Bryan, J. Still, J. Grau-Bové. BUILDING INFORMATION MODELS FOR MONITORING AND SIMULATION DATA IN HERITAGE BUILDINGS. University College London, Gower Street WC1E 6BT London, UK (danae.pocobelli.15, j.boehm, josep.grau.bove)
- Osello, A., n.d. *BIM And InfraBIM For Built Heritage -from CAD to BIM*. Politecnico di Torino. Turin, Italy
- Manzino, A., n.d Geomatica – fotogrammetria_lezione1-5. Politecnico di Torino. Turin, Italy.
- Manzino, A., n.d Geomatica – Cism_trattamento_LIDAR. Politecnico di Torino. Turin, Italy.
- Lingua Andrea, Chiabrando Filiberto, Aicardi Irene, n.d. Droni P1-10. Politecnico di Torino. Turin, Italy.

- Ministero delle Infrastrutture e dei Trasporti, 2020. Linee Guida Per La Classificazione E Gestione Del Rischio, La Valutazione Della Sicurezza Ed Il Monitoraggio Dei Ponti Esistenti. Rome, Italy, Retrieved from <http://www.mit.gov.it/comunicazione/news/mit-approve-le-linee-guida-per-la-sicurezza-dei-ponti>